BROWNIAN SYK MODELS AS EXACTLY SOLVABLE MODELS OF NON-EQUILIBRIUM MANY BODY QUANTUM PHYSICS

A Dissertation

by

LAKSHYA AGARWAL

Submitted to the Graduate and Professional School of
Texas A&M University
in partial fulfillment of the requirements for the degree of

DOCTOR OF PHILOSOPHY

Chair of Committee,	Artem Abanov
Co-Chair of Committee,	Shenglong Xu
Committee Members,	Joe Ross
	Eric Rowell
Head of Department,	Grigory Rogachev

August 2023

Major Subject: Physics

ABSTRACT

The study of quantum many body physics occupies a special place in the landscape of theoretical science, as it behaves like a connective tissue between seemingly disparate domains of inquiry, such as computer science, condensed matter physics and quantum gravity. A major challenge in the field concerns the solvability of strongly-interacting, non-integrable models driven away from equilibrium. Usually, such models can be exactly solved numerically for small-N, or in certain cases one can access their early time behaviour analytically in the infinite-N limit.

In this work, we shed light on the Brownian SYK models as exactly-solvable candidates to study non-equilibrium quantum dynamics. We show that these models have emergent symmetry structures post disorder averaging, where the model built with Majorana fermions (without charge conservation) maps to SO(n) spins and the complex fermionic model with charge conservation maps to SU(n) spins, both of which evolve in imaginary time. This enables us to probe various kinds of dynamical properties, such as charge transport and information scrambling, at both large finite-N and in the infinite-N limit. Apart from the obvious advantage of exact numerical solvability at large-N, the hydrodynamic descriptions that emerge from these models are valid at all time scales, in contrast to other commonly used methods. In case of the model with U(1) symmetry, the emergent hydrodynamics also describe the coupling of the charge-transport with the operator dynamics for arbitrary charge density-profiles.

Using the insights gained from the U(1) symmetric model, we also explicitly demonstrate the difference between commonly used probes of dynamics, such as the Green's functions, and more complicated higher-order correlators such the OTOC (out-of-time ordered correlator) in the study of non-equilibrium quantum dynamics.

DEDICATION

To my family.

ACKNOWLEDGMENTS

This thesis would not have been possible without my advisor, Shenglong Xu. I joined Shenglong's group when I was a young Physics sapling, and he has guided my growth with a special sense of care and purpose. Shenglong has lead by example when it comes to both, numerical and analytical excellence in Physics. He reignited my passion for Physics with his infectious enthusiasm, and taught me how to tackle challenging problems. He also contributed to my personal growth in many ways, as watching him choose grand, risky problems over low hanging fruit with an impressive sense of calmness has taught me to be more confident, and self-correct my own risk averse nature.

A special sense of gratitude is also reserved for my friend Sunny Guha, who was perhaps my first mentor in grad school. Sunny established a benchmark of excellence very early in my Physics journey, which I have tried to live up to ever since. Along with this, he also helped me in numerous other ways, sometimes to the point of my utter confusion over his extreme sense of altruism. Sunny now continues on as my mentor in my deep learning journey as well.

My friend, Chris Langlett, joined Shenglong's group at the same time as me. Chris comes from a different physics background than me, thus conversations with him have been extremely enlightening and have revealed a completely new perspective, previously alien to me. Watching Chris's work ethic has been especially inspiring, and has pushed me to do better myself. Besides this, Chris has personally helped me navigate the treacherous waters of a PhD, and for these reasons I am extremely grateful to him.

I would also like to thank my collaborator Shubhayan Sahu and other physicists that have helped me shape my work through helpful conversations, such as Brian Swingle, Elena Caceres, Anderson Misobuchi, Artem Abanov, DinhDuy Vu and Sankar Das Sarma.

Thanks should also go out to Katrin Becker and William D. Linch for teaching me supersymmetry, along with my friends Ahmed Elezaby, Haoyu Zhang, and other students

in the physics department, such as the ‘Little India’ group consisting of Anindya Sengupta, Aritra Saha and Surya Kiran Kanumilli. They have all been very helpful and I have enjoyed my Physics conversations with them.

Last but not the least, I would like to thank all the committee members for their insightful guidance and my family for their continued support and encouragement, and especially my girlfriend for her exceptional ability to indulge my ramblings about Physics.

CONTRIBUTORS AND FUNDING SOURCES

Contributors

This work was supported by a dissertation committee consisting of Professor Shenglong Xu [advisor], Professor Artem Abanov and Professor Joe Ross of the Department of Physics and Professor Eric Rowell of the Department of Mathematics.

The code to build SU(4) matrices in Chapter 3 using GT-patterns was written by Professor Shenglong Xu. The student analytically built the states and implemented numerical regularization techniques to plot the OTOC.

The work in Chapter 4 is based on a joint collaboration with Dr. Subhayan Sahu and Prof. Xu. The physical interpretation of the results and the analysis of the restricted differential equations was jointly done.

All other work conducted for the dissertation was completed by the student independently.

Funding Sources

Teaching assistance and Shenglong Xu's startup funded the graduate study. The graduate student received no other funding sources.

NOMENCLATURE

SYK	Sachdev-Ye-Kitaev
OTOC	Out-of-time-ordered correlator
q_{syk}	The degree of the polynomial of fermionic operators which appears in the Hamiltonian

TABLE OF CONTENTS

Page

LIST OF FIGURES

FIGURE Page

LIST OF TABLES

TABLE Page

1. INTRODUCTION

1.1 The role of quantum correlations in thermalization

The study of quantum many-body physics has recently seen a surge of interest not just in fields relevant to fundamental physics such as high energy theory, condensed matter physics and quantum information science, but also in applied physics and computer science, such as in the context of quantum computing. The key goal of the field is to understand and classify the structure of many-body quantum-states and describe the dynamics of these states, especially in the presence of strong interactions. A modern classification scheme relies upon the notions of thermalization and ergodicity. This classification is also tied to the puzzle of explaining why local operators in generic, closed, quantum many-body systems behave as if they are a part of a thermal ensemble at late times [1, 2, 3]. It is well known that in statistical mechanics, the density matrix of equilibrium states behaves as a part of the Gibbs ensemble:

$$\rho^{eq} = \frac{e^{-\beta H}}{Z}. \tag{1.1}$$

This is commonly understood as a consequence of interactions between a system and a bath at inverse temperature β. However, it is interesting to think about how this equilibrium is established for a closed quantum system. The seemingly ubiquitous phenomenon of reaching equilibrium is especially puzzling since the quantum system evolves under unitary dynamics. Thus, one would usually expect an initially pure state to evolve into another pure state, and not the thermal ensemble, which is a mixed state. Moreover, the phenomena of thermalization in classical mechanics is linked to chaos and non-linear dynamics, but in quantum mechanics the time-evolution of the density matrix is governed by a strictly linear Schrödinger equation:

$$i\frac{d\rho}{dt} = [H, \rho] \tag{1.2}$$

which is not expected to be chaotic. Along with this, for a time-independent Hamiltonian, the equation does not even host any steady-state solution. In spite of these concerns, given a closed system divided into subsystem A and its complement A^c, it has been observed that the state over the local region A is well-approximated by the thermal ensemble:

$$\rho_A^{eq}(t \to \infty) = \mathrm{Tr}_{A^c}\left(\frac{e^{-\beta H}}{Z}\right) \tag{1.3}$$

where β is the inverse temperature determined by the energy of the initial state and on the right hand side we have traced out the degrees of freedom in A^c. This ensemble is usually determined by measuring expectation values of local observables and other simple correlators over the region A.

The puzzle is resolved when one thinks more carefully about the nature of the observables that display this behaviour. These involve operators which are localized, which usually means their support is negligible when compared to the size of the overall system. Hence the mixed nature appears because the rest of the system (A^c) acts as a bath on the small number of degrees of freedom represented by the region A, even though the whole system $A + A^c$ evolves unitarily. This phenomenon is neatly encoded in the conjecture labelled as the 'Eigenstate Thermalization Hypothesis'. To dispel the notion that this is related to the quantum transport of energy between A and A^c, one can instead use Floquet dynamics, where the system is evolved using two different Unitaries $e^{iH_1\Delta t}$ and $e^{iH_2\Delta t}$ alternatively. In such a scenario energy is not strictly conserved as long as $[H_1, H_2] \neq 0$, but local states still relax to the infinite temperature Gibbs ensemble. Hence what we observe is a consequence of something more general, i.e. a buildup of quantum correlations between A and A^c.

A quantitative way to classify many-body states is through their entanglement structure, which roughly measures the amount of quantum correlations contained within the state. Given a pure state $|\psi\rangle$, the correlations between region A and its complement A^c are encoded in the reduced density matrix $\rho_A = \mathrm{Tr}_{A^c}(|\psi\rangle\langle\psi|)$, where we have traced out the degrees of

freedom contained in A^c. One measure of these correlations is given by the n^{th} Rényi entropy [4, 5, 6, 7], defined as:

$$S^{(n)}(A) = \frac{1}{1-n} \log \text{Tr}\left(\rho_A^n\right) \tag{1.4}$$

where $n \to 1$ limit recovers the Von-Neumann entropy $S(A) = -\text{Tr}(\rho \log \rho)$. The basic ingredient of entanglement can be understood from the simple example of 2 spins, where the entanglement is 0 for a product state such as $|\uparrow\uparrow\rangle$ and maximal for any Bell-pair state such as $|\uparrow\downarrow + \downarrow\uparrow\rangle$. A detailed calculation showing this can be found in [7]. The general expectation is that under quantum dynamics that are thermalizing, any simple state, such as a product state, will develop quantum correlations and will converge to a state with large amount of entanglement [2, 1, 8, 9]. This precisely measures how a local subsystem A builds correlations with its environment A^c.

1.2 Operator growth and the OTOC

A general way to characterize the non-equilibrium journey to these thermalized states in many-body systems is to track the evolution of operators. Under dynamics driven by a Hamiltonian H for example, an initially localized operator W_i will evolve according to

$$W_i(t) = W_i + \frac{it}{\hbar}[H, W_i] + \frac{1}{2!}\left(\frac{it}{\hbar}\right)^2 [H, [H, W_i]] + \dots \tag{1.5}$$

where generically, each nested commutator will make the operator more and more non-local and complicated. As an example, in a system where one starts with a local spin operator σ, it generically grows in 'size' as:

$$\sigma \xrightarrow{t} \sigma + \sigma\sigma + \sigma\sigma\sigma + \dots \tag{1.6}$$

Hence we have posited that entanglement growth and operator spreading are two main features of thermalizing many-body systems. A simple way to track the growth of the

operator is through the out-of-time-ordered correlator (OTOC) [10, 11, 12]:

$$\mathcal{F}(W_i(t), V_r) = \frac{1}{\mathrm{Tr}(I)}\mathrm{Tr}(W_i^\dagger(t)V_r^\dagger W_i(t)V_r) \tag{1.7}$$

which for the case where W_i and V_r are Hermitian and Unitary, such as when they are Pauli operators describing spins, is related to the squared commutator:

$$\mathcal{C}(t) = \frac{1}{\mathrm{Tr}(I)}\mathrm{Tr}\big([W_i(t), V_r]^\dagger\,[W_i(t), V_r]\big) = 2[1 - \mathrm{Re}(\mathcal{F})]. \tag{1.8}$$

Here i and r can be thought of as spatial indices denoting specific spins in a spin chain. Initially, the operator $W_i(t)$ is separated from V_r and they commute, i.e. $\mathcal{C}(t=0) = 0$ and $\mathcal{F}(t=0) = 1$. However, under thermalizing dynamics, the operator W_i grows until its support spreads to the site r and it fails to commute with V_r. This leads to the growth/decay of $\mathcal{C}/\mathcal{F}$, and in spatially extended chaotic systems, the operator W_i typically expands ballistically with a speed known as the butterfly velocity until it has covered the entire chain, and $\mathcal{F}$ reaches its equilibrium value.

The operator $W_i(t)$ is referred to as the dynamical operator in the OTOC, whereas V_r is the probing operator. To understand what $\mathcal{F}$ measures physically, one can imagine evolving a state using two different protocols [13]:

- First, we apply the operator V_r on the state, wait for a time t and then apply W_i

$$|\psi_1\rangle = W_i U V_r\,|\psi\rangle \tag{1.9}$$

- On the second run, apply W_i first at time t, go back in time to $t = 0$ then apply V_r, and then let it evolve naturally to time t again.

$$|\psi_2\rangle = U V_r U^\dagger W_i U\,|\psi\rangle \tag{1.10}$$

- $\mathcal{F}$ then measures the overlap between these two modified states, thereby capturing the effect of reversing the ordering of operators on the state.

$$\mathcal{F} = \langle\psi_2|\psi_1\rangle = \langle\psi| U^\dagger W_i U V_r U^\dagger W_i U V_r |\psi\rangle = \langle\psi| W_i(-t) V_r W_i(-t) V_r |\psi\rangle \tag{1.11}$$

  One can interpret V_r as a sort of 'perturbation', and the OTOC as a measure of how sensitive the system is to such perturbations.

In the more traditional version of the OTOC (Eq. 2.1), we average over all the states ψ in the Hilbert space. To see how the OTOC works in more detail, let's consider a system with N Majorana fermions, where the fermions satisfy the anti-commutation relation $\{\chi_i, \chi_j\} = 2\delta_{ij}$. A suitable way to discuss operator spreading is through the notion of operator-strings

$$\mathcal{S} = s_1 s_2 \dots s_N \ ; \ s_i \in (\chi_i, I) \tag{1.12}$$

where the operator $\mathcal{S}$ is either χ or I on every site/fermion i. This labels the complete set of operators in the model (because $\chi^2 = I$), and is also an orthonormal basis over the operator-space:

$$\frac{1}{\mathrm{Tr}(I)}\mathrm{Tr}(\mathcal{S}^\dagger \mathcal{S}') = \delta(\mathcal{S}', \mathcal{S}), \quad \frac{1}{\mathrm{Tr}(I)} \sum_{\mathcal{S}} \mathcal{S}^\dagger_{mn} \mathcal{S}_{pq} = \delta_{mq}\delta_{np}. \tag{1.13}$$

Due to these properties, we can expand any operator in such a basis. Doing the same for a local Majorana operator at time t, we write:

$$\chi_i(t) = \sum_{\mathcal{S}} c_{\mathcal{S}}(t)\mathcal{S} \ ; \ \mathrm{Tr}(\chi_i(t)\chi_i(t)) = \mathrm{Tr}(I) \implies \sum_{\mathcal{S}} |c_{\mathcal{S}}(t)|^2 = 1 \tag{1.14}$$

where we are expressing the fact that due to unitarity, norms are conserved over time and this leads to the coefficients $|c_{\mathcal{S}}(t)|^2$ describing a probability distribution over the operator-strings $\mathcal{S}$. Now let's plug in the expression for $\chi_i(t)$ into the OTOC averaged over the choice

of the local probing operator:

$$\begin{aligned}\sum_j \mathcal{F}\left(\chi_i(t), \chi_j\right) = \frac{1}{2^{N/2}} \sum_j \mathrm{Tr}\left(\chi_i(t)\chi_j\chi_i(t)\chi_j\right) &= \left(2\sum_{\mathcal{S}} |c_{\mathcal{S}}(t)|^2 \,\mathrm{size}(\mathcal{S}) - N\right) \\ &= (2\overline{\mathrm{size}(\chi_i)} - N)\end{aligned} \tag{1.15}$$

where size($\mathcal{S}$) measures the number of χ in the string $\mathcal{S}$. For example, the size of χ_i at $t = 0$ is 1:

$$\sum_j \mathcal{F}\left(\chi_i(t=0), \chi_j\right) = \frac{1}{2^{N/2}} \sum_j \mathrm{Tr}\left(\chi_i\chi_j\chi_i\chi_j\right) = 1 - (N-1) \tag{1.16}$$

where the 1 on the right is the result when $i = j$ and the $-(N-1)$ comes from the anti-commuting contributions when $i \neq j$. However, the size of the operator will grow with time, as we expect from Eq. (1.5). Under thermalizing dynamics, one expects that the operator will become maximally complex, which means it will flow to all operator-strings in the basis with equal probability. This implies that all sizes will occur with equal probability, and since there are N fermions, the average size will approach $N/2$. In the equation above, this will result in the average OTOC becoming 0, which establishes a precise connection between operator growth and the OTOC. A more detailed version of this calculation can be found in Sec. 3.2.1.

1.3 Scrambling and the OTOC

As it turns out, the OTOC is also useful for characterizing the growth of quantum-correlations under a given unitary channel. This was described in [14], where the authors studied the growth of correlations via the information shared between a quantum system and its time-evolved counterpart. A simple qualitative way to see the connection between operator growth and information scrambling is via the following example. Let's consider a simple product state ψ over N qubits which is time evolved via a generic unitary U:

$$\psi(t=0) = |00...0\rangle \implies \psi(t) = U\,|00...0\rangle \tag{1.17}$$

We can compare this to another similar state $\psi^{'}$, where we initialize the first qubit in the state 1 instead of 0 and evolve it using the same unitary as before:

$$\psi^{'}(t=0) = |10...0\rangle = \sigma_{1,x}\,|00...0\rangle \implies \psi^{'}(t) = U\sigma_{1,x}U^{\dagger}\,\psi(t) \tag{1.18}$$

Hence in the Heisenberg picture, the 'information' about the initial qubit can be viewed from the lens of the growth of the operator $\sigma_{1,x}$. The difference in the two states ψ and $\psi^{'}$, which is encoded in the initialization of the the first qubit, can also be viewed as being stored in the time-evolved operator $\sigma_{1,x}(t)$. As the simple operator grows into a more complex operator, it carries information about the input state into more and more non-local degrees of freedom, thereby making it practically unrecoverable via local measurements. Therefore, the OTOC can measure the growth of such an operator and also provides a measure of information scrambling.

It is important to mention that this connection with the OTOC has been experimentally utilized to measure scrambling in various platforms, such as nuclear magnetic resonance quantum simulators [15, 16, 17, 18], trapped ions [19, 20, 21] and superconducting qubits [22, 23, 24, 25]. The OTOC is also related to the measurement of fidelity during many-body teleportation, which serves as a quantifier of teleportation success [26, 27]. Hence the OTOC serves as a test bed for many quantum simulators and will play an increasingly important role in the quantum information era of physics.

2. GENERAL FORMALISM[1]

In this chapter, we will cover the formalism used to compute the OTOC in later chapters. The strategy revolves around utilizing both the Brownian averaging of the models, as well as rewriting the OTOC in terms of four copies of the Hilbert space. The procedure can also be similarly applied to arbitrarily complex correlators. For completeness and notational clarity, we will redefine the OTOC as

$$\mathcal{F}(W(t),V) = \frac{1}{\mathrm{Tr}I}\mathrm{Tr}(W^\dagger(t)V^\dagger W(t)V) \tag{2.1}$$

2.1 Operator to state mapping on 4 copies of the Hilbert Space

To compute the OTOC, we map it to the overlap between two quantum states in four replicas of the original Hilbert space, labelled by a, b, c, d. The OTOC in Eq. (2.1) can be written as

$$\mathcal{F}(W(t),V) = \mathrm{Tr}I \,\langle \mathrm{out}|\, \mathbb{U}\, |\mathrm{in}\rangle \tag{2.2}$$

where $|\mathrm{in}\rangle$ and $|\mathrm{out}\rangle$ are the input and output states defined as

$$\begin{aligned} |\mathrm{in}\rangle &= \frac{1}{\mathrm{Tr}I}\sum W^\dagger_{mn}W_{pq}\,|m\otimes n\otimes p\otimes q\rangle \\ |\mathrm{out}\rangle &= \frac{1}{\mathrm{Tr}I}\sum V^\dagger_{mq}V_{pn}\,|m\otimes n\otimes p\otimes q\rangle \end{aligned} \tag{2.3}$$

and m, n, p, q are the computational basis states spanning the Hilbert space of each replica. On the other hand, terms such as V_{pn} refer to the element of the matrix representation of the operator V, in the row p and column n. The time evolution operator $\mathbb{U}$ is given by

$$\mathbb{U} = U\otimes U^*\otimes U\otimes U^*. \tag{2.4}$$

[1]Reprinted with permission from "Emergent Symmetry in Brownian SYK models and charge dependent scrambling" by L. Agarwal and S. Xu [28]

The time evolved state $|\text{in}(t)\rangle$ is

$$|\text{in}(t)\rangle = \mathbb{U}\,|\text{in}\rangle = \frac{1}{\text{Tr}I}\sum W^\dagger(t)_{mn}W(t)_{pq}\,|m\otimes n\otimes p\otimes q\rangle \tag{2.5}$$

One can verify that $\langle\text{out}|\text{in}(t)\rangle$ does indeed lead to $\mathcal{F}(W(t),V)$. To simplify the notation, we rewrite $|\text{in}\rangle$ as

$$|\text{in}\rangle = \frac{1}{\text{Tr}I}\,|W^\dagger\otimes W\rangle\,. \tag{2.6}$$

On the other hand, using a complete operator basis $\mathcal{S}$, we rewrite the state $|\text{out}\rangle$ as

$$\begin{aligned}|\text{out}\rangle &= \frac{1}{\text{Tr}^2 I}\sum V^\dagger_{mm'}\mathcal{S}^\dagger_{m'n'}V_{n'n}\mathcal{S}_{pq}\,|m\otimes n\otimes p\otimes q\rangle \\ &= \frac{1}{\text{Tr}^2 I}\sum_{\mathcal{S}}|V^\dagger\mathcal{S}^\dagger V\otimes\mathcal{S}\rangle\,.\end{aligned} \tag{2.7}$$

Therefore, the OTOC is written as

$$\mathcal{F}(W_i(t),V_j) = \frac{1}{\text{Tr}^2(I)}\sum_{\mathcal{S}}\langle V_j^\dagger\mathcal{S}^\dagger V_j\otimes\mathcal{S}|\,\mathbb{U}\,|W_i^\dagger\otimes W_i\rangle\,. \tag{2.8}$$

This is equivalent to Eq. (2.2) and does not reduce the computational complexity in general. However, as we will show in the following sections, for a special class of chaotic quantum many-body models called Brownian models, the symmetry and algebraic structure of $\mathbb{U}$ after the random averaging significantly reduces the computational complexity. This allows us to calculate the OTOC exactly for all time scales, including the early time growth and late-time saturation, for large system size.

2.2 General structure of Brownian models

The Hamiltonian of Brownian models takes the following general form,

$$H(t) = \sum_A J_A(t)\hat{X}_A + h.c. \tag{2.9}$$

where $\hat{X}_A$ describes few body interactions, i.e. spin-spin interactions or 4-body fermionic interactions between the different degrees of freedom, and A is a generic index labeling the degrees of freedom this term acts on. The model is Brownian because the coupling strength $J_A(t)$ is a Gaussian white noise uncorrelated in time obeying

$$\overline{J_A(t)} = 0, \quad \overline{J_A(t)J^*_{A'}(t')} = J\delta_{AA'}\delta(t-t'). \tag{2.10}$$

Because the disorder is uncorrelated in time, the disorder average can be computed independently at different times. At each time slice, we have

$$\overline{d\mathbb{U}} = \overline{dU^a dU^{b,*} dU^c dU^{d,*}} = (1 + \mathbb{H}dt) \tag{2.11}$$

where

$$\begin{aligned} \mathbb{H} &= -\frac{J}{2}\sum_A \left(\mathbb{X}_A\mathbb{X}_A^\dagger + \mathbb{X}_A^\dagger\mathbb{X}_A\right), \\ \mathbb{X}_A &= X_A^a - X_A^{b,*\dagger} + X_A^c - X_A^{d,*\dagger}. \end{aligned} \tag{2.12}$$

The operator $\mathbb{H}$ is Hermitian and semi-negative, namely all the eigenvalues are either zero or negative. As is evident from the expression above, there is a discrete symmetry under the exchange of replicas $a \leftrightarrow c$ and $b \leftrightarrow d$, along with a conjugation symmetry between the pairs (a, c) and (b, d). These discrete symmetries have been studied in detail recently [29].

In addition $\mathbb{H}$ has two zero energy eigenstates that are independent of the details of $\hat{X}_A$. We have

$$e^{\mathbb{H}t}\left|I\otimes I\right\rangle = \left|I\otimes I\right\rangle, \quad e^{\mathbb{H}t}\sum_{\mathcal{S}}\left|\mathcal{S}^\dagger\otimes\mathcal{S}\right\rangle = \sum_{\mathcal{S}}\left|\mathcal{S}^\dagger\otimes\mathcal{S}\right\rangle. \tag{2.13}$$

This is because the identity operator stays the same under unitary time evolution (Fig. 2.1(b) and (c)). This condition is useful for consistency checks when we build $\mathbb{H}$ for specific models. If the Hamiltonian has additional symmetries, the corresponding operator-states are also zero-energy eigenstates with respect to the emergent Hamiltonian. As an example, the parity operator-state $|\prod\chi\otimes\prod\chi\rangle$ has null energy with respect to the emergent Hamiltonian

in the case of the Brownian SYK model.

The unitary time evolution operator on the replicated Hilbert space after Brownian average $\overline{\mathbb{U}}$ becomes $\exp(\mathbb{H}t)$. In other words, the Brownian disorder average converts the unitary real-time evolution to the imaginary time evolution governed by the Hamiltonian $\mathbb{H}$ acting on four copies of the original Hilbert space. This property follows from the observation that the term corresponding to first order time in dU has to be paired with another first order term to be nonzero after disorder average. Then the OTOC in Eq. (2.8) after the disorder average can be written as

$$\mathcal{F}(W_i(t), V_j) = \frac{1}{\mathrm{Tr}^2(I)} \sum_{\mathcal{S}} \langle V_j^\dagger \mathcal{S}^\dagger V_j \otimes \mathcal{S}| \exp(\mathbb{H}t) |W_i^\dagger \otimes W_i\rangle \tag{2.14}$$

which measures the overlap between the input state and output state after quenched *imaginary* time evolution. This is valid for any Brownian model described by Eq. (2.9). In general, with this formalism, it is still very challenging to obtain the OTOC $\mathcal{F}$ because one needs to diagonalize the Hamiltonian $\mathbb{H}$ numerically, which is limited to small system sizes.

In the following sections, we will show that for a certain class of Brownian models, namely the Brownian-SYK models, the Hamiltonian $\mathbb{H}$ exhibits elegant symmetry structures that only appear after the disorder average. By exploiting the symmetry structures, we show that the largest Hilbert space involved in the computation of $\mathcal{F}$ scales linearly with the number of Majoranas or complex fermions in the systems, making results for large but finite N accessible. More specifically, we find that

- For the Brownian Majorana SYK model without charge conservation, the operator dynamics can be mapped to imaginary time dynamics of an SU(2) spin with angular momentum $\sim N/2$.

- For the complex Brownian SYK model with charge conservation, the operator dynamics can be mapped to imaginary time dynamics of an SU(4) spin with fixed weight.

In what follows, we discuss each model individually. For the Brownian Majorana SYK model,

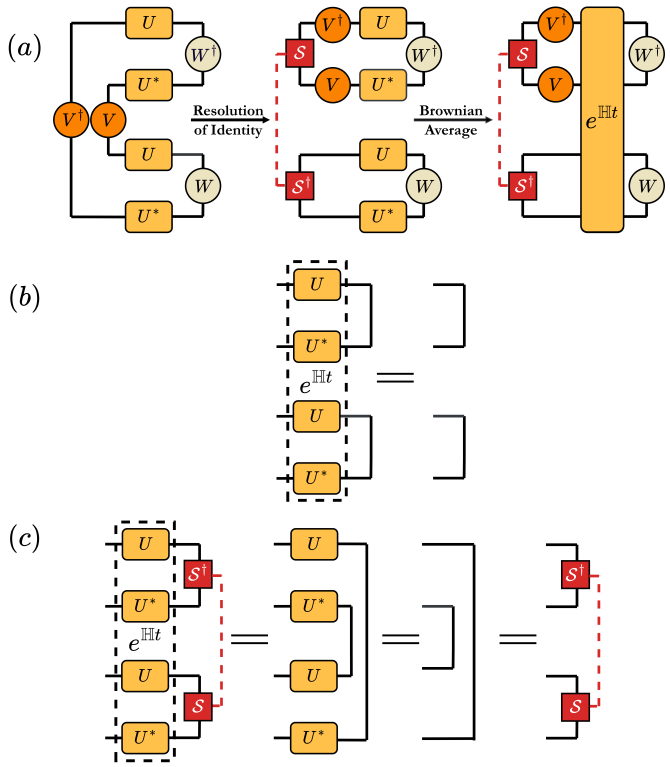

Figure 2.1: (a) Resolution of the identity in the OTOC, followed by the Brownian average. (b) The invariance of the Identity operator-state $|I \otimes I\rangle$ under the effective imaginary-time evolution. (c) The invariance of the complete set of operator-states $\sum_{\mathcal{S}} |\mathcal{S}^\dagger \otimes \mathcal{S}\rangle$ under the effective imaginary-time evolution. Both operator-states considered in (b) and (c) remain eigenstates of the effective Hamiltonian $\mathbb{H}$ because they are invariants of the circuit even before the random averaging.

our approach, inspired by [30], simplifies the method used therein and unifies the approach used in [30] and [31, 32, 33]. More importantly, our approach can be generalized to the complex Brownian SYK model, which is the primary focus of the thesis.

3. NON-EQUILIBRIUM DYNAMICS IN 0+1 DIMENSIONS[1]

3.1 Chapter Summary

The goal of this chapter is to show how Brownian SYK models make good candidates to study non-equilibrium phenomenon in $0+1$ dimensions, both analytically and numerically. This is shown both for the model without symmetry, and for the U(1) symmetric model as well. The steps are as follows:

- First, we take advantage of the uncorrelated nature of the model along the time direction, to describe the dynamics on four time contours in terms of an effective imaginary time Schrodinger equation. This is covered in detail in Chapter 2.

- This evolution is governed by an emergent Hamiltonian, which is composed of 'replica' fermions on four time contours.

- For the regular Brownian SYK model built with Majorana fermionsa, we show that these replica fermions follow the commutation relations of an SU(2) algebra, therefore the emergent Hamiltonian can be viewed as a spin model and this drastically reduces the computational time complexity of the problem from $\mathcal{O}(2^{N/2}) \to \mathcal{O}(N)$.

- This is utilized to plot the OTOC in the model for $N = 10000$ fermions. Along with this, the spin description also helps us to derive the hydrodynamic equation in the infinite-N limit.

- Following this, we discuss operator dynamics in the complex Brownian SYK model built with complex fermions and with a U(1) symmetry. For this model, we show that the replica complex fermions follow the commutation rules for the SU(4) algebra, thereby allowing us to interpret the emergent Hamiltonian as an SU(4) spin model.

[1]Reprinted with permission from "Emergent Symmetry in Brownian SYK models and charge dependent scrambling" by L. Agarwal and S. Xu [28]

- Since the U(1) symmetry in the original model causes the SU(4) spin model to conserve weights, this leads to a reduction in computational time complexity ($\mathcal{O}(2^N) \to \mathcal{O}(N)$), which is then utilized to plot the behaviour of the OTOC within each charge sector, for $N = 500$ fermions. Knowledge about Gelfand-Tsetlin patterns is used to construct the emergent Hamiltonian within fixed weight sectors numerically.

- From this, we extract insights about the charge-dependence of information scrambling, which is then verified analytically as well, in the infinite-N limit.

3.2 The case without symmetry : Brownian SYK model

Our first goal will be to understand dynamics in a dimensionless dot with many interacting quantum particles. Initially, we will compute the OTOC ($\mathcal{F}$ in Eq. (2.1)) in a model without symmetries, i.e. the Brownian SYK model, at both large finite-N and in the infinite-N limit. In all-to-all interacting models with few-body interactions and a large number of degrees of freedom, such as the Sachdev-Ye-Kitaev model [34, 35, 36, 37, 38], $\mathcal{F}$ typically grows exponentially fast in the early-time regime, $\mathcal{F} \sim \frac{1}{N} e^{\lambda_L t}$ [39, 40, 41, 42], where λ_L is the Lyapunov exponent. In a local extended system, the support of $W(t)$ typically grows ballistically, and $\mathcal{F}$ features a wavefront travelling at the butterfly velocity [43, 44, 45, 46, 47, 48, 49, 50, 51, 52, 53, 54, 31, 55]. More generally, the behavior of $\mathcal{F}$ depends on the interaction between the different degrees of freedom [56, 57]. The OTOC has been experimentally measured in nuclear magnetic resonance quantum simulators [15, 16, 17, 18], trapped ions [19, 20, 21] and superconducting qubits [22, 23, 24, 25, 58].

On the other hand, Brownian many-body models [40, 59, 60, 31, 33, 30, 32], in which the couplings are random variables uncorrelated in the time direction, are useful for understanding scrambling dynamics. In the absence of conserved quantities, the operator dynamics in Brownian models can be mapped to a Markovian process [31, 33, 61] or imaginary time dynamics of bosonic models [30] post disorder average, in which case the OTOC can be calculated efficiently for all time at large finite N. The analytical expression of the OTOC

in the large N limit can also be derived, which obeys a logistic type differential equation [33] for all-to-all connected models and reaction-diffusion equation [44, 31] in higher dimensions. Related to Brownian models, scrambling for random Hamiltonians [62] and noisy spin systems [63, 64] has also been studied.

Building on previous work on the Majorana Brownian SYK model [30], we demonstrate that Brownian SYK models have a simple symmetry structure for arbitrary N after taking the random disorder average, which makes the numerical calculation of the OTOC at large finite N possible even in the case with charge conservation. The operator dynamics can be organized into various irreducible representations (irreps) of the symmetry group. We show that in the case of the Majorana Brownian SYK model, this approach maps the operator dynamics to that of an SU(2) spin in imaginary time, with the angular momentum being related to N. In what follows, we will first revisit the notion of how the OTOC is tied to operator growth in models built with Majorana fermions, which is relevant when we want to consider non-symmetric models.

3.2.1 Operator growth for Majorana fermions

We begin with the analysis of the operator dynamics of Majorana fermions, which is relevant in the case of the regular and Brownian SYK models. Although this has been talked about in the Introduction, here we will flesh it out in more detail and cover edge cases as well. We consider a system of N Majoranas with the Hilbert space dimension $\mathrm{Tr}(I) = 2^{N/2}$, where the Hamiltonian is a function of the Majorana operators χ_i, and the subscript i goes from 1 to N. The operators obey the anti-commutation relation $\{\chi_i, \chi_j\} = 2\delta_{ij}$. A good basis for the operator dynamics are the Majorana strings [10], which are products of local operators, either χ_i or I_i. The Majorana strings take the form

$$\mathcal{S} = s_1 s_2 \cdots s_N \tag{3.1}$$

Where each s_i in the string is either the identity (I) or the Majorana operator (χ) at that site. We define the size of the Majorana string as size($\mathcal{S}$), which counts the number of χ's in the string. The Majorana strings satisfy the orthogonality and completeness relations in Eq. (1.13). Therefore, any Heisenberg operator at arbitrary time can be expanded in this basis with coefficients $c(\mathcal{S}, t)$:

$$W(t) = \sum_{\mathcal{S}} c(\mathcal{S}, t)\mathcal{S}. \tag{3.2}$$

We choose the operator W to have the normalization $\mathrm{Tr}(W^\dagger W) = \mathrm{Tr}I$ and this leads to the constraint $\sum_{\mathcal{S}} |c(\mathcal{S}, t)|^2 = 1$. Thus the coefficients $|c(\mathcal{S}, t)|^2$ have the interpretation of a probability distribution over the different strings of operators. Quantum information scrambling is tied to the fact that a simple initial operator becomes as complicated as possible under Heisenberg time evolution. This suggests that the operator probability distribution, starting with one localized at a single operator-string, would approach uniform distribution in the late time regime where every operator is equally probable and the system becomes fully scrambled. An important caveat to keep in mind is that the operator cannot spread to the identity or parity operator at late times if it has a null overlap with the specified steady operators at zero time.

Physical systems usually conserve the fermionic parity, since the Hamiltonian only contains an even number of Majorana operators and commutes with the parity operator $\prod \chi$. As a result, the parity of an operator, whether it starts with an even or odd number of Majorana operators, remains invariant under the unitary time evolution. Only the $\mathcal{S}$ with even (odd) lengths appear in the expansion of the operator $W(t)$ with even (odd) parity. In the late time regime, the operator probability becomes uniform in the parity sector determined by the initial operator but remains zero in the opposite sector. The simplest quantity to characterize scrambling of an initially simple operator, such as $\chi(t)$, is the average size of the Majorana strings $\sum_{\mathcal{S}} |c(\mathcal{S}, t)|^2 \mathrm{size}(\mathcal{S})$. This average size is precisely measured by the OTOC. Using the operator expansion and the anti-commutation relation of Majorana operators, one

can show that

$$\begin{aligned}\sum_i \mathcal{F}(W(t),\chi_i) &= \frac{1}{2^{N/2}}\sum_i \mathrm{Tr}(W^\dagger(t)\chi_i W(t)\chi_i) \\ &= \pm\left(N - 2\,\overline{\mathrm{size}(W)}\right).\end{aligned} \tag{3.3}$$

The plus or minus sign depends on whether $W(t)$ is parity even or odd. Each OTOC in the sum $\sum_i \mathcal{F}(W(t),\chi_i)$ is related to the probability of the operator χ_i appearing in the operator string. For the simple OTOC $\mathcal{F}(\chi_i(t),\chi_j)$, the initial and final values are

$$\mathcal{F}(\chi_i(0),\chi_j) = -1 + 2\delta_{ij}, \quad \mathcal{F}(\chi_i(\infty),\chi_j) = 0. \tag{3.4}$$

We will compute the time evolution of $\mathcal{F}$ from $t = 0$ to $t = \infty$ in the Brownian Majorana SYK model and also show that the general expectation is violated when the system becomes non-interacting. Here we emphasize that the late-time value goes to zero because as intuitively expected, starting from an operator in the parity odd sector will result in the operator spreading uniformly to all the operator-strings in the odd sector, therefore odd operator-sizes will be binomially distributed and the average operator size will be $N/2$. On the other hand, if we consider a bosonic initial operator, say $\chi_i\chi_{i'}$, the late-time operator distribution will be uniform over the operator-strings in the even sector, with the exception of the identity and parity operator which are static. The binomial distribution of all operators with even sizes excluding the identity and the parity operator also leads to average operator size $N/2$. Therefore, in the majorana system where the only symmetry is the fermionic parity, the late-time value of the OTOC in Eq. (3.3) approaches zero. This is in contrast with general spin models, where the only operator excluded from the late-time distribution would be the identity. In this case, the late-time value of the OTOC contains a finite-size correction exponentially small as a function of the system size [65].

3.2.2 Defining the Brownian SYK model

In this section we will review the work done on the Brownian SYK model for the purpose of completeness and notational clarity. We start with the Hamiltonian

$$H(t) = i^{\frac{q_{\text{syk}}}{2}} \sum_{i_1<\ldots<i_{q_{\text{syk}}}} J_{i_1,\ldots,i_{q_{\text{syk}}}}(t)\chi_{i_1}\chi_{i_2}\cdots\chi_{i_{q_{\text{syk}}}} \tag{3.5}$$

where the generalised index i_j can take values between 1 and N. The couplings for general q_{syk} are distributed according to

$$\overline{J_{i_1\ldots,i_{q_{\text{syk}}}}(t)J_{i'_1\ldots,i'_{q_{\text{syk}}}}(t')} = \delta_{i_1 i'_1}\cdots\delta_{i_{q_{\text{syk}}}i'_{q_{\text{syk}}}}\delta(t-t')\,\frac{(q_{\text{syk}}-1)!}{2N^{(q_{\text{syk}}-1)}}. \tag{3.6}$$

We are interested in computing the OTOC, which can be rewritten in terms of four copies of the Hilbert space, as shown in Sec. 2.1. The four copies of the unitary operator $d\mathbb{U}$ that encode the time evolution in the OTOC are built using operators of the form

$$\begin{aligned} \chi_j^a &:= \chi_j \otimes I \otimes I \otimes I \quad \chi_j^b := I \otimes \chi_j^* \otimes I \otimes I \\ \chi_j^c &:= I \otimes I \otimes \chi_j \otimes I \quad \chi_j^d := I \otimes I \otimes I \otimes \chi_j^* \end{aligned} \tag{3.7}$$

These operators satisfy the (anti-)commutation relations $\left[\chi_j^\alpha, \chi_k^\beta\right] = 0$ for $\alpha \neq \beta$ and $\left\{\chi_j^\alpha, \chi_k^\alpha\right\} = 2\delta_{j,k}$. We can use the parity operator $\mathcal{Q}$ on each copy

$$\mathcal{Q}^\alpha = \prod_{k=1}^{N} \chi_k^\alpha, \quad \alpha = a, b, c, d \tag{3.8}$$

to turn χ_i^α into purely anti-commuting operators as follows [30]

$$\begin{aligned} \psi_j^a &= i\mathcal{Q}^a\chi_j^a, & \psi_j^b &= \mathcal{Q}^a\chi_j^b \\ \psi_j^c &= i\mathcal{Q}^a\mathcal{Q}^b\mathcal{Q}^c\chi_j^c, & \psi_j^d &= \mathcal{Q}^a\mathcal{Q}^b\mathcal{Q}^c\chi_j^d. \end{aligned} \tag{3.9}$$

These new operators obey the relation $\left\{\psi_j^\alpha, \psi_k^\beta\right\} = 2\delta_{\alpha,\beta}\delta_{j,k}$, and since $(Q^\alpha)^2 = 1$ (for $N \equiv 0 \bmod 4$), we can exploit the identity $\prod_{k=1}^M \chi_{j_k}^\alpha = \prod_{k=1}^M \psi_{j_k}^\alpha$ to rewrite $d\mathbb{U}$ and thus the effective Hamiltonian $\mathbb{H}$ in terms of these new operators. We introduce the bilinear operators $S^{\alpha\beta} = \sum_i \psi_i^\alpha \psi_i^\beta$, and remark that the effective Hamiltonian takes the following general form :

$$\mathbb{H} = \mathbb{H}\left(S^{\alpha\beta}\right), \quad \alpha, \beta \in a, b, c, d. \tag{3.10}$$

The explicit expression, which depends on q_{syk}, is provided in the appendix. The main observation is that the Hamiltonian $\mathbb{H}$ is always a function of the six operators $S^{\alpha\beta}$ for $\alpha \neq \beta$ (the term with $\alpha = \beta$ contributes a constant term to the Hamiltonian).

3.2.3 The emergent SU(2) $\otimes$ SU(2) algebra

The emergent Hamiltonian $\mathbb{H}$ acts on a Hilbert space of dimension 4^N. The system contains N sites, each one hosting 4 local states, which can be thought of as the vacuum state ($|I \otimes I\rangle$), doubly-occupied state ($|\mathcal{Q}\chi_i \otimes \mathcal{Q}\chi_i\rangle$), and two singly occupied states ($|\mathcal{Q}\chi_i \otimes I\rangle, |I \otimes \mathcal{Q}\chi_i\rangle$), much like those in the Fermi-Hubbard model. Here $\mathcal{Q}$ is the parity operator $\prod_i \chi_i$. The vacuum and doubly occupied state are even parity states whereas the singly occupied states have odd parity. Now we explore the symmetry of $\mathbb{H}$ to block-diagonalize the Hamiltonian and reduce the effective dimension. First, $S^{\alpha\beta}$ and $\mathbb{H}$ commute with the onsite parity operator $\psi_i^a \psi_i^b \psi_i^c \psi_i^d$. As a result, the number of fermions per site stays even or odd. One can show that for the input state of the form $2^{N/2}|\text{in}\rangle = |W^\dagger \otimes W\rangle$, the parity on each site is even, either the empty state or doubly occupied state. This reduces the total Hilbert space dimension to 2^N. To this end, we map the system to N two-level systems.

In order to further reduce the Hilbert space dimension, we will rely on additional sym-

metries of the emergent Hamiltonian. Let us define the following quantities:

$$\begin{aligned} L_x &= \frac{1}{4i}(S^{bc} + S^{ad}), \quad J_x = \frac{1}{4i}(S^{bc} - S^{ad}) \\ L_y &= \frac{1}{4i}(S^{ca} + S^{bd}), \quad J_y = \frac{1}{4i}(S^{ca} - S^{bd}) \\ L_z &= \frac{1}{4i}(S^{ab} + S^{cd}), \quad J_z = \frac{1}{4i}(S^{ab} - S^{cd}). \end{aligned} \tag{3.11}$$

These operators are the generators of the $\mathrm{SU}(2) \otimes \mathrm{SU}(2)$ algebra, which can by checked by verifying the commutation relations

$$[L_i, L_j] = i\epsilon_{ijk} L_k, \ [J_i, J_j] = i\epsilon_{ijk} J_k, \ [L_i, J_j] = 0. \tag{3.12}$$

The full emergent Hamiltonian can now be written as a function of both the L and the J operators (Eq. (3.10)). Identifying the SU(2) algebras in the Hamiltonian has reduced the maximum dimensionality of the dynamical subspace to be of order N^2 since the input state will split into the irreps of the algebras, and the Hamiltonian evolves separate irreps independently. Consider the four states on a site. They split into a $\mathbf{2} \oplus \mathbf{2}$ representation of the $\mathrm{SU}(2) \otimes \mathrm{SU}(2)$ group. The empty and doubly occupied states form a doublet of the L algebra and a singlet of the J algebra, while the two singly occupied states form a singlet of the L algebra and a doublet of the J algebra. Since the input state $|\mathrm{in}\rangle$ has an even number of fermions per site, it is a singlet state of the J algebra and we have $J_\alpha |\mathrm{in}\rangle = 0$ ($\alpha = x, y, z$). Thus the emergent Hamiltonian will now have only one copy of the SU(2) algebra, i.e. the L algebra. The effective Hamiltonian in this form does not depend on the details of the system but is fully determined by the irrep of the SU(2) algebra. More explicitly, for $q_{\mathrm{syk}} = 2$, the emergent Hamiltonian $\mathbb{H}$ is

$$\mathbb{H}_{q_{\mathrm{syk}}=2} = \frac{1}{2N}\left(-2\binom{N}{2} - 3N + 4L^2\right). \tag{3.13}$$

The Hamiltonian is SU(2) invariant as it only contains the total angular momentum L^2, and is a c number once the irrep is fixed. On the other hand, for $q_{\text{syk}} = 4$, the Hamiltonian is

$$\mathbb{H}_{q_{\text{syk}}=4} = \frac{3}{N^3}\left(-2\begin{pmatrix} N \\ 4 \end{pmatrix} + \frac{1}{4!}\Big(H_x + H_z - H_y\Big)\right), \tag{3.14}$$

where

$$H_\alpha = 32L_\alpha^4 + 8(8-6N)L_\alpha^2 + 6N(N-2); \quad \alpha = x, y, z. \tag{3.15}$$

The full SU(2) symmetry in the $q_{\text{syk}} = 2$ case is reduced to a discrete rotation symmetry in the xz plane. For general q_{syk}, the part of the emergent Hamiltonian which depends on the angular momentum takes the form $H_x + H_z - (-1)^{q_{\text{syk}}/2} H_y$, and hence the symmetry is either discrete $\pi/2$ rotations within the xz plane or between the x, y, z axes, depending on whether $q_{\text{syk}}/2$ is even or odd respectively. The additional symmetry in the case where $q_{\text{syk}}/2$ is odd occurs as a result of the time-reversal symmetry operator commuting with the unitary time evolution operator [60].

The emergent Hamiltonian is always a function of the angular momentum $\vec{L}$ for arbitrary q_{syk}. When $q_{\text{syk}} = 2$, the Hamiltonian is also an SU(2) invariant, making it analytically tractable. For $q_{\text{syk}} > 2$, the Hamiltonian only has a square or cubic symmetry. The enhanced symmetry in the $q_{\text{syk}} = 2$ case makes the operator dynamics non-scrambling and distinct from general q_{syk}. This is expected since the original Brownian SYK is quadratic at $q_{\text{syk}} = 2$.

Although we still need to diagonalize $\mathbb{H}$ to obtain the dynamics for general q_{syk}, the largest Hilbert space dimension, which is determined by the angular momentum, is $N + 1$. This is drastically reduced from the original Hilbert space size of 4^N and enables the exploration of operator scrambling dynamics for large but finite N and arbitrary time scales. Furthermore, as we will show in Sec. 3.2.6, this formalism also makes it possible to derive an analytical expression for the OTOC in the large N limit for arbitrary time scales and is naturally connected to the previously known approach which consists of mapping to a stochastic

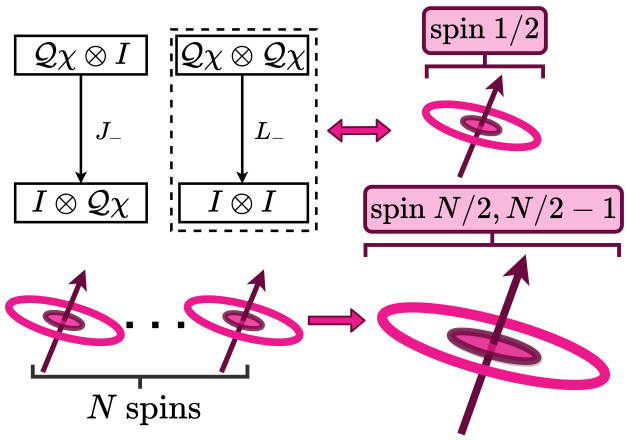

Figure 3.1: The four local operator-states form two doublets of the emergent SU(2) $\otimes$ SU(2) algebra. The J doublets do not contribute to the OTOC because they have odd local parity. The operator dynamics of N Majoranas are mapped to the imaginary time dynamics of N 1/2-spins from the L doublets, which compose to form $N/2$ and $N/2-1$ spins of the global SU(2) algebra generated by $\vec{L}$ in Eq. (3.11). The largest Hilbert space dimension is $N+1$.

model.

3.2.4 Classifying the states in the SU(2) algebra

We are interested in studying the operator dynamics of the Majorana fermions $\chi(t)$ through the OTOC $\mathcal{F}(\chi_i(t), \chi_j)$, which, based on Eq. (2.14), takes the following form:

$$\begin{aligned} &\mathcal{F}(\chi_i(t), \chi_j) = 2^{N/2} \langle \text{out}| \exp(\mathbb{H}t) |\text{in}\rangle \\ &|\text{in}\rangle = \frac{1}{2^{N/2}} |\chi_i \otimes \chi_i\rangle\,, \quad |\text{out}\rangle = \frac{1}{2^N} \sum_{\mathcal{S}} |\chi_j \mathcal{S}^\dagger \chi_j \otimes S\rangle\,. \end{aligned} \tag{3.16}$$

Now that we have described the structure of the emergent Hamiltonian, the next task is to decompose the input state $|\text{in}\rangle$ and the output state $|\text{out}\rangle$. The problem is very similar to decomposing states of N 1/2-spins into various irreps of the total angular momentum. In general, we have

$$2 \otimes 2 \cdots 2 \otimes 2 = (N+1) \oplus \underbrace{(N-1)}_{N-1 \text{ copies}} \oplus \cdots \tag{3.17}$$

There is a single irrep with largest angular momentum $L = N/2$, $(N-1)$ irreps with $L = N/2 - 1$, etc. However, in calculating the OTOC $F(\chi_i(t), \chi_j)$, only the irreps with $L = N/2$ and $L = N/2 - 1$ appear in the decomposition (As shown in Fig. 3.1). Now we construct the input and the output state explicitly from the SU(2) algebra.

Input State–We first notice that the operator states corresponding to the identity operator $|I \otimes I\rangle$ and the parity operator $|\mathcal{Q} \otimes \mathcal{Q}\rangle$ are the two fully polarized states in the z direction and thus belong to the unique $L = N/2$ irrep. This can be checked explicitly as

$$L_z|I \otimes I\rangle = -\frac{N}{2}|I \otimes I\rangle, \quad L_z|\mathcal{Q} \otimes \mathcal{Q}\rangle = \frac{N}{2}|\mathcal{Q} \otimes \mathcal{Q}\rangle. \tag{3.18}$$

Therefore, the parity operator state and the identity state can be regarded as the N up spin state and N down spin state, respectively. Generally, the eigenstates of the L_z operator are classified as follows :

$$L_z|\mathcal{Q}\chi_{i_1}...\mathcal{Q}\chi_{i_j} \otimes \mathcal{Q}\chi_{i_1}...\mathcal{Q}\chi_{i_j}\rangle = \left(j - \frac{N}{2}\right)|\mathcal{Q}\chi_{i_1}...\mathcal{Q}\chi_{i_j} \otimes \mathcal{Q}\chi_{i_1}...\mathcal{Q}\chi_{i_j}\rangle. \tag{3.19}$$

In the same spirit, the input state is obtained by flipping a local spin at site i from the fully polarized state $|\mathcal{Q} \otimes \mathcal{Q}\rangle$. In the picture of N 1/2-spins, the input state is

$$|\text{in}\rangle = -|\uparrow_1 ... \uparrow_{i-1}\downarrow_i\uparrow_{i+1} ... \uparrow_N\rangle\,. \tag{3.20}$$

This state splits into two irreps of the total angular momentum L as

$$\begin{aligned} |\chi_i \otimes \chi_i\rangle &= \left(\frac{1}{N}\sum_j |\chi_j \otimes \chi_j\rangle\right) + \left(|\chi_i \otimes \chi_i\rangle - \frac{1}{N}\sum_j |\chi_j \otimes \chi_j\rangle\right) \\ &= -\sqrt{\frac{1}{N}}\left|\frac{N}{2}, \frac{N}{2} - 1\right\rangle_z + \sqrt{\frac{N-1}{N}}\left|\frac{N}{2} - 1, \frac{N}{2} - 1\right\rangle_{z,i} \end{aligned} \tag{3.21}$$

in the $|l, m\rangle$ notation.

Output State–The output state is more non-trivial to interpret in the spin formalism

because it requires us to insert a complete set of operators and resolve the identity, as shown in Fig. 2.1(a)

$$|\text{out}\rangle = \frac{1}{2^N} \sum_{\mathcal{S}} |\chi_j \mathcal{S}^\dagger \chi_j \otimes \mathcal{S}\rangle \,. \tag{3.22}$$

For an intuitive understanding of expressing this state in the SU(2) language, one can start with the state corresponding to the complete set of operators and its respective spin representation

$$\frac{1}{2^N} \sum_{\mathcal{S}} |\mathcal{S}^\dagger \otimes S\rangle = \frac{1}{2^{N/2}} \prod_i (\uparrow - \downarrow)_i = |\leftarrow \cdots \leftarrow\rangle \,. \tag{3.23}$$

This is just the lowest weight state polarised along the x-direction, which is a steady state with respect to the emergent Hamiltonian because of the discrete rotational square (or cubic) symmetry. For the output state, the term in the summation gains a relative minus sign when the Majorana string $\mathcal{S}$ contains χ_j. As a result, the jth spin is flipped from $\leftarrow$ to $\rightarrow$, and we have

$$|\text{out}\rangle = -\,|\leftarrow_1 \ldots \leftarrow_{j-1} \rightarrow_j \leftarrow_{j+1} \ldots \leftarrow_N\rangle \,. \tag{3.24}$$

This output state splits into two irreps of SU(2) as well, similar to the input state, but in the x direction

$$|\text{out}\rangle = -\sqrt{\frac{1}{N}} \left| \frac{N}{2}, 1 - \frac{N}{2} \right\rangle_x + \sqrt{\frac{N-1}{N}} \left| \frac{N}{2} - 1, 1 - \frac{N}{2} \right\rangle_{x,j} . \tag{3.25}$$

3.2.5 The OTOC

The problem reduces to the time evolution of the input state followed by the computation of the overlap with the output state. Because the Hamiltonian only depends on the total angular momentum $\vec{L}$, the two irreps in the input state do not mix during the time evolution. As a result, the OTOC can be can be succinctly written as the contribution from the two irreps

$$\mathcal{F}(\chi_i, \chi_j) = \mathcal{F}_{N/2}(t) + \left(\frac{N\delta_{ij} - 1}{N - 1} \right) \mathcal{F}_{N/2-1}(t) \tag{3.26}$$

where

$$\begin{aligned}\mathcal{F}_{N/2}(t) &= \frac{2^{N/2}}{N}\,{}_x\langle l, 1-l|e^{\mathbb{H}t}|l, l-1\rangle_z \\ \mathcal{F}_{N/2-1}(t) &= 2^{N/2}\left(\frac{N-1}{N}\right){}_x\langle l-1, 1-l|e^{\mathbb{H}t}|l-1, l-1\rangle_z\end{aligned} \tag{3.27}$$

and $2l = N$. Therefore the operator dynamics have been exactly mapped to the imaginary time dynamics of SU(2) spins with angular momenta $L = N/2, N/2-1$.

3.2.5.1 Analytical results for the non-interacting model ($q_{syk} = 2$)

We first discuss the non-interacting case, i.e. $q_{\text{syk}} = 2$ in Eq. (3.5). This special case is manifest in the effective Hamiltonian $\mathbb{H}$, since it only depends on the total angular momentum L^2 and the SU(2) algebra is promoted to an exact symmetry. Recall that the effective Hamiltonian for $q_{\text{syk}} = 2$ takes the form

$$\mathbb{H}_{q_{\text{syk}}=2} = \frac{1}{2N}\left(-2\begin{pmatrix} N \\ 2 \end{pmatrix} - 3N + 4L^2\right).$$

Where $L^2 = L_x^2 + L_y^2 + L_z^2$ is the total angular momentum squared, which is the Casimir of the SU(2) group, and hence the Super-Hamiltonian becomes a constant within a given irrep. For the irreps relevant to the computation of the OTOC,

$$\mathbb{H}_{l,q_{\text{syk}}=2} = 0; \quad \mathbb{H}_{l-1,q_{\text{syk}}=2} = -2. \tag{3.28}$$

Hence the OTOC for $q_{\text{syk}} = 2$ becomes:

$$\mathcal{F}_{q_{\text{syk}}=2}(\chi_i(t), \chi_j) = \left(-1 + \frac{2}{N}\right) + 2\left(\frac{N\delta_{ij} - 1}{N}\right)e^{-2t}. \tag{3.29}$$

It exponentially decays to the late-time value $(-1 + 2/N)$, which is nonzero and in contrast with the expectation from scrambling (Eq. (3.4)), because the model for $q_{\text{syk}} = 2$ is not interacting.

3.2.5.2 Scrambling dynamics for $q_{syk} = 4$

For $q_{\rm syk} > 2$, the model becomes interacting and the effective $\mathbb{H}$ is not only a function of the total angular momentum L^2 but depends on L_x, L_y and L_z. An example (for $q_{\rm syk} = 4$) is shown in Eq. (3.14). Therefore, to obtain the OTOC one needs to diagonalize $\mathbb{H}$ for the two irreps $L = N/2$ and $L = N/2 - 1$. The Hilbert space dimension scales linearly with N, permitting calculation from small to large but finite N.

In Fig. 3.2(a) we plot the overall OTOC for the cases $i = j$ and $i \neq j$, for $N = 10000$, which agrees with the results in [30] up to an overall time scale due to the different convention of J used in this work. The results for smaller N are also benchmarked with exact diagonalization on the original model in Eq. (3.5), averaged over 200 noise realizations in the appendix. This demonstrates the validity of our method. The two curves start with different values and both relax to the late time value 0, in contrast with $q_{\rm syk} = 2$ and agreeing with the general expectation for scrambling dynamics. The difference between $i = j$ and $i \neq j$ drastically decreases as time increases, the latter characterized by the Lyapunov growth in the early time.

From Eq. (3.26), the difference between $i = j$ and $i \neq j$ is proportional to $\mathcal{F}_{N/2-1}$, the contribution from the smaller irrep. In this irrep, one can show that the initial state $|l-1, l-1\rangle_z$ displays an exponential decay, as shown in Fig. 3.2(b), which also fits the ansatz $\mathcal{F}_{N/2-1}(\chi(t), \chi) \simeq 2\,(1 - 1/N)\, e^{-2t}$. As a result, the difference in $\mathcal{F}(\chi_i(t), \chi_j)$ between $i = j$ and $i \neq j$ vanishes at a short time scale. On the other hand, the scrambling dynamics is contained in $\mathcal{F}_{N/2}(t)$, the contribution from the largest irrep which corresponds to the angular momentum $L = N/2$. This irrep shows early time Lyapunov growth and late time exponential decay and follows the ansatz

$$\mathcal{F}_{N/2}(t) \sim \begin{cases} -1 + \frac{2}{N} e^{4t} & t \ll \frac{1}{4} \ln N \\ e^{-2t} & t \gg \frac{1}{4} \ln N \end{cases} \tag{3.30}$$

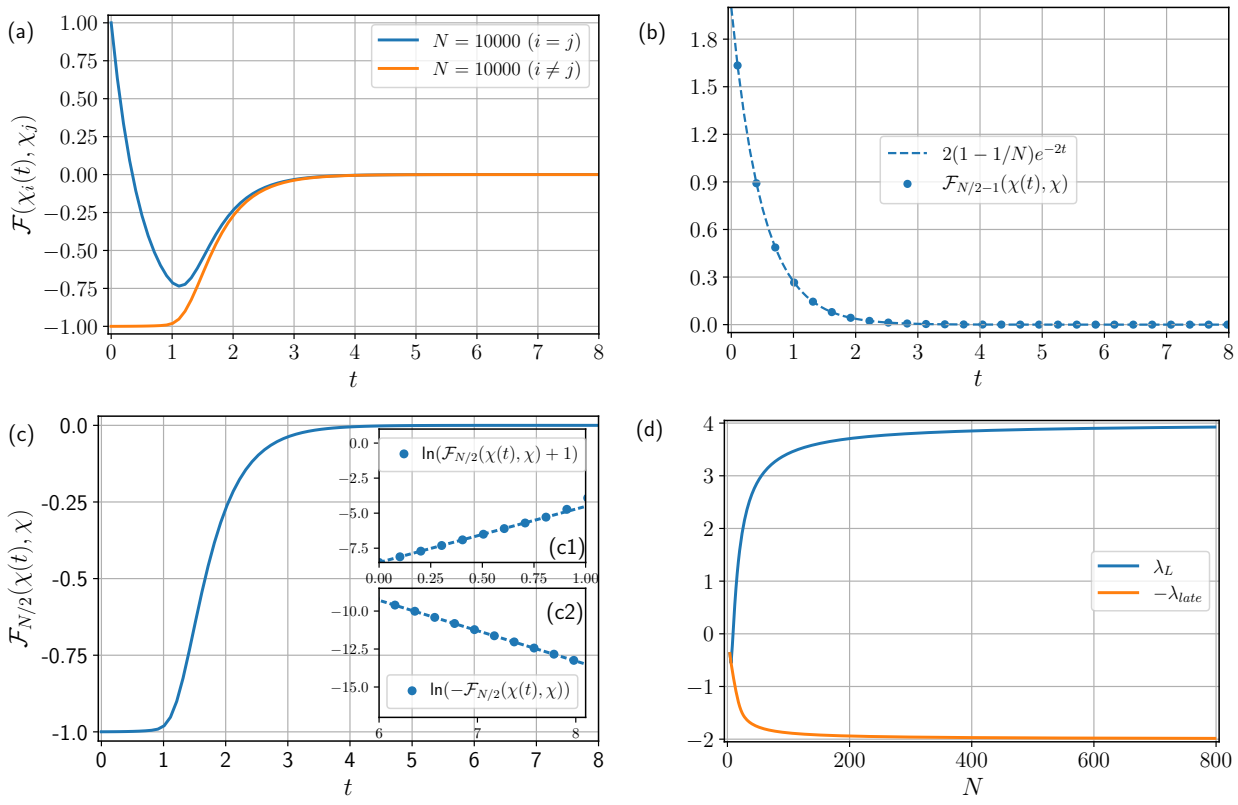

Figure 3.2: (a) The OTOC $\mathcal{F}(\chi_i(t), \chi_j)$ for $i = j$ and $i \neq j$, computed according to Eq. (3.26), for $N = 10000$ fermions. (b) The contribution to the OTOC from the irrep $L = N/2 - 1$ exponentially decays with time. The curve is fitted against e^{-2t}. (c) The contribution to the OTOC from the irrep $L = N/2$, vs time for $N = 10000$ fermions, displaying scrambling behavior. The insets (c1) and (c2) show exponential Lyapunov growth in the early time regime and exponential decay in the late time regime, fitted against the lines $4t - \ln(N)$ and $-2t + \ln(15)$ respectively. Thus the curve follows the ansatz in Eq. (3.30). (d) The plot of λ_L and $-\lambda_{late}$ as a function of N.

As discussed in Eq. (3.27),

$$\mathcal{F}_{N/2}(t) = \frac{2^{N/2}}{N}\langle N/2, 1-N/2|e^{\mathbb{H}t}|N/2, N/2-1\rangle$$

where $\mathbb{H}$ given in Eq. (3.14) is a negative $N+1$ dimensional Hermitian matrix with all eigenvalues smaller or equal to 0. As a result, $\mathcal{F}_{N/2}(t)$ in general is a sum of $N+1$ exponentially decaying terms. Therefore, it is natural to expect that $\mathcal{F}_{N/2}(t)$ decays exponentially in the late time, where the exponents are given by the largest nonzero eigenvalue of $\mathbb{H}$. On the other hand, the early-time Lyapunov exponential growth emerges from the interplay of sufficiently many exponentially decaying terms. For example, when $N=4$, $\mathbb{H}$ only has five eigenvalues, including four zeros modes ($\mathbb{H}$ is identically zero for $N=2, q_{\text{syk}}=4$). As a result, $F_{N/2}(t)$ would display an exponential decay for all time scales, instead of exponential growth at early time. Therefore, the Lyapunov growth only occurs for sufficiently large N, the time scale for which increases logarithmically with N.

To investigate how the early time behavior changes from the exponential decay to exponential growth as N increases, we use a more general ansatz $\mathcal{F}_{N/2}(t\sim 0) \sim a + be^{\lambda_L t}$ for the early time regime of $\mathcal{F}_{N/2}$, and study how λ_L change as N increases. By Taylor expanding the ansatz and the definition of $\mathcal{F}_{N/2}$ in Eq. (3.27) and comparing coefficients, we get

$$\lambda_L = \frac{{}_x\langle l, 1-l|\mathbb{H}^2|l, l-1\rangle_z}{{}_x\langle l, 1-l|\mathbb{H}|l, l-1\rangle_z}. \tag{3.31}$$

This is a more accurate approach to extract λ_L than curve fitting, especially for relatively small N where the Lyapunov growth can be short-lived.

We plot the λ_L obtained using this approach as a function N in Fig. 3.2(d), and we also include the largest non-zero eigenvalue λ_{late} that controls the late time relaxation for comparison ($\mathcal{F}_{N/2}(t\to\infty) \sim ce^{-\lambda_{late}t}$). At $N=4$, because there is only decaying mode from $\mathbb{H}$, both λ_L and $-\lambda_{late}$ start with the same value. As N increases, λ_L also increases, changes sign at $N=10$ and asymptotes to 4, while λ_{late} increases and asymptotes to 2.

To understand why $\lambda_L = 2\lambda_{late}$ in the large N limit and provide an analytical understanding of $\mathcal{F}_{N/2}(t)$'s behavior for all time scales, in the next subsection, we will derive $\mathcal{F}_{N/2}(t)$ directly in the infinite N limit (It should be noted that the ratio of λ_L/λ_{late} is a function of q_{syk} and the behavior for general q_{syk} is provided in the appendix. The results obtained there agree with the analysis in [66]). In particular, we will see precisely how the early time Lyapunov growth emerges from many exponentially decaying modes.

3.2.6 Hydrodynamic equation for the Brownian SYK model

We focus on the sector given by $L = N/2$, which contains the scrambling behavior. In this sector, the OTOC is

$$\mathcal{F}_{N/2}(t) = 2^{N/2} \langle \text{out}|\text{in}(t)\rangle = \sum_m \psi_{\text{out}}(m)\psi_{\text{in}}(m,t) \tag{3.32}$$

where

$$\psi_{\text{out}}(m) = -\frac{2m}{N}\binom{N}{N/2-m}^{1/2}. \tag{3.33}$$

The coefficient of the input state satisfies the imaginary time Schrodinger equation

$$\partial_t \psi_{\text{in}}(m,t) = \sum_{m'} \mathbb{H}_{m,m'}\psi_{\text{in}}(m',t). \tag{3.34}$$

To proceed to derive $\mathcal{F}$ in the large N limit, we exploit a similarity transformation to remove the non-uniform N dependence of $\psi_{\text{out}}(m)$ such that,

$$\psi_{\text{out}}(m) \to \tilde{\psi}_{\text{out}}(m) = -\frac{2m}{N}. \tag{3.35}$$

The OTOC therefore becomes $\mathcal{F}_{N/2}(t) = -2/N \sum_m m\tilde{\psi}_{\text{in}}(m,t)$. After the similarity transformation, the ladder operator takes the following simple form

$$(\tilde{L}_+)_{m+1,m} = \frac{N}{2} - m, \quad (\tilde{L}_-)_{m-1,m} = \frac{N}{2} + m \tag{3.36}$$

while $\tilde{L}_z$ is the same as L_z. From these angular momentum operators, The transformed effective Hamiltonian $\tilde{\mathbb{H}}$ can be constructed from Eq. (3.14) and becomes non-hermitian.

The transformed input state now obeys,

$$\partial_t \tilde{\psi}_{\text{in}}(m,t) = \sum_{m'} \tilde{\mathbb{H}}_{mm'} \tilde{\psi}_{\text{in}}(m',t). \tag{3.37}$$

Remarkably, $\tilde{\mathbb{H}}$ satisfies the property that $\sum_m \tilde{\mathbb{H}}_{mm'} = 0$. This is because one of the eigenstates of $\mathbb{H}$, the fully polarized state in the x direction becomes uniform after the transformation, and is a left eigenvector of $\tilde{\mathbb{H}}$. As a result, Eq. (3.37) is a master equation and $\tilde{\psi}_{\text{in}}(m,t)$ has the interpretation of a probability because $\sum_m \tilde{\psi}_{\text{in}}(m,t)$ is conserved for all time.

Following this, we take the large N limit of the master equation by using the continuous variable $\xi = 2m/N$. To the leading order of $1/N$, the master equation becomes

$$\partial_t \tilde{\psi}_{\text{in}}(\xi,t) = -2\partial_\xi \left(\xi(\xi^2-1)\tilde{\psi}_{\text{in}}(\xi,t) \right) \tag{3.38}$$

which can be solved analytically. In particular, if $\tilde{\psi}_{\text{in}}$ starts with a Delta distribution , it remains a Delta distribution $\tilde{\psi}_{\text{in}}(\xi,t) = \delta(\xi - \xi(t))$ for all time. As a result, $\mathcal{F}_{N/2}(t) = -\xi(t)$. The peak value $\xi(t)$ obeys a logistic differential equation

$$\xi'(t) = 2\xi(t)\big(\xi^2(t) - 1\big). \tag{3.39}$$

There are 3 static solutions; $\xi = \pm 1$ are the unstable solutions corresponding to the states $|I \otimes I\rangle$ and $|\mathcal{Q} \otimes \mathcal{Q}\rangle$, while $\xi = 0$ is the stable solution corresponding to complete scrambling. When $\xi(0) = 1 - 2\delta$, i.e., slightly deviates away from the unstable solution, we obtain the OTOC $\mathcal{F}$ as

$$\mathcal{F}_{N/2}(t) = -\xi(t) = -\frac{1}{\sqrt{1 + 4e^{4t}\delta}}. \tag{3.40}$$

It demonstrates the characteristic early-time Lyapunov exponential growth and late-time

exponential relaxation,

$$\mathcal{F}_{N/2}(t) \sim \begin{cases} -1 + 2e^{4t}\delta & t \ll -\frac{1}{4}\ln\delta \\ e^{-2t} & t \gg -\frac{1}{4}\ln\delta \end{cases} \tag{3.41}$$

Which is in agreement with the numerical results in Sec. 3.2.4 and [30]. With the analytical expression in hand, one can expand $\mathcal{F}_{N/2}(t)$ as

$$\mathcal{F}_{N/2}(t) = \sum_{n=0}^{\infty} \frac{(-1)^n (2n)!}{2^{4n+1}(n!)^2 \delta^{n+1/2}} \exp\left(-2(2n+1)t\right). \tag{3.42}$$

This demonstrates the emergence of the Lyapunov growth from many decaying modes with alternating sign.

Several remarks are in order. First, $\tilde{\psi}_{\text{in}}(\xi, t)$ remains a Delta probability distribution over time only in the infinite N limit. One can include the $1/N$ term in Eq. (3.38) when expanding the master equation and will obtain a Fokker-Planck equation. The $1/N$ term would broaden the distribution, which is a result of quantum fluctuations. Such terms can lead to observable effects, such as wavefront broadening in higher dimensions [50, 51, 31]. Second, the analytical form of $\mathcal{F}$ in Eq. (3.40) does not have to precisely match the numerics in Sec. 3.2.4. This is because in the numerics, we always use the simplest initial operator state corresponding to $\delta = 1/N$ while the analytical form is valid when δ is kept a constant as one approaches the infinite N limit. Finally, the master equation we obtained in Eq. (3.37) precisely matches that obtained by solving the model using the stochastic method [32]. Thus our approach, by taking advantage of the emergent symmetry structure after the random disorder average, reveals that the stochastic approach and the Hamiltonian approach used to solve the model are simply connected by a similarity transformation. The logistic equation we obtain in Eq. (3.39) is slightly different from that obtained in the spin Brownian model [31, 33], where there are only two steady solutions because of the absence of the fermionic parity operator. In the spin Brownian model, λ_L and λ_{late} are the same. In the Majorana case, the relation

between λ_L and λ_{late} depends on q_{syk}, as discussed in the appendix.

Our approach, exactly mapping the operator dynamics to the imaginary-time dynamics of a spin, is readily generalized to the complex Brownian SYK model with charge conservation, which we will present next.

3.3 The case with U(1) symmetry : complex Brownian SYK model

Now we move on to the primary goal of the program, which is to understand quantum information dynamics in charged models. There have been many fruitful discussions on the interplay between scrambling dynamics, conserved quantities such as energy [41, 46, 47, 67, 68, 69, 70, 71, 72, 73, 74, 75], charge [76, 77, 78, 79, 80, 81, 82, 83], dipole [84, 85, 86] and other symmetries [29, 87]. It has been shown that the presence of conserved quantities bounds the operator growth [41, 82] and also slows down the relaxation of OTOC in higher dimensions when the conserved quantities display diffusive transport [77, 78, 75]. From the opposite perspective, operator growth can also influence transport properties [88, 46, 70]. In systems with conserved quantities, the operator dynamics contain contributions from different sectors of the Hilbert space, each labelled by the corresponding value of the conserved charge. A natural curiosity therefore arises, concerning the relation between scrambling dynamics and the density of the conserved quantities. In all-to-all interacting models, most studies related to this question focus on the early time behavior of $\mathcal{F}$ characterized by the Lyapunov exponent. In the SYK model, it is found that the Lyapunov exponent $\lambda_L = 2\pi T$ at low energy [35, 38], saturating the conjectured chaos bound [41]. More recently, the bound on λ_L from the charge density ρ has also been computed, showing λ_L vanishes algebraically at low density [82]. These results are consistent with the intuition that scrambling should slow down at low density of conserved quantities because of the restricted Hilbert space. However, most calculations of the Lyapunov exponent are in the large N limit or at small N up to ~ 60 in the Majorana case [89]. Furthermore, precise results concerning the OTOC beyond the early time exponential regime are difficult to obtain, even in the large N limit. Therefore, to further understand the interplay between conserved quantities and scrambling,

exact large but finite N calculations of the OTOC at a given energy or charge are required.

Although the Brownian model does not conserve energy because of the time-dependent couplings, one can design such a model to conserve charge. These properties make such models appealing for understanding the interplay between conserved quantities and scrambling. One of the simplest Brownian models that conserves charge is the complex Brownian SYK model. However, the technique used to solve Brownian models previously does not directly apply to this case, because of the charge conservation. So far, only the charge dependence of the Lyapunov exponent is available in the large N limit based on a standard field theory calculation [82].

In the case of the complex Brownian SYK model, which is the primary focus of this work, our approach maps the operator dynamics to an SU(4) spin with conserved weights and the particular irrep is related to N. The largest Hilbert space dimension required to compute the OTOC scales linearly with N, drastically reduced from the original Hilbert space that scales exponentially with N. This allows for numerical computation of the OTOC for large but finite N and also makes the derivation of the OTOC possible for all times in the large N limit. We emphasize that the original Brownian SYK model does not have the specified symmetry structure, which only appears after taking the random average. This work is also related to recent studies on the emergent discrete symmetry resulting from the disorder average over replicas in random circuit models [50, 90, 91, 92, 29, 93, 94] and large N field theory calculations of the static SYK model [95, 96]. These discrete symmetries can be intuitively understood as the interplay between permutation among replicas and the physical symmetries of the model. This work demonstrates that the effective model emerging from the Brownian SYK model at any N is not only invariant under these discrete symmetries, but is closed within a larger continuous symmetry group, SU(2) in the case without charge conservation, or SU(4) with charge conservation, for which the discrete symmetry group is a subgroup. Furthermore, when the model is non-interacting, i.e., quadratic in the fermionic operators, it is invariant under the continuous symmetry group [97, 98].

We will next discuss operator dynamics in the context of complex fermions, where we define a suitable operator basis which respects the U(1) symmetry. We also use this knowledge to compute the OTOC analytically for different correlators, which will be verified numerically for the complex Brownian SYK model.

3.3.1 Operator dynamics of complex fermions

In this section, we discuss the operator dynamics of complex fermions in systems with charge conservation. In general, we consider a system of N fermions, and a Hamiltonian that is a function of the creation and annihilation operators $\chi_i^\dagger$ and χ_i, where the subscript i goes from 1 to N. These operators obey the standard anti-commutation relation $\{\chi_i^\dagger, \chi_j\} = \delta_{ij}$. We define the operator $n_i = \chi_i^\dagger \chi_i$, which measures the local charge. We also define $\bar{n}_i = I - n_i$ for later convenience. The Hamiltonian conserves the total charge, meaning that $[H, \sum_i n_i] = 0$. As a result, given an initial state with a fixed charge, its dynamics is always restricted to the corresponding charge-sector of the Hamiltonian.

One can also define the conserved charge for an operator in such systems. Unlike the state, the operator has two conserved quantities, resulting from measuring the total charge on the left or on the right. An eigen-operator W of two U(1) symmetries is defined as

$$\left(\sum_i n_i\right) W = m_a W, \quad W \left(\sum_i n_i\right) = m_b W. \tag{3.43}$$

In general, m_a and m_b are independent and the tuple (m_a, m_b) is labelled as the charge-profile of the operator. Because the Hamiltonian conserves the total charge $\sum n_i$, the Heisenberg operator $W(t)$ remains an eigen-operator with the same conserved quantities m_a and m_b. The appropriate local eigen-operators have the charge profile :

$$\chi^\dagger : (1,0) \quad \chi : (0,1) \quad n : (1,1) \quad \bar{n} : (0,0). \tag{3.44}$$

Note that the identity operator is not an eigen-operator of the two U(1) symmetries.

Using the operators in Eq. (3.44), one can construct a complete operator basis for N fermions that fully respects the two U(1) symmetries of the operator dynamics

$$\mathcal{S} = 2^{N/2} s_1 s_2 \cdots s_N, \quad s_i \in \{\chi^\dagger, \chi, n, \bar{n}\}. \tag{3.45}$$

One can also show that $m_a(\mathcal{S})$ counts the number of $\chi^\dagger$ plus the number of n in the string, while $m_b(\mathcal{S})$ counts the number of χ plus n. Under unitary time evolution driven by the charge-conserving Hamiltonian, the only permissible building block for the dynamics of the operator-states of the form $\mathcal{S}$ is the move

$$\bar{n}n \longleftrightarrow \chi^\dagger \chi \tag{3.46}$$

which preserves the charge-profile. Following this, one can immediately detect the set of operators that may have time-dependence but display no operator spreading, i.e. $W(t) = e^{ict} W$ where c is a real constant. For example, it is evident that the operators of the form $\prod_{i=1}^{N} \chi_i^\dagger$ and $\prod_{i=1}^{N} \chi_i$ are the unique operators with the charge profiles $(N, 0)$ and $(0, N)$ respectively, therefore they simply gain a phase under the dynamics. The identity operator is more special because it always commutes with the unitary and therefore does not have dynamics. We can further expand I in the basis $\mathcal{S}$ as

$$\begin{aligned} I &= \prod_{i=1}^{N} (n_i + \bar{n}_i) = \sum_{m=0}^{N} I_{m,N} \\ I_{m,N} &= \sum_{i_1 < \ldots < i_m} n_{i_1} \ldots n_{i_m} \bar{n}_{i_{m+1}} \ldots \bar{n}_{i_{N-m}}. \end{aligned} \tag{3.47}$$

Here the operator $I_{m,N}$ is a component of the identity over N fermions in the U(1) basis, with the charge profile (m, m). Since the identity does not have time dependence, each component with a different m is also static under the charge-conserving dynamics.

We can determine the dynamics of a local operator $W_i I$ after expanding the identity over

$N-1$ fermions in the basis $\mathcal{S}$

$$W_i I = W_i \prod_{j\neq i}(n_j + \bar{n}_j) = \sum_{m=0}^{N-1} W_i I_{m,N-1}. \tag{3.48}$$

Each component $I_{m,N-1}$ has profile (m, m). Thus it is apparent that when a local operator chosen from the set $\{\chi_i^\dagger, \chi_i, n_i, \bar{n}_i\}$ is expanded in such a basis, each operator-string in the sum has a fixed charge profile (m_a, m_b), where $m_a - m_b$ is invariant across all the components and takes the values $\{1, -1, 0, 0\}$ corresponding to the choice of operator from the set respectively. Once the expansion is obtained, the dynamics, in the form of the charge conserving move, take place independently within each charge sector (labelled by m).

Given an initially simple operator W_i, one way to track its complexity under Heisenberg time evolution is using the OTOC

$$\mathcal{F}(W_i(t), V_j) = \frac{1}{2^N}\mathrm{Tr}\left(W_i^\dagger(t)V_j^\dagger W_i(t)V_j\right) \tag{3.49}$$

where V_j is a local probing operator. Since $W_i(t)$ is a local operator, it does not respect the two U(1) symmetries and has the expansion shown in Eq. (3.48). Therefore the OTOC $\mathcal{F}$ contains contributions from different charge sectors,

$$\begin{aligned}\mathcal{F}(W_i(t), V_j) =& \sum_m \frac{\mathrm{Tr}(P_m)}{2^N}\mathcal{F}^m(W_i(t), V_j)\\ \mathcal{F}^m(W_i(t), V_j) =& \frac{1}{\mathrm{Tr}(P_m)}\mathrm{Tr}(P_m W_i^\dagger(t)V_j^\dagger W_i(t)V_j)\end{aligned} \tag{3.50}$$

where $P_m = \sum_m |\psi_m\rangle \langle\psi_m|$ is the projection operator for the subspace of the Hamiltonian with charge m and dimension $\binom{N}{m}$. We denote $\mathcal{F}^m$ as the charge-resolved OTOC, contributing to the overall $\mathcal{F}$ based on the binomial distribution. To illustrate this, let us consider $\mathcal{F}(\chi_i(t), \chi_j^\dagger)$ where one can start with χ_i and use $\chi_j^\dagger$ to probe its growth. In $\mathcal{F}^m(\chi_i(t), \chi_j^\dagger)$ given by

$$\mathcal{F}^m(\chi_i(t), \chi_j^\dagger) = \frac{1}{\mathrm{Tr}(P_m)}\mathrm{Tr}(P_m \chi_i^\dagger(t)\chi_j\chi_i(t)\chi_j^\dagger). \tag{3.51}$$

The charge profiles of the operator $\chi_i^\dagger(t)$ (notice the dagger) and $\chi_i(t)$ are fixed to be $(m, m-1)$ and $(m, m+1)$ respectively for all time as a result of the charge conserving dynamics. Therefore, $\mathcal{F}^m(\chi_i(t), \chi_j^\dagger)$ probes the correlation between the components of the operator $\chi_i^\dagger(t)$ in two different charge sectors $(m, m-1)$ and $(m+1, m)$. It is generally true that $\mathcal{F}^m(W_i(t), \chi_j)$ probes the correlation between different charge sectors of W_i. To probe the operator growth within a charge sector, one can also use n_j instead as the probing operator and study the charge resolved OTOC $\mathcal{F}^m(W_i(t), n_j)$. For example, in $\mathcal{F}^m(\chi_i(t), n_j)$ the charge profiles of $\chi_i^\dagger(t)$ and $\chi_i(t)$ are fixed to be $(m, m-1)$ and $(m-1, m)$. Therefore, $\mathcal{F}^m(\chi_i(t), n_j)$ probes the operator dynamics of $\chi_i(t)$ within one charge sector $(m-1, m)$. Using combinatorics and the assumptions that the Heisenberg operator $W(t)$ becomes as complicated as possible at late times, we obtain the initial and late-time values of the charge resolved OTOC $\mathcal{F}^m(\chi_i(t), \chi_j^\dagger)$ and $\mathcal{F}^m(\chi_i(t), n_j)$, which are summarized in Table 3.1.

We also consider the Heisenberg dynamics of the operator $n_i(t)$. The operator growth can be probed by the charge resolved OTOC $\mathcal{F}^m(n_i(t), \chi_j^\dagger)$ and $\mathcal{F}^m(n_i(t), n_j)$. When the local probing operator is $\chi_j^\dagger$, $\mathcal{F}^m$ probes the correlation between the charge sectors (m, m) and $(m+1, m+1)$ of n_i. When the local probing operator is n_j, $\mathcal{F}^m$ probes the operator growth of n_i within the charge sector (m, m). In the case of the OTOCs $\mathcal{F}^m(n_i(t), \chi_j^\dagger)$ and $\mathcal{F}^m(n_i(t), n_j)$, the late-time values are more nontrivial to compute than when the initial operator is chosen to be $\chi_i(t)$, because $n_i(t)$ is not traceless. Within each charge sector, we have $\mathrm{Tr}(P_m n(t))/\mathrm{Tr}(P_m) = m/N$, and this will put constraints on the coefficients of the operators present in the component of the identity in the charge sector (i.e., all the different operators that make up $I_{m,N}$ in Eq. (3.47)). These constraints will in turn lead to non-uniform operator spreading. To remedy this, one can investigate the OTOC through the operator-spreading of a modified operator $n(t) - \Delta_m I$ within each charge sector, which is related to the OTOC of $n(t)$ in a simple way. The constant Δ_m can be chosen to precisely guarantee uniform operator spreading at late times, through the equation $\mathrm{Tr}(P_m(n_i - \Delta_m I)) = \sqrt{(m/N)(1 - 2\Delta_m + \Delta_m^2 N/m)}$. The initial and late-time

values for $\mathcal{F}^m(n_i(t), \chi_j^\dagger)$ and $\mathcal{F}^m(n_i(t), n_j)$ are also listed in Table 3.1, and one can use them to compute the late time values of the overall OTOCs $\mathcal{F}$ from the weighted average $\mathcal{F} = \sum_m \mathrm{Tr}(P_m)\mathcal{F}^m/\mathrm{Tr}(I)$

$$\begin{aligned}
&\mathcal{F}(\chi_i(t \to \infty), \chi_j^\dagger) = 0 \\
&\mathcal{F}(\chi_i(t \to \infty), n_j) = \frac{(N-1)(N+2)}{8N^2} \overset{N\to\infty}{=} \frac{1}{8} \\
&\mathcal{F}(n_i(t \to \infty), \chi_j^\dagger) = \frac{(N-1)(N+2)}{8N^2} \overset{N\to\infty}{=} \frac{1}{8}
\end{aligned} \tag{3.52}$$

For the OTOC $\mathcal{F}(n_i(t), n_j)$, it is difficult to obtain a closed form expression for the overall OTOC. However, from the charge-resolved value, one can compute the large-N expansion and find that the leading order piece at late times is $\mathcal{F}(n_i(t \to \infty), n_j) \overset{N\to\infty}{=} 3/16$. This OTOC will also have finite sized effects in its late time value, similar to both the other OTOCs computed where one of the operators is chosen to be n. In Sec. 3.3.6, we verify these late-time values in the case of the complex Brownian SYK model (The values for the charge-resolved case are verified in the appendix). Furthermore, we also provide an exact formalism to track the time evolution of various OTOCs from the initial value to the late-time value in different charge sectors.

Using the result in Table. 3.1, one can also compute the late-time value of the overall OTOC between traceless operators by summing over the contribution from each charge sector and compare the result without charge conservation. For example, we can consider the overall OTOC between χ_i and $n_j - I/2$. Importantly, within each symmetry sector, the operator $n_j - I/2$ is not traceless, and the charge resolved OTOC approaches a finite value that depends on m. Summing over contributions from each charge sector leads to a late-time value $(N-2)/8N^2$, scaling as $\sim 1/N$ in sharp contrast with $1/\exp(\alpha N)$ that is found in systems without symmetry [65]. The $1/N$ corrections to the late-time value are present for all pairs of operators in Table. 3.1, except $\mathcal{F}(\chi_i(t), \chi_j^\dagger)$ because the operators involved are traceless in each charge sector. Related to this, the $1/\mathrm{poly}(N)$ correction to the late-time

W_i	V_j	$\mathcal{F}^m(W_i(t=0),V_j)$	$\mathcal{F}^m(W_i(t\to\infty),V_j)$
χ_i	$\chi_j^\dagger$	$(1-\delta_{ij})\frac{m(m-N)}{N(N-1)}$	0
χ_i	n_j	$(1-\delta_{ij})\frac{m(m-1)}{N(N-1)}$	$\frac{m^2(m-1)}{N^3}$
n_i	$\chi_j^\dagger$	$(1-\delta_{ij})\frac{m(m-N)}{N(N-1)}$	$\frac{m(m+1)(N-m)}{N^3}$
n_i	n_j	$\frac{m(m(1-\delta_{ij})-1)}{N(N(1-\delta_{ij})-1)}$	$\frac{m^3}{N^3}+(\frac{m}{N}-(\frac{m}{N})^2)\left(\frac{\binom{N-1}{m-1}^2-m/N}{\binom{N}{m}^2-1}\right)$

Table 3.1: The early and late time value of the charge resolved OTOC in Eq. (3.50) for each charge sector labelled by m and for different choices of the operators W and V.

value of the OTOC is found in energy conserving systems as well [73].

We also note that some subtlety arises for the late value of $\mathcal{F}^m(W_i(t),V_j)$ when the Hamiltonian is q_{syk}-uniform and only contains terms of the form $\chi^\dagger_{i_1}\cdots\chi^\dagger_{i_{q_{\text{syk}}/2}}\chi_{j_1}\cdots\chi_{j_{q_{\text{syk}}/2}}$. In this case, some operators in sectors of dilute charge ($m\sim\mathcal{O}(1)$) have restricted dynamics owing to the symmetries of the q_{syk}-uniform Hamiltonian, and the late time value of the OTOC can be different for the cases $i=j$ and $i\neq j$, due to imperfect scrambling.

3.3.2 Defining the complex Brownian SYK model

We start with the Brownian version of the complex SYK model [36] with N complex fermionic pairs $(\chi,\chi^\dagger)$ and ($q_{\text{syk}}=4$)-body interactions with complex time-dependent couplings J

$$H(t)=\sum_{j_1,j_2,k_1,k_2}J_{j_1,j_2,k_1,k_2}(t)\chi^\dagger_{j_1}\chi^\dagger_{j_2}\chi_{k_1}\chi_{k_2}+h.c. \tag{3.53}$$

These fermions satisfy the usual anti-commutation relations

$$\{\chi_j,\chi_k\}=0\quad\left\{\chi_j^\dagger,\chi_k\right\}=\delta_{jk}. \tag{3.54}$$

The couplings J are sourced independently from a Gaussian distribution with zero mean and variance

$$\overline{J_{j_1,j_2,k_1,k_2}(t)J^*_{j_1',j_2',k_1',k_2'}(t')} = \delta^{j_1}_{j_1'}\delta^{j_2}_{j_2'}\delta^{k_1}_{k_1'}\delta^{k_2}_{k_2'}\,\delta\,(t-t')\,\frac{1}{2N^3} \tag{3.55}$$

This relation can be generalized for other q_{syk} as well, although in this work we primarily focus on $q_{\text{syk}} = 4$. In the main text, as an example, we will primarily be focusing on computing the OTOC $\mathcal{F}(\chi_i(t), \chi_j^\dagger)$ and its charge resolved version $\mathcal{F}^m(\chi_i(t), \chi_j^\dagger)$

$$\begin{aligned}\mathcal{F}(\chi_i(t), \chi_j^\dagger) =& \sum_m \frac{\text{Tr}(P_m)}{2^N}\mathcal{F}^m(\chi_i(t), \chi_j^\dagger)\\ \mathcal{F}^m(\chi_i(t), \chi_j^\dagger) =& \frac{1}{\text{Tr}(P_m)}\text{Tr}(P_m\chi_i^\dagger(t)\chi_j\chi_i(t)\chi_j^\dagger).\end{aligned} \tag{3.56}$$

We will quote the result for the other OTOCs but leave the details of the calculation in the appendix.

One can rewrite the OTOC as shown in Sec. 2.1. This gives us the idea to work with four copies of the Hilbert space, occupied by four "replica" fermions labelled by the indices (a, b, c, d). This larger Hilbert space is spanned by the basis vectors

$$\begin{aligned}\chi_j^a &:= \chi_j \otimes I \otimes I \otimes I \qquad \chi_j^b := I \otimes \chi_j^\intercal \otimes I \otimes I\\ \chi_j^c &:= I \otimes I \otimes \chi_j \otimes I \qquad \chi_j^d := I \otimes I \otimes I \otimes \chi_j^\intercal\end{aligned} \tag{3.57}$$

and their Hermitian conjugates $(\chi_j^{a\dagger}, \chi_j^{b\dagger}, \chi_j^{c\dagger}, \chi_j^{d\dagger})$. Here we use the notation $\chi_j^\intercal = \chi_j^{*\dagger}$, which implies that we have performed a particle-hole transformation on copies b, d. This is just a convention which makes things easier when defining the operators of the SU(4) algebra in the next section. The replica fermions with different indices commute with each other. This 'mixed' species of particles populating the Hilbert space is rather inconvenient to work with, and we convert them to fermions that anti-commute with each other by using the parity

operator similar to the Majorana case

$$\mathcal{Q}^\alpha = \prod_{k=1}^{N} \exp(i\pi n_k^\alpha), \quad \alpha = a, b, c, d. \tag{3.58}$$

One can check that this operator satisfies the following relations : $\{\mathcal{Q}^\alpha, \chi_k^\alpha\} = 0$, $\left\{\mathcal{Q}^\alpha, \chi_k^{\alpha\dagger}\right\} = 0$, $\left(\mathcal{Q}^\alpha\right)^2 = 1$. Following this, we define

$$\begin{aligned} \psi_j^a &= \mathcal{Q}^a \chi_j^a, & \psi_j^b &= \mathcal{Q}^a \chi_j^b \\ \psi_j^c &= \mathcal{Q}^a \mathcal{Q}^b \mathcal{Q}^c \chi_j^c, & \psi_j^d &= \mathcal{Q}^a \mathcal{Q}^b \mathcal{Q}^c \chi_j^d \end{aligned} \tag{3.59}$$

These operators are purely fermionic, i.e. they anti-commute with themselves and fermions from other replicas, satisfying : $\left\{\psi_j^{\alpha\dagger}, \psi_k^\beta\right\} = \delta_{\alpha,\beta}\delta_{j,k}$, $\left\{\psi_j^\alpha, \psi_k^\beta\right\} = 0$. One can also confirm that

$$\psi_{j_1}^{\alpha\,\dagger} \ldots \psi_{j_q}^{\alpha\,\dagger} \psi_{k_1}^\alpha \ldots \psi_{k_q}^\alpha = \chi_{j_1}^{\alpha\,\dagger} \ldots \chi_{j_q}^{\alpha\,\dagger} \chi_{k_1}^\alpha \ldots \chi_{k_q}^\alpha \tag{3.60}$$

and hence we can replace the operators in the original Hamiltonian with these new purely fermionic operators.

We can now take the disorder average of each time step in the discretized time-evoluton independently using the approach outlined in Sec. 2 and arrive at the averaged time evolution operator, as well as the effective Hamiltonian $\overline{\mathbb{U}}(t) = \exp(\mathbb{H}t)$. Although the full expression of $\mathbb{H}$ is quite complicated (which is given in the Appendix), it takes a general simple form that results from the general construction as well as the charge conservation on each replica $a \sim d$.

We introduce the bilinear operators

$$S^{\alpha\beta} = \sum_i \psi_i^{\alpha\dagger} \psi_i^\beta. \tag{3.61}$$

The total charges $\sum_i \chi_i^\dagger \chi_i$ on each replica are given by $(S^{aa}, N - S^{bb}, S^{cc}, N - S^{dd})$, which measures the charge profile of an operator state. Note the particle-hole transformation on

replicas b and d. In terms of these bilinear operators, the Hamiltonian takes the following general form:

$$\mathbb{H} = \mathbb{H}(S^{\alpha\beta}S^{\beta\alpha}, S^{\alpha\alpha}), \quad \alpha, \beta \in a, b, c, d. \tag{3.62}$$

Which results from the independent charge conservation on the four replicas. One can explicitly verify that $\mathbb{H}$ commutes with all four operators $S^{\alpha\alpha}$ in this functional form.

3.3.3 Emergence of the SU(4) $\otimes$ U(1) algebra

Now we analyze the full symmetry structure of $\mathbb{H}$. The dimension of the total Hilbert space of the effective Hamiltonian $\mathbb{H}$ is 16^N since it contains 4 copies of the original system. The dimension scales exponentially with N even with the charge conservation. In this section, we exploit the additional symmetry structure of $\mathbb{H}$ in Eq. (3.62) to further reduce the dimension.

From the bilinear operator introduced in Eq. (3.61), we define $\tilde{S}^{\alpha\beta} = S^{\alpha\beta} - \frac{1}{4}\delta^{\alpha\beta}S^{\sigma\sigma}$. The operators satisfy the commutation relations

$$[\tilde{S}^{\alpha\beta}, \tilde{S}^{\gamma\sigma}] = \delta^{\beta\gamma}\tilde{S}^{\alpha\sigma} - \delta^{\alpha\sigma}\tilde{S}^{\gamma\beta}. \tag{3.63}$$

There are 15 independent operators because $\sum_\alpha \tilde{S}^{\alpha\alpha} = 0$ and they are generators of the SU(4) algebra. Along with this, the operator $Q = \sum_\alpha S^{\alpha\alpha}$ commutes with all the operators of the SU(4) algebra and defines the U(1) charge to make the overall algebra SU(4)$\otimes$U(1).

Since the emergent Hamiltonian commutes with the four operators $S^{\alpha\alpha}$, in addition to commuting with the total charge operator, it also commutes with the three operators that form the Cartan-subalgebra of the SU(4) algebra. Each subsector of $\mathbb{H}$ can therefore be labeled by the irrep of the SU(4) algebra, the three weights in the weight diagram of the irrep, and the total U(1) charge. This fully resolves the symmetry structure of $\mathbb{H}$. It is well known that there are multiple states corresponding to the same weights in SU(n) irreps for $n > 2$. In our case, the dimensions of the irreps of the SU(4) algebra scales as $\mathcal{O}(N^4)$ and fixing the weights decreases the scaling to $\mathcal{O}(N)$. In other words, the largest dimension of

subsectors of $\mathbb{H}$ scales linearly with N, drastically reducing the computational cost.

Let us compare the structure of $\mathbb{H}$ between the Majorana case and the complex case. In the Majorana case, $\mathbb{H}$ can be written as a function of SU(2) generators, and the dimension of largest subsector scales linearly with N. Here in the complex case, $\mathbb{H}$ is a function of SU(4) generators. In addition, it commutes with the weight of the SU(4) algebra, and as a result, the largest Hilbert space dimension also scales linearly with N.

The strategy for calculating the OTOC in the complex case is similar to the Majorana case. We need to decompose the input and the output state into different subsectors of $\mathbb{H}$, let the different components of the input state evolve in the imaginary time given by $\mathbb{H}$, and then take the overlap with the different components of the output state. Thus the OTOC contains the contribution from the different irreps of SU(4) as well as different charge sectors (weights). This method therefore naturally provides us the OTOC in the charge resolved manner.

Before proceeding to discuss the decomposition of the initial and the final states into irreps of SU(4), we note that the non-interacting nature of the quadratic model ($q_{\text{syk}} = 2$) manifests itself in the effective Hamiltonian, similar to the Majorana case. A straightforward calculation reveals that the emergent Hamiltonian $\mathbb{H}_{q_{\text{syk}}=2}$ takes the following simple form,

$$\mathbb{H}_{q_{\text{syk}}=2} = \frac{1}{N}(C_2 + \frac{Q^2}{8} - 2N - \frac{QN}{2}) \tag{3.64}$$

where Q is the total charge and C_2 is the quadratic Casimir of SU(4)

$$C_2 = \frac{1}{2}\sum_{\alpha,\beta} S^{\alpha\beta}S^{\beta\alpha} - \frac{Q^2}{8}. \tag{3.65}$$

In this case, $\mathbb{H}_{q_{\text{syk}}=2}$ commutes with all $S^{\alpha\beta}$ and becomes a constant within a given irrep, i.e. the algebra structure is enhanced to an exact symmetry. These properties make it possible to solve the OTOC analytically for $q_{\text{syk}} = 2$, which will be presented in Sec. 3.3.5. Other than $q_{\text{syk}} = 2$, the emergent Hamiltonian $\mathbb{H}_{q_{\text{syk}}}$ only conserves the weights within the SU(4)

irrep. This remarkable difference between $q_{\text{syk}} = 2$ and $q_{\text{syk}} \neq 2$ leads to the distinct operator dynamics.

The full emergent Hamiltonian for $q_{\text{syk}} = 4$ is present in the appendix. The general structure of the Hamiltonian for all q_{syk} takes the form in Eq. (3.62), which manifestly preserves the charges for each of the four replicas. This is a powerful property that will be exploited to 'chop up' the input state in the OTOC into states with different weights within the SU(4) irreps so that each piece will only have dynamics within its own fixed-weight (charge) subspace.

3.3.4 Classification of states in the SU(4) algebra

The emergent Hamiltonian acts on four replicas of the original Hilbert space. In other words, the input states correspond to two copies of operators, in total 16^N independent states. In the last section, we demonstrated that the emergent Hamiltonian is closed within the irreps of the SU(4) algebra. In this section, we organize the input states and the output states into various irreps of SU(4), from which the operator dynamics and OTOC can be efficiently computed exactly using Hilbert space of size $\mathcal{O}(N)$.

3.3.4.1 $N = 1$ representation

We first consider the operators acting on the same fermionic index, i.e., $N = 1$. There are four independent operators per site, $\chi^\dagger$, χ, $n = \chi^\dagger\chi$ and $\bar{n} = \chi\chi^\dagger$. As discussed in Sec. 3.3.1, this basis fully utilizes the U(1) symmetry of the complex Brownian model. The identity operator I is $n+\bar{n}$. Combinations from the 4 operators on each copy leads to 16 independent operator states. The 16 operator states can be grouped into irreps of SU(4) in the following way,

$$\mathbf{16} = \mathbf{1} \oplus \mathbf{4} \oplus \mathbf{6} \oplus \bar{\mathbf{4}} \oplus \mathbf{1}. \tag{3.66}$$

The initial operator state of interest, $|\chi_i^\dagger I \otimes \chi_i I\rangle$, contains the operator state $\chi^\dagger \otimes \chi$ and $I \otimes I$ acting on different fermions, which belong to the six dimensional irrep $(0, 1, 0)$. In other words, the initial states are only made using states per fermion within the $(0, 1, 0)$ irrep. The

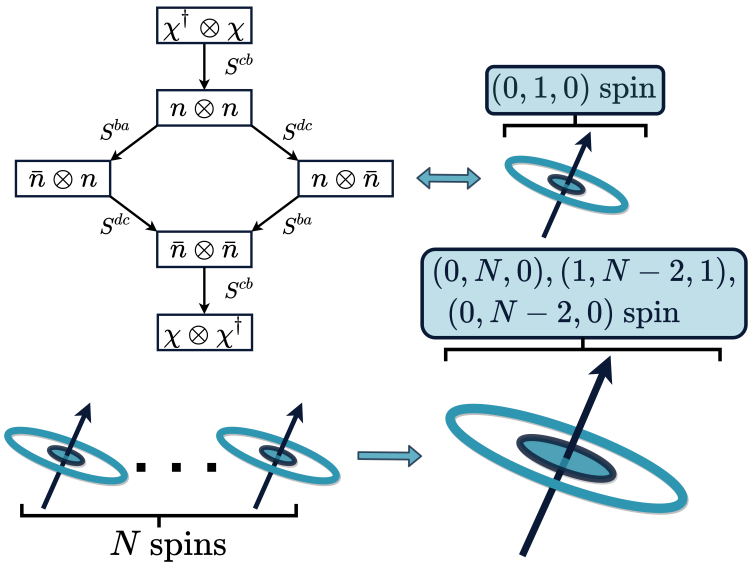

Figure 3.3: The six onsite operator-states for the complex Brownian SYK model form the SU(4) irrep $(0, 1, 0)$. Here $\bar{n} = 1 - n$ and the construction of the generators is provided in Eq. (3.61). The operator dynamics of N complex fermions with charge conservation is mapped to the imaginary time dynamics of N SU(4) spins in the $(0, 1, 0)$ irrep, which compose to form $(0, N, 0)$, $(1, N-2, 1)$ and $(0, N-2, 0)$ irreps of the global SU(4) algebra as shown in Eq. (3.68). In addition, the weights of the global SU(4) spin are also conserved because of the charge conservation. The largest Hilbert space dimension for a fixed weight sector within a given global SU(4) irrep scales linearly with N.

operator states in the $(0, 1, 0)$ irrep and their transformation under SU(4) generators are shown in Fig. 3.3. Since the emergent Hamiltonian only contains the generators of SU(4), the other single fermion irreps do not contribute to the dynamics. To this end, the operator dynamics is mapped to the dynamics of N six-dimensional SU(4) spins. This is in the same spirit with the operator dynamics of the Majorana model mapping to N spin-1/2 SU(2) spins. Crucially, unlike the Majorana case, the operator on each copy does not have to match during the dynamics, and the configuration $n \otimes \bar{n}$, for example, can be generated in the dynamics. This leads to the rich charge-dependent operator dynamics of the complex model.

3.3.4.2 Representation for general N

Taking into account the SU(4) irreps of operator states at each site reduces the Hilbert space dimension from 16^N to 6^N, a significant reduction which however is still difficult to work with. Since the Hamiltonian only depends on the SU(4) $\otimes$ U(1) generators, the dynamics must be closed within the SU(4) irreps of N total fermions. Hence the next step is to build SU(4) irreps of N fermions from N copies of the irrep $(0,1,0)$ corresponding to a single fermion, based on the composition rule of SU(4) irreps,

$$\underbrace{(0,1,0)\otimes ...\otimes (0,1,0)}_{N \text{ times}} = (0,N,0)\oplus \underbrace{(1,N-2,1)}_{N-1 \text{ copies}} \oplus ..., \tag{3.67}$$

and then decompose the initial operators into the various irreps, which evolve *independently* under the emergent Hamiltonian. The dimension of each irrep scales polynomially with N, drastically reduced from 6^N. The dimension of the Hilbert space can be further reduced to linear scaling because the emergent Hamiltonian also conserves the weight of the states within the irrep.

This is a well-defined but tedious procedure for a general initial operator state $|W^\dagger \otimes W\rangle$ since many SU(4) irreps can appear in the composition. However, for simple initial operator states of interest, this procedure is significantly simplified, and at most three irreps appear in the composition. The initial operator states we consider are local operators of the form $|W_1^\dagger I \otimes W_1 I\rangle$, made from the identity operators except for one fermion, which is located at site 1 without loss of generality. We notice that the operator state $|I\otimes I\rangle$ on the remaining $N-1$ fermions belongs to a single SU(4) irrep $(0,N-1,0)$. Therefore the composition in Eq. (3.67) is reduced to the composition of two irreps,

$$(0,1,0)\otimes(0,N-1,0) = (0,N,0)\oplus(1,N-2,1)\oplus(0,N-2,0). \tag{3.68}$$

Now we present the explicit decomposition of the initial operators into the three irreps,

which will then be used to calculate OTOC later. We will assume that N is even throughout this work for simplicity. The notation we use will assume that unless an index is specified, it is implied that the operator has support on all sites which are not populated by other operators in the given operator string, i.e.:

$$O \equiv \Pi_{i=1}^{N} O_i; \quad \tilde{O}_j O \equiv \tilde{O}_j \Pi_{i \neq j} O_i. \tag{3.69}$$

Our strategy is to build the states from the highest weight state within each of the three irreps, just like building the state from the fully polarized state using $L_\pm$ in the Majorana case. The highest weight state is defined so that it is annihilated by S^{ab}, S^{bc} and S^{cd}, using the following convention

$$\begin{aligned} |W_{(0,N,0)}\rangle &= \frac{1}{N} |\chi^\dagger \otimes \chi\rangle \\ |W_{(1,N-2,1)}\rangle &= -|n_1\chi^\dagger \otimes n_1\chi\rangle + \frac{1}{N}\sum_{i=1}^{N} |n_i\chi^\dagger \otimes n_i\chi\rangle . \end{aligned} \tag{3.70}$$

Input state – We will first demonstrate the procedure to build all the states required to compute the OTOC, using the OTOC $\mathcal{F}(\chi_i(t), \chi_j^\dagger)$ as an example. We start with the operator state $|\chi_1^\dagger I \otimes \chi_1 I\rangle$, which corresponds to the input state in the OTOC. Using the $\mathrm{SU}(2) \otimes \mathrm{SU}(2)$ sub-algebra of SU(4) generated by S^{ba} and S^{dc}, one can show that,

$$|\chi_1^\dagger I \otimes \chi_1 I\rangle = \sum_{k,l=0}^{N-1} (-1)^{k+l} \frac{(S^{ba})^k}{k!} \frac{(S^{dc})^l}{l!} |\chi_1^\dagger n \otimes \chi_1 n\rangle . \tag{3.71}$$

Each term in the summation has the fixed charge profile $(N-k, N-1-k, N-1-l, N-l)$. The operator state $|\chi_1^\dagger n \otimes \chi_1 n\rangle$ can be built from the highest weight states using the operator S^{cb} from the following simple relation:

$$|\chi_1^\dagger n \otimes \chi_1 n\rangle = (-1)^{N/2+1} \left(\frac{(S^{cb})^{N-1}}{(N-1)!} |W_{(0,N,0)}\rangle + \frac{(S^{cb})^{N-2}}{(N-2)!} |W_{(1,N-2,1)}\rangle \right). \tag{3.72}$$

Thus the initial operator state $|\chi_1^\dagger I \otimes \chi_1 I\rangle$ is completely decomposed into the two irreps and built from the highest weight states. This state does not have a component in the $(0, N-2, 0)$ irrep. Each term in the summation can therefore be restricted to one irrep and has fixed charges, thus evolving independently under the emergent Hamiltonian. The dimension of each subspace is given in Eq. (A.23), which scales linearly with N. The other initial state of interest $|n_1 I \otimes n_1 I\rangle$ can be built from the highest weight state in a similar fashion, but has components in all three irreps. The details can be found in the appendix.

Output state – Now we discuss building the output state using SU(4) irreps. Similar to the case of the Majorana model, building the output state requires inserting the resolution of the identity operator to ensure a proper overlap with the input state. We again consider the operator state $|\chi_1^\dagger I \otimes \chi_1 I\rangle$. After inserting the resolution of the identity, the state becomes

$$\frac{1}{4^N}\sum_{\mathcal{S}} |\chi_1 \mathcal{S}^\dagger \chi_1^\dagger \otimes \mathcal{S}\rangle = \sum_{\mathcal{S}^c} \frac{P(S_c)}{2^{2N-1}} |\bar{n}_1 \mathcal{S}^{c\dagger} \otimes n_1 \mathcal{S}^c\rangle \tag{3.73}$$

where $P(S^c)$ is the parity of the string S^c, equaling 1 if the total number of χ and $\chi^\dagger$ in the string S^c is even, and -1 otherwise. The string S^c represents all complex fermionic strings over the fermions except site 1. Using the SU(2)⊗SU(2) sub-algebra of SU(4) generated by S^{cb} and S^{da}, one can show that

$$\begin{aligned}&\sum_{\mathcal{S}^c} \frac{P(S^c)}{2^{N-1}} |\bar{n}_1 \mathcal{S}^{c\dagger} \otimes n_1 \mathcal{S}^c\rangle \\ &= \sum_{k,l=0}^{N-1} (-1)^{N/2+k} \frac{(S^{cb})^k}{k!} \frac{(S^{da})^l}{l!} (-S^{ba}) |n_1 \chi^\dagger \otimes n_1 \chi\rangle \,.\end{aligned} \tag{3.74}$$

where the operator state $|n_1 \chi^\dagger \otimes n_1 \chi\rangle$ is built from the highest weight states as

$$|n_1 \chi^\dagger \otimes n_1 \chi\rangle = S^{cb} |W_{(0,N,0)}\rangle - |W_{(1,N-2,1)}\rangle \,. \tag{3.75}$$

Thus this completes the prescription of constructing the output state from the highest weight

states.

3.3.5 The OTOC

As is evident from the sum in Eqs. (3.71) and (3.74), both the input and output states are composed of N^2 different weights. Since the Hamiltonian preserves weights and states with different weights are orthogonal, it is important to check how many of the weights are shared between the input and output states. One can deduce that there are $N-1$ such weights, and they can be labelled by a single integer m that also labels the charge in each corresponding sector, and ranges between $[1, N-1]$

$$\begin{aligned}
|\text{in}_m\rangle &= -\frac{1}{2^N}\frac{(S^{dc})^{N-m-1}(S^{ba})^{N-m}}{(N-m-1)!(N-m)!}\,|\chi_1^\dagger n\otimes\chi_1 n\rangle \\
|\text{out}_m\rangle &= \frac{(-1)^{N/2-m-1}}{2^N}\frac{(S^{da})^{N-m-1}(S^{cb})^{m-1}}{(N-m-1)!(m-1)!}\,|\bar{n}_1\chi^\dagger\otimes n_1\chi\rangle
\end{aligned} \tag{3.76}$$

This is exactly equivalent to restricting the OTOC to a specific charge sector, as shown in Sec. 3.3.1. The states $|\chi_1^\dagger n\otimes\chi_1 n\rangle$ and $|\bar{n}_1\chi^\dagger\otimes n_1\chi\rangle$ have been built in the previous section. One can check that the states defined above have equal weight for the corresponding m, hence the problem reduces to dynamics within $N-1$ subspaces, each of maximum size $\mathcal{O}(N)$. Following this, the OTOC is governed by the equation

$$\begin{aligned}
\mathcal{F}(\chi_i(t),\chi_j^\dagger) &= \mathcal{F}_{(0,N,0)}(t) + \left(\frac{N\delta_{ij}-1}{N-1}\right)\mathcal{F}_{(1,N-2,1)}(t) \\
\mathcal{F}_{(0,N,0)}(t) &= 2^N\sum_{m=1}^{N-1}\langle\text{out}_m|e^{\mathbb{H}_m t}|\text{in}_m\rangle_{(0,N,0)} \\
\mathcal{F}_{(1,N-2,1)}(t) &= 2^N\sum_{m=1}^{N-1}\langle\text{out}_m|e^{\mathbb{H}_m t}|\text{in}_m\rangle_{(1,N-2,1)}.
\end{aligned} \tag{3.77}$$

From here on out, we will use the notation $\mathcal{F}_{\text{irrep}}(t)$ to refer to the OTOC $\mathcal{F}(\chi_i(t),\chi_j^\dagger)$ and the notation $\mathcal{F}^m_{\text{irrep}}(t)$ to discuss its charge resolved version restricted to the particular irrep, unless other operators are explicitly specified. As we will see in the upcoming sections, the scrambling dynamics are present solely in the contribution from the symmetric $(0,N,0)$ irrep

(for $q_{\text{syk}} \geq 4$) and all other irrep contributions are marked by exponential decays at all times.

3.3.5.1 Analytical results for the non-interacting model ($q_{syk} = 2$)

One can compute the OTOC for the free case ($q_{\text{syk}} = 2$) using the emergent Hamiltonian which in the case of the non-interacting model depends only on the quadratic Casimir C_2 and the total charge Q, as shown below

$$\mathbb{H}_{q_{\text{syk}}=2} = \frac{1}{N}(C_2 + \frac{Q^2}{8} - 2N - \frac{QN}{2}).$$

In this case the dynamics are analytically accessible and the two different irreps involved in the OTOC are a constant. These are given by

$$C_2^{(0,N,0)} = \frac{N^2}{2} + 2N; \quad C_2^{(1,N-2,1)} = \frac{N^2}{2} + N. \tag{3.78}$$

Utilizing this knowledge and the fact that the total charges of both irreps are $Q = 2N$, one can compute the emergent Hamiltonian corresponding to both irreps

$$\mathbb{H}_{q_{\text{syk}}=2}^{(0,N,0)} = 0; \quad \mathbb{H}_{q_{\text{syk}}=2}^{(1,N-2,1)} = -1. \tag{3.79}$$

This implies that the dynamics within each irrep takes the following simple form $\mathcal{F}_{(0,N,0)}(t) = a$, $\mathcal{F}_{(1,N-2,1)} = be^{-t}$. The constant parameters a and b can be conveniently obtained from the initial value of the overall OTOC $\mathcal{F}_{q_{\text{syk}}=2}(\chi_i(t), \chi_j^\dagger)$

$$\mathcal{F}_{q_{\text{syk}}=2}(\chi_i(t=0), \chi_j^\dagger) = \begin{cases} 0 & (i = j) \\ -\frac{1}{4} & (i \neq j) \end{cases} \tag{3.80}$$

The OTOC is then written as

$$\mathcal{F}_{q_{\text{syk}}=2}(\chi_i(t), \chi_j^\dagger) = \left(\frac{N-1}{4N}\right)\left[-1 + \left(\frac{N\delta_{ij} - 1}{N-1}\right)e^{-t}\right]. \tag{3.81}$$

Hence the OTOC starts from a value dependent on δ_{ij} and N, and exponentially decays to $-(N-1)/4N$ instead of 0 as in the case of scrambling dynamics.

3.3.5.2 Scrambling dynamics for $q_{syk} = 4$

The effective Hamiltonian is not a constant anymore for $q_{\text{syk}} > 2$. One needs to diagonalize $\mathbb{H}$ for each irrep and every charge sector to compute the OTOC in Eq. (3.77). This can be done for large but finite N because the Hilbert space for each sector is at most of size $\mathcal{O}(N)$, given the symmetry structure of $\mathbb{H}$. Constructing the effective Hamiltonian for each sector requires us to build the matrix representation for the bilinear operators $S^{\alpha\beta}$ for both irreps $(0, N, 0)$ and $(1, N-2, 1)$. Unlike the SU(2) case in which all the states within an irrep can be uniquely labelled by L_z, or equivalently the weight, for SU(n) and $n > 2$, there are multiple states within each irrep that are labelled by the same weight. In fact, these subspaces labelled by the weights are the ones leading to the operator dynamics within each charge sector in the complex Brownian SYK model. Fortunately, there are well-established schemes to uniquely label the states of arbitrary irreps for SU(n) groups, called Gelfand-Tsetlin patterns [99], a brief introduction to which is provided in the appendix. Based on GT patterns, the matrix representation of $S^{\alpha\beta}S^{\beta\alpha}$ for each irrep and fixed weight subsectors and thus the effective Hamiltonian $\mathbb{H}$ can be constructed efficiently, which is local in this basis.

Using this approach, we compute the overall OTOC $\mathcal{F}(\chi_i(t), \chi_j^\dagger)$ for N up to 500 and plot the results in Fig. 3.4(a) and (b) for $i = j$ and $i \neq j$, respectively. Similar to the Majorana model, the two cases start with distinct initial values but quickly approach the same behavior that exponentially decays to zero. Furthermore, the case with $i \neq j$ develops the characteristic early time Lyapunov growth as N increases. As shown in Eq. (3.77), the difference between the two cases is from $\mathcal{F}_{(1,N-2,1)}$, the contribution from the $(1, N-2, 1)$ irrep. We plot $\mathcal{F}_{(0,N,0)}(t)$ and $\mathcal{F}_{(1,N-2,1)}(t)$ in Fig. 3.4(b). Evidently, $\mathcal{F}_{(1,N-2,1)}(t)$ shows purely exponential decay, explaining the early time difference between $i = j$ and $i \neq j$ in $\mathcal{F}(\chi_i(t), \chi_j^\dagger)$. On the other hand, the early time Lyapunov growth is from $\mathcal{F}_{(0,N,0)}(t)$. This

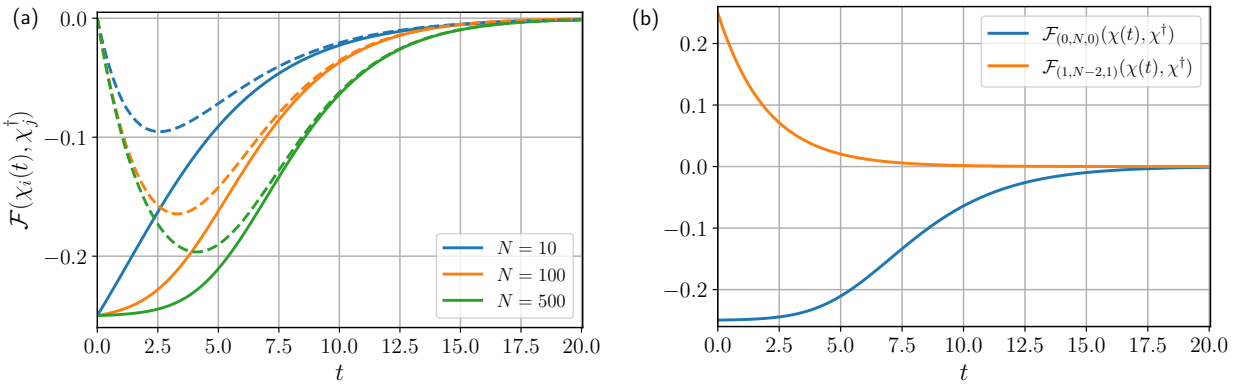

Figure 3.4: (a) The overall OTOC $\mathcal{F}(\chi_i(t), \chi_j^\dagger)$ vs time for $i = j$ (dashed lines) and $i \neq j$ (solid lines) for different values of N. The OTOC decays to zero at late times as expected from scrambling, which is in contrast with the non-interacting ($q_{\text{syk}} = 2$) case given in Eq. (3.81). (b) The OTOC resolved into the contributing irreps, according to Eq. (3.77), for $N = 500$ particles. The scrambling behavior is present in the $(0, N, 0)$ irrep while the $(1, N-2, 1)$ irrep displays an exponential decay at all times.

demonstrates scrambling in the interacting complex Brownian SYK model for local operators of the type $|\chi^\dagger \otimes \chi\rangle$.

OTOCs $\mathcal{F}(W(t), V)$ for other operators, even non local ones and other q_{syk} can be in principle calculated following the same procedure, which we summarize below

1. Find the form of $\mathbb{H}$ as a function of the operators $S^{\alpha\beta}$

2. Decompose the input and output states, $|\text{in}\rangle$ and $|\text{out}\rangle$, which depend on the operators W and V respectively, into different irreps and weight sectors of SU(4).

3. Construct the matrix representation of $\mathbb{H}$ using GT patterns, for the sectors in which the component of the input and output states have a non-zero overlap.

4. Evolve the input state in imaginary time, using the Hamiltonian constructed in the last step, for each sector, and take the overlap with the output state.

Among all these steps, step 2 is the most tedious. In what follows, we discuss the other OTOCs, $\mathcal{F}(\chi_i(t), n_j)$ and $\mathcal{F}(n_i(t), n_j)$. Note that $\mathcal{F}(\chi_i(t), n_j)$ and $\mathcal{F}(n_j(-t), \chi_i)$ are identical. The calculation involves the same two irreps $(0, N, 0)$ and $(1, N-2, 1)$ for $\mathcal{F}(\chi_i(t), n_j)$

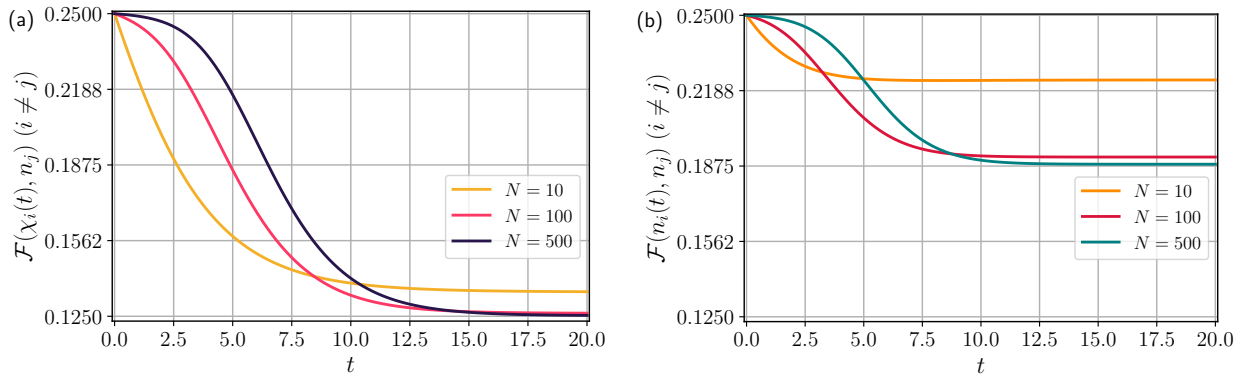

Figure 3.5: The overall OTOC $\mathcal{F}(\chi_i(t), n_j)$ in (a) and $\mathcal{F}(n_i(t), n_j)$ in (b), for $i \neq j$ and different values of N. Both the OTOCs display pronounced finite-sized effects in their late-time values, which remain finite as $N \to \infty$, in contrast with that of $\mathcal{F}(\chi_i(t), \chi_j^\dagger)$.

but involves the third irrep $(0, N-2, 0)$ for $\mathcal{F}(n_i(t), n_j)$. The details of decomposing the input state and the output state can be found in Appendix A.4. Similar to the previous example, the scrambling behavior results from the dynamics in the irrep $(0, N, 0)$, while the contributions from the other irreps are purely exponential decay. In Fig. 3.5, we plot both $\mathcal{F}(\chi_i(j), n_j)$ and $\mathcal{F}(n_i(t), n_j)$ for $i \neq j$ both N up to 500, the behavior of which is dominated by the contribution from the irrep $(0, N, 0)$. Evidently, they develop the characteristic early time Lyapunov growth as N increases. Unlike $\mathcal{F}(\chi_i(t), \chi_j)$, the late time value has a strong finite-size effect and asymtotes to 1/8 and 3/16 for large N, in agreement with Eq. (3.52) [2].

This concludes our discussion on the behavior of the overall OTOC in the complex Brownian SYK model. The overall OTOC contains contributions from each charge sector that we label $\mathcal{F}^m$ in Sec. 3.3.6, where m denotes the charge. Remarkably, our approach naturally provides full access to $\mathcal{F}^m$ from each charge sector and can be exploited to understand charge dependent scrambling for finite but large N and all time scales, which we discuss in the next section.

[2]Since we are working with a q_{syk}-uniform model, sectors corresponding to dilute charge will display imperfect scrambling and there will be small corrections to the predicted values of the overall OTOC

3.3.6 Charge-dependent scrambling

As discussed in Sec. 3.3.1, in systems with charge conservation the dynamics of a generic operator splits into sectors with different charge profiles. We expect that dynamics with restricted access to states within the full Hilbert space will display slower operator growth as the restrictions are made more stringent. In other words, OTOCs involving operators confined to specific sectors of the Hilbert space should experience Lyapunov growth as a function of the size of the sector. In the case of U(1) conservation, these sectors can be labelled using the charge. The overall OTOC is a weighted sum of the charge resolved OTOC defined in Sec. 3.3.1

$$\mathcal{F}^m(W,V) = \frac{1}{\mathrm{Tr}(P_m)}\mathrm{Tr}(P_m W^\dagger(t) V^\dagger W(t) V). \tag{3.82}$$

We also define $\rho = m/N$ as the charge density. Our approach, which is based on the SU(4)⊗U(1) symmetry structure of the emergent Hamiltonian in the complex Brownian SYK model, can be naturally used to compute $\mathcal{F}^m(W,V)$ for each m.

Take the charge resolved OTOC $\mathcal{F}^m(\chi_i(t),\chi_j)$ for example. After resolving the symmetry structure of $\mathbb{H}$, the common subsectors for the input state and the output state are labeled by conserved quantities $S^{\alpha\alpha}$ for α in $a \sim d$, which are directly related to m as $(m, N-m+1, m, N-m-1)$. Furthermore each charge sector splits into two irreps $(0,N,0)$ and $(1,N-2,1)$. Then from Eq. (3.77), we can directly obtain the charge resolved OTOC from each term in the summation. They are

$$\begin{aligned}
\mathcal{F}^m(\chi_i(t),\chi_j^\dagger) &= \mathcal{F}^m_{(0,N,0)}(t) + \left(\frac{N\delta_{ij}-1}{N-1}\right)\mathcal{F}^m_{(1,N-2,1)}(t) \\
\mathcal{F}^m_{(0,N,0)}(t) &= \frac{4^N}{\mathrm{Tr}(P_m)}\langle \mathrm{out}_m | e^{\mathbb{H}_m t} | \mathrm{in}_m\rangle_{(0,N,0)} \\
\mathcal{F}^m_{(1,N-2,1)}(t) &= \frac{4^N}{\mathrm{Tr}(P_m)}\langle \mathrm{out}_m | e^{\mathbb{H}_m t} | \mathrm{in}_m\rangle_{(1,N-2,1)}.
\end{aligned} \tag{3.83}$$

where the states $|\mathrm{in}_m\rangle$ and $|\mathrm{out}_m\rangle$ for each charge sector are given in Eq. (3.76). The other

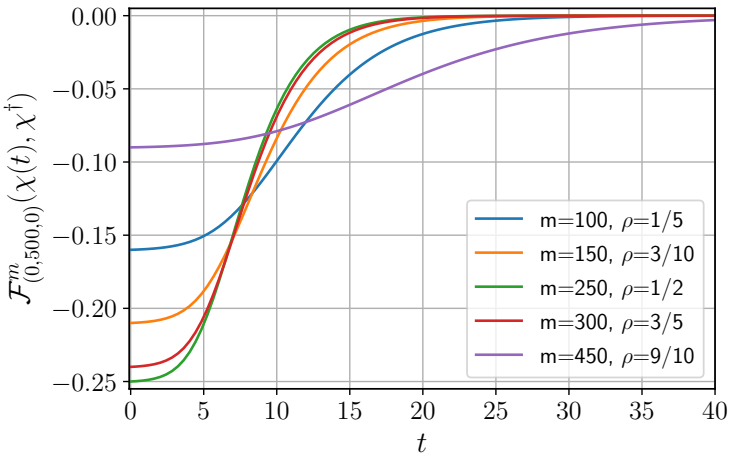

Figure 3.6: Contributions to the OTOC from different charge densities $\rho = m/N$, for the OTOC $\mathcal{F}^m(\chi_i(t), \chi_j^\dagger)$. The OTOC has been restricted to the $(0, N, 0)$ irrep with $N = 500$. This can be compared with the overall OTOC for the case $i \neq j$ for large N. The charge resolved OTOC $\mathcal{F}^m$ shows different initial values and time scales.

charge resolved OTOCs share a similar structure, and more irreps might be involved in their computation, for example, in the case of $\mathcal{F}^m(n_i(t), n_j)$.

As discussed in the last section, the irrep $(0, N, 0)$ contributes to scrambling dynamics while the contribution from other irreps exponentially decays to zero. Therefore we focus on $\mathcal{F}^m_{(0,N,0)}(t)$ and study how the scrambling dynamics depend on the charge m both numerically for large finite N, and analytically directly in the infinite N limit.

Using our approach, we compute $\mathcal{F}^m_{(0,N,0)}(\chi(t), \chi^\dagger)$ and plot the results for different m in Fig. 3.6 for $N = 500$. They start with different initial values and relax to zero, consistent with Table. 3.1. Since $\mathcal{F}^m_{0,N,0}(\chi(t), \chi^\dagger)$ is related to the overall one as $\sum_j \mathcal{F}^m(\chi_i(t), \chi_j^\dagger)/N$, we obtain the exact initial values as $-\rho(1-\rho)$. The early time behavior is characterized by the Lyapunov growth. Remarkably, in addition to the different initial values, the time scale in which $\mathcal{F}^m$ relaxes to zero only strongly depends on m or the charge density ρ, which we analyze in full detail below.

To examine the early time growth and extract the Lyapunov coefficients for each charge

sector, we will begin by assuming an early time ansatz of the form

$$\mathcal{F}^{m}_{(0,N,0)}(\chi(t\sim 0),\chi^{\dagger}) \sim -\rho(1-\rho)+\frac{a_\rho}{N}(e^{\lambda^{\rho}_{L}t}-1). \tag{3.84}$$

By Taylor expanding both the ansatz and Eq. (3.83) and matching coefficients, we can relate λ^{ρ}_{L} to the moments of the effective Hamiltonian

$$\lambda^{\rho}_{L}=\frac{\langle \text{out}_m|\mathbb{H}^2_m|\text{in}_m\rangle_{(0,N,0)}}{\langle \text{out}_m|\mathbb{H}_m|\text{in}_m\rangle_{(0,N,0)}}. \tag{3.85}$$

This is a more accurate method to extract λ^{ρ}_{L} than curve fitting. We plot the Lyapunov coefficients obtained in Fig. 3.7(a) for $N = 500$, via the method outlined above. We see that the Lyapunov exponent grows with the density till it reaches $\rho = 1/2$ after which it starts decreasing again, and the behavior is exactly described by an inverted parabola. The curve has been fitted against the function

$$\lambda^{\rho}_{L}(\rho)=4\rho(1-\rho) \tag{3.86}$$

which agrees with [82]. We also plot the magnitude of the late-time relaxation exponent λ^{ρ}_{late}, which is given by the largest nonzero eigenvalues for each sector of $\mathbb{H}$ labelled by m, as a function of the charge density ρ. It follows the same behavior as λ^{ρ}_{L} described by the inverted parabola, but half in magnitude, $\lambda^{\rho}_{late} = 2\rho(1-\rho) = \lambda^{\rho}_{L}/2$. This relation is reminiscent of the Majorana case shown in Fig. 3.2(c).

In Fig. 3.7(b) we plot the maximal Lyapunov exponent and relaxation exponent at half filling as a function of N. Similar to the Majorana case, λ^{max}_{L}, starts with a negative value $-1/4$, changes sign and asymptotes to the large N value 1 as N increases, while $-\lambda^{max}_{late}$, starts with the same value, remains negative, and asymptotes to $-1/2$. The positive Lyapunov exponent is an effective behavior that emerges from a pool of a large number of eigenvalues, all of which are negative. For small Hilbert spaces (corresponding to low N), this pool is

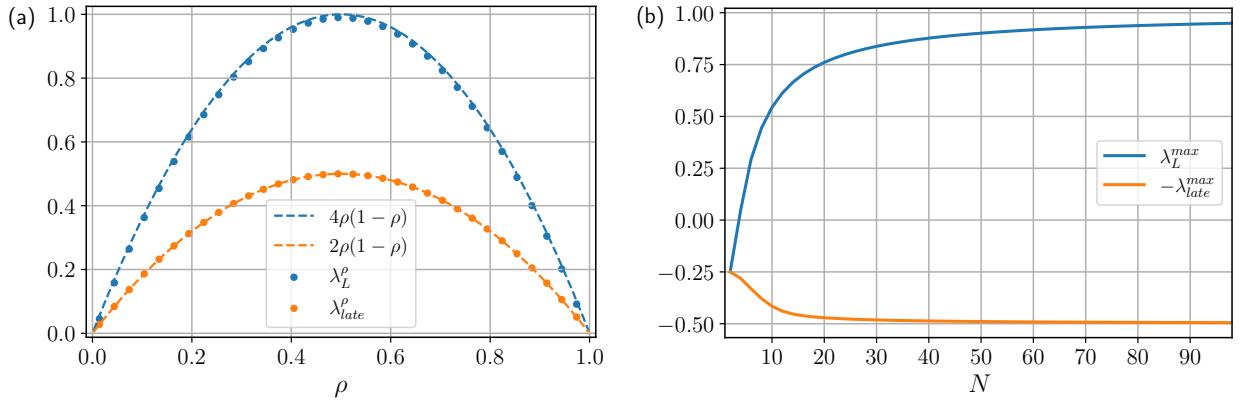

Figure 3.7: (a) The plot of the Lyapunov exponent λ_L^ρ and the late-time exponent λ_{late}^ρ vs ρ for $N = 500$. (b) The maximal Lyapunov exponent λ_L^ρ and late-time exponent corresponding to the half filled state $\rho = 1/2$ plotted as a function of N. The exponents in both (a) and (b) have been extracted from a given charge sector within the irrep $(0, N, 0)$ for $\mathcal{F}(\chi_i(t), \chi_j^\dagger)$. The exponents of OTOCs involving other local operators, restricted to the $(0, N, 0)$ irrep, show similar behavior.

not large enough to produce a positive exponent. It should also be noted that although we obtain positive exponents for some small N, this behavior is short-lived and therefore difficult to obtain using standard curve-fitting techniques. In the large N limit, this λ_L^{max} is also the overall Lyapunov coefficient of the contribution from the $(0, N, 0)$ irrep since it corresponds to the sector (half-filled) which dominates, and of the overall OTOC in the case $i \neq j$ since the contribution from the $(0, N, 0)$ irrep dominates in that case.

To capture the charge dependence of $\mathcal{F}^m_{(0,N,0)}$ beyond early time, we consider the rescaled OTOC $\widetilde{\mathcal{F}}^m = \mathcal{F}^m/(-\rho(1-\rho))$, which starts from 1 and relaxes to 0 for each m. We define a new parameter

$$\tilde{t}_N^\rho = \ln\left(\frac{e^{\lambda_L^\rho t} - 1}{N\rho(1-\rho)}\right). \tag{3.87}$$

Then the early time behavior of $\tilde{\mathcal{F}}^m_{(0,N,0)}$ is given by $1 - a_\rho e^{\tilde{t}_N^\rho}$. Using the numerical data, one can fix $a_\rho = 1$. Remarkably, we find that $\tilde{\mathcal{F}}^m_{(0,N,0)}$ for $N = 200$ and $N = 500$, and various m collapses to a single curve as a function of $\tilde{t}_N^\rho$ for all time scales, as shown in Fig. 3.8. This indicates that the leading charge dependence and also N dependence of $\mathcal{F}^m_{(0,N,0)}$ is captured

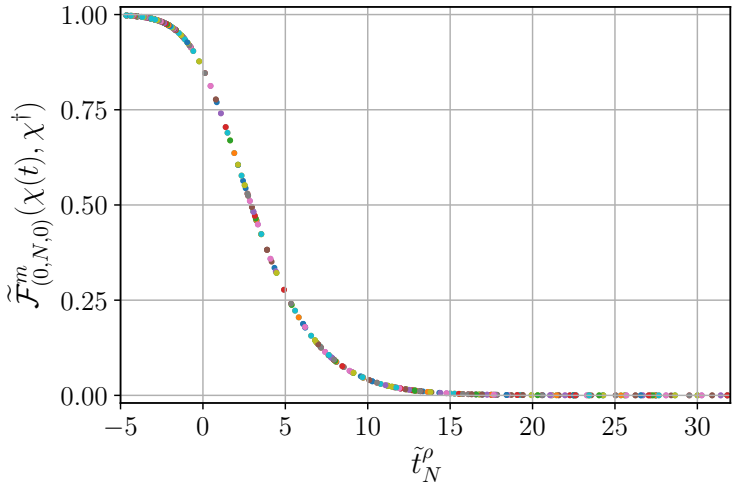

Figure 3.8: The rescaled OTOC $\widetilde{\mathcal{F}}^m_{(0,N,0)}(\chi(t),\chi^\dagger)$ for different charge sectors and two values of N : $m = \{50, 60, ..., 440, 450\}$ for $N = 500$, and $m = \{50, 60, ..., 140, 150\}$ for $N = 200$, plotted against the transformed time variable $\tilde{t}^\rho_N$. The OTOCs for all different m corresponding to both the values of N collapse into a single function.

by the following simple form

$$\mathcal{F}^m_{(0,N,0)}(\chi(t),\chi^\dagger) = -\rho(1-\rho)f(\tilde{t}^\rho_N). \tag{3.88}$$

It must be emphasized that the collapsing behavior is only observed for charge sectors of finite charge density ρ, which have Hilbert-spaces that are large enough to produce a positive Lyapunov exponent.

3.3.7 Charge-dependent hydrodynamic equation

To gain analytical understanding of the charge dependent scrambling and its relation to the Majorana case, we derive the charge resolved OTOC in the large N limit analytically in this section. Similar to the procedure in the Majorana case, we focus on the irrep $(0, N, 0)$ that gives rise to the scrambling behavior, and write the OTOC $\mathcal{F}^m(\chi_i(t),\chi^\dagger_j)$ as follows:

$$\mathcal{F}^m_{(0,N,0)}(t) = \frac{4^N}{\mathrm{Tr}(P_m)}\langle \mathrm{out}_m|\mathrm{in}_m(t)\rangle = \sum_k \psi^m_{\mathrm{out}}(k)\psi^m_{\mathrm{in}}(k,t). \tag{3.89}$$

Since all the states within a fixed-m subspace have equal weights in the eyes of the algebra, we use GT-patterns to distinguish them, labelled by the integer k. In this basis k takes integer values ranging from 0 to $\min(m-1, N-m-1)$ and the output state takes the form:

$$\begin{aligned} \psi^m_{\text{out}}(k) &= -g(N,k)\sqrt{(N-m-k)(m-k)}/N \\ g(N,k) &= \left(\binom{N+1}{k+1}\binom{N+1}{k}\frac{N-2k}{N+1}\right)^{1/2}. \end{aligned} \tag{3.90}$$

We define a similarity transformation to make the N-dependence of $\psi^m_{\text{out}}(k)$ uniform, just as shown in Sec. 3.2.6, and the output state is transformed as

$$\psi^m_{\text{out}}(k) \to \tilde{\psi}^m_{\text{out}}(k) = -\sqrt{(N-m-k)(m-k)}/N. \tag{3.91}$$

After the transformation, the Hamiltonian and the input state are

$$\tilde{H}_{kk'} = g(N,k)H_{kk'}g(N,k)^{-1};\ \tilde{\psi}^m_{\text{in}}(k) = g(N,k)^{-1}\psi^m_{\text{in}}(k). \tag{3.92}$$

The dynamics of $\tilde{\psi}^m_{\text{in}}$ is governed by the equation $\partial_t\tilde{\psi}^m_{\text{in}}(t) = \tilde{H}\tilde{\psi}^m_{\text{in}}$, which now is ready to be expanded in the large-N continuum limit.

The strategy is similar to that in the Majorana case. We use the continuous variables $x = k/N$ and $\rho = m/N$, where $0 \le x \le \min(\rho, 1-\rho)$. In the large N limit, the building blocks of the Hamiltonian $S^{\alpha\beta}S^{\beta\alpha}$ can be written as differential operators in terms of x after the similarity transformation, from which the Hamiltonian $\tilde{H}$ as a differential operator acting on $\tilde{\psi}^m_{\text{in}}$ can be obtained. In the infinite N limit, $\tilde{\psi}^m_{\text{in}}$ obeys

$$\partial_t\tilde{\psi}^m_{\text{in}} = \partial_x\left(-\frac{4(x-1)x(x^2-x+\rho(1-\rho))}{2x-1}\tilde{\psi}^m_{\text{in}}\right). \tag{3.93}$$

Similar to the Majorana case, this equation predicts that $\int dx\,\psi^m_{\text{in}}(x)$ is a constant and that $\psi^m_{\text{in}}(x)$ can be interpreted as a probability distribution function. If $\tilde{\psi}^m_{\text{in}}$ starts with a delta

function, it will remain a delta function $\sqrt{\rho(1-\rho)}\delta(x-x(t))$, with the peak value $x(t)$ obeying an ordinary differential equation

$$\partial_t x(t) = \frac{4(x-1)x(x^2-x+\rho(1-\rho))}{2x-1}. \tag{3.94}$$

Then the charge resolved OTOC is given by

$$\begin{aligned} \mathcal{F}^m_{(0,N,0)} &\sim \int \psi^m_{\text{out}}(x)\psi^m_{\text{in}}(x)dx \\ &= -\sqrt{(1-\rho)\rho(1-\rho-x(t))(\rho-x(t))}. \end{aligned} \tag{3.95}$$

It should be noted that the transformed effective Hamiltonian $\tilde{\mathbb{H}}$ at finite N is not stochastic due to the lack of a steady state for the OTOC we are considering, unlike the Majorana case. As a result, the interpretation of $\psi^m_{\text{in}}(x)$ as a probability distribution is only valid in the infinite N limit and breaks by a $1/N$ effect. We will discuss some interesting $1/N$ effects in the end of this section.

To solve Eq. (3.94), we introduce a new variable ξ as a function of x

$$\xi = \left(\frac{(1-\rho-x)(\rho-x)}{(1-\rho)\rho}\right)^{1/2} \tag{3.96}$$

which ranges from 0 to 1. In the transformed variables Eq. (3.94) becomes

$$\partial_t \xi(t) = 2\rho(1-\rho)\xi(\xi^2-1), \tag{3.97}$$

which is the same as the logistic differential equation derived for the Majorana case in Eq. (3.39) up to a ρ dependent factor that can be absorbed into t. This factor clearly demonstrates the characteristic time scale associated with the sector of charge density ρ. The differential equation has two unstable steady solutions $\xi = \pm 1$ and one stable steady solution $\xi = 0$. Initially ξ starts with a value close to 1, corresponding to x near 0, and relaxes to the stable steady solution over time.

In the new variable ξ, the output state is $-\sqrt{\rho(1-\rho)}\xi$, and OTOC is proportional to $\xi(t)$. Solving the logistic equation, we obtain

$$\mathcal{F}^m_{(0,N,0)}(t) = A_\rho \xi(t) = \frac{A_\rho}{\sqrt{e^{4t\rho(1-\rho)}\delta_\rho + 1}}, \tag{3.98}$$

where δ_ρ and A_ρ are determined by the input operator. We have assumed that $\delta_\rho \ll 1$. The early and late time behavior are given by

$$\mathcal{F}^m_{(0,N,0)}(t) \sim \begin{cases} A_\rho - \frac{1}{2}e^{4\rho(1-\rho)t}A_\rho\delta_\rho & t \ll -\frac{\ln\delta}{4\rho(1-\rho)} \\ e^{-2\rho(1-\rho)t} & t \gg -\frac{\ln\delta}{4\rho(1-\rho)} \end{cases} \tag{3.99}$$

which results from the competition between $e^{4t\rho(1-\rho)}$ and δ_ρ. The exponents λ^ρ_L and λ^ρ_{late} agree with the leading order of the numerical results. The same comments that apply to the Majorana case apply here as well, namely the analytical expression is not expected to match the numerical data as the initial state corresponding to local operators implies an initial condition of the form $x(0) \propto 1/N$, and the analytical technique is only applicable in cases where the input state is independent of N.

This result illustrates that the majority of the density dependence in the large-N limit is contained in the initial value and the Lyapunov exponent, and scaling them appropriately will result in all sectors of finite charge density displaying the same behavior. Given the analytical expression, one can also expand the solution in a manner very similar to Eq. (3.42) to observe the emergence of positive Lyapunov exponents from the negative eigenvalues of the emergent Hamiltonian.

There are also some interesting $1/N$ effects that we briefly mention here. Similar to the Majorana case, adding $1/N$ corrections will result in the dynamical equation for $\tilde{\psi}^m_{\text{in}}$ (Eq. (3.93)) transforming into a second-order differential equation in x, which will lead to the initial delta function broadening under the time-evolution. However, there are two $1/N$ effects that are absent in the Majorana case. Firstly, the new logistic equation obtained

will have zeros which when corrected for the $1/N$ effect, will lead to steady solutions being shifted outside of the physical Hilbert space. Secondly, since there will be no steady-state solutions within the physical Hilbert space, $\int dx\, \tilde{\psi}^m_{\text{in}}$ will no longer be conserved and the interpretation of $\tilde{\psi}^m_{\text{in}}$ as a probability distribution will no longer be valid. Hence we will see that this quantity will show a late-time decay away from its constant value, which can be numerically verified as well.

3.3.8 Other OTOCs

We now discuss two other kinds of OTOCs, namely $\mathcal{F}^m_{(0,N,0)}(\chi(t), n)$ and $\mathcal{F}^m_{(0,N,0)}(n(t), n)$. We are again restricting the discussion to the irrep $(0, N, 0)$ because it contains all of the interesting scrambling dynamics. The relevant charge sector labelled by $S^{\alpha\alpha}$ are $(m, N - m + 1, m - 1, N - m)$ and $(m, N - m, m, N - m)$ for $\mathcal{F}^m_{(0,N,0)}(\chi(t), n)$ and $\mathcal{F}^m_{(0,N,0)}(n(t), n)$, respectively. The main difference from the previous OTOC $\mathcal{F}^m_{(0,N,0)}(\chi(t), \chi^\dagger)$ is that there reside steady states within these charge sectors. In other words, the effective Hamiltonian $\mathbb{H}$ has a zero eigenvalue in addition to other negative eigenvalues. As a result, when the input state and the output state both have a finite overlap with the steady state, the OTOC develops a finite late-time value. This indeed is what is observed here. In Fig. 3.9 (insets (a1) and (b1)), we plot both OTOCs for different m, which relax to different final values consistent with those given in Table 3.1.

To study the charge dependence, we rescale $\mathcal{F}^m_{(0,N,0)}$ as

$$\widetilde{\mathcal{F}}^m_{(0,N,0)}(t) = \frac{\mathcal{F}^m_{(0,N,0)}(t) - \mathcal{F}^m_{(0,N,0)}(\infty)}{\mathcal{F}^m_{(0,N,0)}(0) - \mathcal{F}^m_{(0,N,0)}(\infty)}. \tag{3.100}$$

The rescaling removes the dependence of the initial and the late-time values, and the rescaled OTOC monotonically decreases from 1 to 0 as time increases, for all m. Remarkably, as we show in Fig. 3.9, the rescaled OTOC for different m and two values of N, 200 and 500, also collapses to a function of the variable $\tilde{t}^\rho_N$ defined in Eq. (3.87). This indicates that the leading charge dependence of all OTOCs considered in this work, apart from the initial and

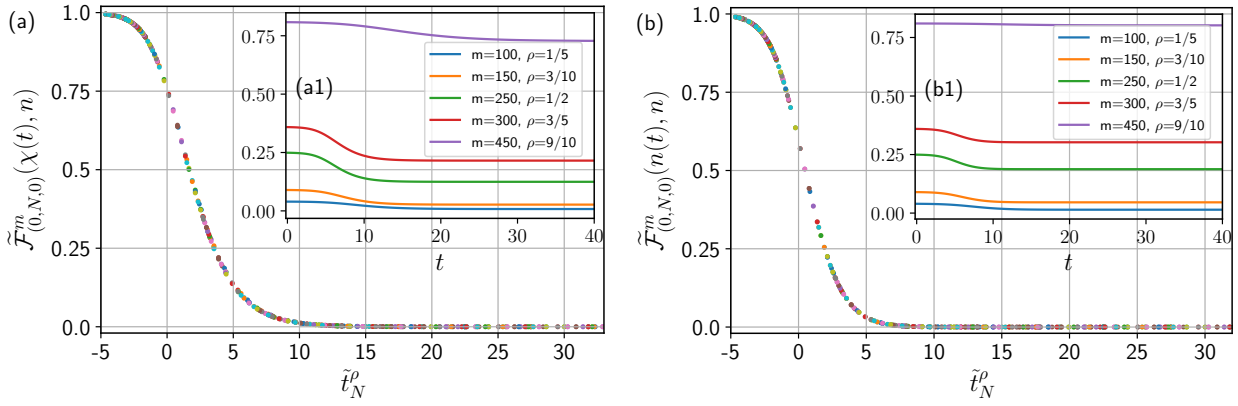

Figure 3.9: The rescaled charge resolved OTOCs $\widetilde{\mathcal{F}}^{m}_{(0,N,0)}(\chi(t),n)$ in (a) and $\widetilde{\mathcal{F}}^{m}_{(0,N,0)}(n(t),n)$ in (b) for different m and N plotted against the transformed time variable $\tilde{t}^{\rho}_N$. We choose $m = \{50, 60, ..., 440, 450\}$ for $N = 500$, and $m = \{50, 60, ..., 140, 150\}$ for $N = 200$. The OTOCs for different m and both the values of N collapse into a single functional form. Insets (a1) and (b1) show the corresponding unrescaled charge-resolved OTOCs $\mathcal{F}^{m}_{(0,N,0)}(\chi(t),n)$ and $\mathcal{F}^{m}_{(0,N,0)}(n(t),n)$ for different m at $N = 500$ as a function of t.

the late-time values, can be captured by $\tilde{t}^{\rho}_N$.

As is evident from the discussions in this section, all OTOCs display a late-time exponential decay behavior. Some studies [77, 78, 75] have found late time power law relaxations of the OTOC in systems with U(1) conservation or energy conservation due to diffusion, which scales as $\sim t^{d/2}$, where d is the number of spatial dimensions. However, we are working in 0 spatial dimensions where the charge is static and therefore the OTOC still exponentially decays in the late-time regime.

3.4 Discussion and summary

In this chapter we studied the Brownian SYK model with and without charge conservation. We introduced a symmetry-based approach which maps the Brownian SYK dynamics to SU(n) spin dynamics after taking the disorder average, where $n = 2$ for the Majorana model and 4 for the model with complex fermions. This mapping drastically reduces the dimension of the effective dynamical Hilbert space from $\sim e^N$ to $\sim \mathcal{O}(N)$, allowing us to numerically compute the OTOCs exactly for large system size and all time scales. For the

non-interacting case ($q_{\text{syk}} = 2$), one finds that the SU(n) algebras are promoted to exact symmetries and the OTOCs can be solved analytically. We also provided a method to connect the Hamiltonian approach used in the formalism to the approach which maps to a stochastic model, via a similarity transformation, and utilized it to derive a hydrodynamical description of the OTOC in the large-N limit. In this limit, we find that the OTOC in the complex model follows the same differential equation as the Majorana model, up to a density dependent overall scaling.

For the Majorana model, we verified previously known results using the new formalism and compute the OTOC for $N = 10000$ fermions. We also utilized the approach to analyze the early and late time exponents as a function of N and demonstrate how they reach their asymptotic values for large N. In this context we also discuss the emergence of the positive Lyapunov exponent which arises from the combined effect of the negative eigenvalues of the emergent Hamiltonian.

For the complex model, multiple kinds of OTOCs are discussed which involve different operators. We study the scrambling dynamics of these different operators and provide exact early and late-time values of the OTOC restricted to different charge sectors in a general complex model with charge conservation, which are later verified numerically for the case of the complex Brownian model. We also make use of the formalism to numerically compute the exact OTOC for $N = 500$ fermions, and analyze how the OTOC approaches the late time value starting from the initial value. We find that for $q_{\text{syk}} = 4$ the Lyapunov exponent has density dependence $\lambda_L^\rho = 4\rho(1-\rho)$ and that the late time dynamics is marked by an exponential decay as well, with an exponent that has a similar functional dependence on the charge density, i.e. $\lambda_{late}^\rho = 2\rho(1-\rho)$. Since the formalism provides access to the dynamics for finite N, we study how these exponents change and approach their asymptotic values starting from $N = 2$ to $N \gtrsim 100$.

The approach used in this work has several directly visible extensions. One direction is to explore higher order correlators which will involve more than 4 time-contours and

therefore for the Brownian model will still have an emergent SU(n) algebra, albeit with a higher n and more complex symmetry structure when compared with the conventional OTOC. As an example, the complex Brownian fermionic model will give rise to an SU(n) $\otimes$ U(1) algebra on n time contours, while the Majorana model will display an SO(n) algebra. Another direction is to start with some Brownian model with a non-abelian symmetry such as SU(n), instead of U(1), and explore the behavior of the correlators as a function of n to probe the relation between the rank of the continuous symmetry in the model, and scrambling. Furthermore, it would be very interesting to generalize the procedure given in this work to higher dimensions, especially for the charge conserved case where one can derive the hydrodynamic equations to describe the interplay between local Lyapunov growth and ballistic operator spreading [31, 100] as well as charge diffusion. We expect that the coupled diffusion equation of the charge and the FKPP equation of the operator [44, 31] can lead to algebraic decay of OTOC [77, 78] in the late time. We will explore this direction in the next chapter. From the coupled equations between charge and operator, one can also study the charge dependence of the butterfly velocity and the relation between the diffusion constant, butterfly velocity, and the Lyapunov exponent at different charge density. Some other directions for future work are studying related observables such as entanglement entropy, tripartite mutual information and spectral form factors in the presence of the U(1) symmetry.

4. NON-EQUILIBRIUM DYNAMICS IN 1+1 DIMENSIONS [1]

4.1 Chapter Summary

In this chapter, we will explore interesting features of quantum dynamics in extended spatial dimensions. While scrambling in the dimensionless case is marked by the presence of a Lyapunov exponent at early times, in general dimensions, travelling wave solutions emerge which carry 'quantum information' with a well-defined butterfly velocity. We will first understand these solutions deeply by analyzing the case without symmetry, following which we will proceed to the richer situation where the charge transport couples to the spread of information. The steps will be as follows:

- We begin by describing the dynamics of the OTOC for a chain of clusters of the Brownian SYK model built with Majorana fermions. As shown previously, the couplings, which are uncorrelated in the time direction, allow us to describe the computation of the OTOC in terms of an SU(2) spin chain which evolves in imaginary time.

- Expanding the SU(2) spin operators in the infinite-N limit, gives us a partial differential equation describing the evolution of the OTOC.

- For the purely inter-site non-interacting model, the equation describes diffusive operator spreading. When intra-site interactions are added, the OTOC follows dynamics described by the class of FKPP equations.

- We demonstrate how the Lyapunov exponent and butterfly velocity emerge from these solutions, and compute them for the Brownian SYK chain.

- Moving on to the case with charge conservation, the dynamics of the OTOC in the chain of clusters of the complex Brownian SYK model map to an SU(4) spin chain

[1] Reprinted with permission from "Charge transport, information scrambling and quantum operator-coherence in a many-body system with U(1) symmetry" by L. Agarwal, S. Sahu and S. Xu [101] (accepted into JHEP)

which evolves in imaginary time

- We describe states within the SU(4) algebra, in the GT-pattern basis. This description allows us to neatly separate the description of the charge dynamics from the operator spreading.

- We consider both intra-site interactions and inter-site non-interacting models together. The former causes information scrambling within each cluster, whereas the latter gives rise to the charge dynamics.

- Expanding the SU(4) spin operators in the GT-pattern basis provides us with the equations which couple charge transport with operator spreading. We obtain the charge-dependent Lyapunov exponent and butterfly velocity from these equations, and simulate them in different domain-wall density backgrounds to explore rich features of charged information scrambling.

4.2 The case without symmetry : Brownian SYK chain

To keep things simpler, we will first consider a chain of clusters in one dimension, each containing N Majorana fermions. The results from this analysis can be easily generalized to higher dimensions.

4.2.1 The non-interacting chain

In this section, we will exactly solve the dynamics in the Brownian SYK chain coupled using quadratic, i.e. non-interacting, expressions of the Majorana operators:

$$H(t) = i \sum_{r,j,k} K_{r,j,k}(t)\, \chi_{r,j}\, \chi_{r+1,k} \quad ; \quad \overline{K_{r,j,k}(t) K_{r',j',k'}(t')} = \frac{1}{4N} \delta_{j,j'} \delta_{k,k'} \delta_{r,r'} \delta(t-t') \tag{4.1}$$

Here r labels the cluster index on the chain of length L, whereas j, k label the N fermions within each cluster. One can now use the same protocol as before (Sec. 3.2.2), generating

Majorana fermions on four-time contours that anti-commute with each other and follow the anti-commutation relation:

$$\{\chi^{\alpha}_{r,i}, \chi^{\beta}_{r',j}\} = 2\delta_{i,j}\delta_{r,r'}\delta_{\alpha,\beta} \quad ; \quad \alpha, \beta = a, b, c, d \tag{4.2}$$

Using this, one can define an SU(2) algebra within each cluster, such that we can map the computation of the OTOC in the original Brownian SYK chain to an SU(2) spin-chain that evolves in imaginary time (Eq. 3.11). This gives rise to the following emergent Hamiltonian (Assuming periodic boundary conditions without loss of generality):

$$\mathbb{H} = \frac{1}{4N}\bigg(- 2N^2 L + 8\sum_{r}(L_{x,r}L_{x,r+1} + L_{y,r}L_{y,r+1} + L_{z,r}L_{z,r+1})\bigg) \tag{4.3}$$

Hence the free Brownian chain on four contours reduces to the SU(2) symmetric Heisenberg model. First, let's perform some consistency checks to make sure this result is accurate. One expects the global identity to be static under unitary dynamics and the global parity operator to be static due to the underlying parity symmetry in the original model. Under the SU(2) decomposition, these operators map to the fully spin up and the fully spin down states respectively (Eq. 3.18), which do not move due to the SU(2) symmetry in the Heisenberg model:

$$\mathbb{H}\,|I \otimes I\rangle = 0 \quad ; \quad \mathbb{H}\,|\mathcal{Q} \otimes \mathcal{Q}\rangle = 0 \tag{4.4}$$

Now, let's look at the dynamics of local operators, or in other words, compute the OTOC $\mathcal{F}(\chi_r(t), \chi_{r'})$ where the operators are assumed to be symmetrized in each cluster to make computations simpler. Although we can solve this exactly at finite-N, here we will solve this in the large-N limit, using the procedure in Sec. 3.2.6. We perform a similarity transformation on each site, following which the emergent Hamiltonian is also transformed $\mathbb{H} \to \tilde{\mathbb{H}}$. Writing the overall input state as $\psi_{\text{in}}(\vec{m}, t)$, where $\vec{m} = (m_1, \ldots, m_L)$ labels the state in the z-basis on each site, the evolution in the infinite-N limit is given by the Fokker-Planck

equation:

$$\partial_t \psi_{\text{in}}(\vec{m},t) = \tilde{\mathbb{H}}\,\psi_{\text{in}}(\vec{m},t) \to \partial_t \psi_{\text{in}}(\vec{m},t) = -\sum_r \partial_r\big((2m_r - m_{r+1} - m_{r-1})\psi_{\text{in}}(\vec{m},t)\big) \quad (4.5)$$

Hence the evolution of m_r is modelled by a Langevin equation:

$$\partial_t m_r(t) = 2m_r - m_{r+1} - m_{r-1} \implies \partial_t m(r,t) = \partial_r^2 m(r,t) \quad (4.6)$$

The OTOC on the other hand, after the similarity transformation, is simply given by $\mathcal{F} = -2m_{r'}/N$. After the transformation $\xi = 2m_{r'}/N$, the OTOC $(-\xi(r',t))$ is given by the equation:

$$\partial_t \xi(r,t) = \partial_r^2 \xi(r,t) \quad (4.7)$$

It is well known that the OTOC follows diffusive dynamics in a free model, and we have reproduced that result here starting from a microscopic model. Thus, a free model has neither a Lyapunov exponent, nor a butterfly velocity. In what follows, we will add interactions back into the model, reproducing these desired features.

4.2.2 Adding interactions: The FKPP equation

In this section, we will analyze the FKPP equation, which is commonly studied in fields such as population dynamics, crystallography, physiology and plasma physics. To derive this from the microscopic model, we will simply add intra-site interactions to the inter-site free model described in the previous section:

$$\begin{aligned} H(t) &= H_{\text{inter}}(t) + \sum_r H_{\text{intra},r}(t) \\ H_{\text{intra},r}(t) &= g \sum_{i_1<\ldots<i_4} J_{i_1,i_2,i_3,i_4,r}(t)\chi_{i_1,r}\chi_{i_2,r}\chi_{i_3,r}\chi_{i_{q_4},r} \\ H_{\text{inter}}(t) &= i\sum_{r,j,k} K_{r,j,k}(t)\,\chi_{r,j}\,\chi_{r+1,k} \end{aligned} \quad (4.8)$$

The couplings are sourced from the distributions:

$$\begin{aligned}\overline{J_{i_1\ldots,i_4}(t)J_{i'_1\ldots,i'_4}(t')} &= \delta_{i_1 i'_1}\cdots\delta_{i_4 i'_4}\delta\left(t-t'\right)\frac{6}{2N^3}\\ \overline{K_{r,j,k}(t)K_{r',j',k'}(t')} &= \frac{1}{4N}\delta_{j,j'}\delta_{k,k'}\delta_{r,r'}\delta(t-t')\end{aligned} \tag{4.9}$$

Since each of these models have been individually solved for the OTOC ξ in the infinite-N limit (Eq. 3.39), we will write their combined result here:

$$\partial_t\xi = \partial_r^2\xi + 2g^2\xi(\xi^2-1) \tag{4.10}$$

This is a particular instance of the FKPP equation and in the following subsection we will analyze its important properties.

4.2.3 Properties of the FKPP equation

The Fisher-Kolmogorov-Petrovsky-Piskun (FKPP) equation is a non-linear partial differential equation of the form:

$$\partial_t\xi = D\partial_r^2\xi + F(\xi) \tag{4.11}$$

with the constraints $F(0) = F(1) = 0, F'(0) = c > 0$ and $F(v) > 0, F'(1) < c$ for all $0 < v < 1$. To simplify calculations, we will assume that F takes the general form : $F(\xi) = c\,\xi(1-\xi^n)$, which is similar to the one we obtain from the Brownian model. It is well known that at late-times, this equation supports wave-like solutions:

$$\phi = \exp(\lambda_L\left(t - \frac{r}{v_B}\right)) \tag{4.12}$$

The velocity v_B is known as the butterfly velocity in an information theory context. It is also the minimal velocity with which such a wave solution can travel within the FKPP equations. The Lyapunov exponent and butterfly velocity can be computed by plugging the form of the

solution into a linearized equation (around $\xi = 0$):

$$\partial_t \phi = D\partial_r^2 \phi + c\phi \implies v_B = D\frac{\lambda_L}{v_B} + c\frac{v_B}{\lambda_L} \tag{4.13}$$

Now, to find the minima of this function, which will give us the butterfly velocity, we set the derivative of v_B with respect to the ratio λ_L/v_B as zero. This gives us the identity:

$$v_B = 2\sqrt{Dc} \tag{4.14}$$

From this, we can also compute the Lyapunov exponent by using the value of λ_L/v_B at which the minima occurs:

$$\frac{\lambda_L}{v_B} = \sqrt{\frac{c}{D}} \implies \lambda_L = 2c \tag{4.15}$$

where in the implication statement we have used the value of the butterfly velocity in Eq. 4.14. Hence the Lyapunov velocity of the wave-like solution is twice that expected from naive linearization of the equation (or just with the $H_{\text{intra},r}$ term).

The FKPP equation thus obtained from the Majorana model can be obtained by similarly linearizing the equation around the unstable point ($\xi = 1$), and has the following exponents:

$$\lambda_L = 8g^2 \quad ; \quad v_B = 4g \tag{4.16}$$

Although we have derived this interesting phenomenon from a simple microscopic model, in the next section we will see even richer phenomenon, where the wave-like solution is also coupled to the moving charge density background.

4.3 The case with U(1) symmetry : complex Brownian SYK chain

Previous work on random circuits and noisy-driven models has established several related effective classical models of operator dynamics, including biased random walk [50], reaction diffusion process [31] and population dynamics [102]. These classical models are used to fit

and understand experimental data of the OTOC on quantum platforms [24, 103]. The models are obtained by mapping the unitary operator dynamics to a classical stochastic process by disorder average. While this approach is feasible for usual noisy/random models without symmetry, adding charge conservation makes the problem more difficult as it causes quantum coherence to persist at the operator level, even after disorder-averaging (Fig. 4.1(e)). However, such a classical description is important to obtain for charged models, as thermalization in systems with charge conservation has recently become accessible on quantum simulators [104].

The primary mechanism through which charge, or other conserved quantities, can influence operator growth is by confining the access of growing operators to a specific (symmetry) sector of the Hilbert space. In addition, within extended systems, the conservation law leads to transport of local conserved quantities, which couples to the operator dynamics. Therefore the correct semi-classical picture of operator dynamics in the presence of a symmetry should at least contain two dynamical variables, the operator size and the local density of the conserved quantity. In this work, we study operator dynamics in the presence of charge transport. We derive the required semi-classical equations which couple the charge and the operator, that are valid even in inhomogeneous and dynamical charge-density backgrounds:

$$\begin{aligned} \partial_t \rho &= \partial_r^2 \rho \\ \partial_t \xi &= \partial_r^2 \xi + 2g^2 \xi(\xi^2 - \rho(1-\rho)) \end{aligned} \tag{4.17}$$

Here $\rho(r,t)$ is the charge density, which obeys the diffusion equation, while $\xi(r,t)$ is the analog of operator-size in models with symmetries that measures local scrambling of the operator. The dynamics of ξ is described by a diffusion-reaction equation that depends on the dynamical charge density. In particular, the local density bounds the range of ξ from 0 to $\sqrt{\rho(1-\rho)}$. We note that this class of equations has been independently studied in the context of bacterial population growth in diffusive media, where it is denoted as the 'Diffusive Fisher–Kolmogorov equation' [105]. To derive these equations, we use the complex Brownian

SYK model on a lattice with U(1) symmetry.

In this work, we show that the extended complex Brownian model is mapped to a quantum SU(4) spin chain with inter-site Heisenberg coupling and intra-site interaction. In the large N limit, the microscopic quantum model is reduced to the semi-classical equations in Eq. (4.17). We provide a complete picture of the coupled dynamics between operators and charge. Our approach can also be extended to systems with other symmetries.

4.3.1 Summary of the main results

The primary result of our work is captured by Eq (4.17). The equation effectively models the evolution of the OTOC depicted in Eq. (2.1), for a charge-conserving fermionic model defined on a chain (Fig. 4.1(a)). The steps via which this connection is established are:

- To begin, one specifies the charge density on each site r. This fixes the profile of $\rho(r, t = 0)$.

- Because the initial charge on every site has been fixed, the simplest initial operator is the projection operator onto a symmetry sector with a given charge density on every site.

- In models where the charge is conserved on each site, this projector is static. However, once the charge is allowed to flow from site to site, this operator becomes dynamical as well.

- Just as there are multiple states within each charge sector, there are also multiple operators [28]. The variable ξ controls the choice of the operator once the charge is fixed. For example, the maximal value of $\xi = \sqrt{\rho(1-\rho)}$ represents a simple operator such as a projector, while $\xi = 0$ represents a local scrambled operator within the charge sector. This is consistent with $\xi = 0$ being a stable solution of Eq. (4.17), as all simple operators will eventually evolve into the most complex one.

- Fixing both $\rho(t = 0)$ and $\xi(t = 0)$ also completely fixes the initial global operator

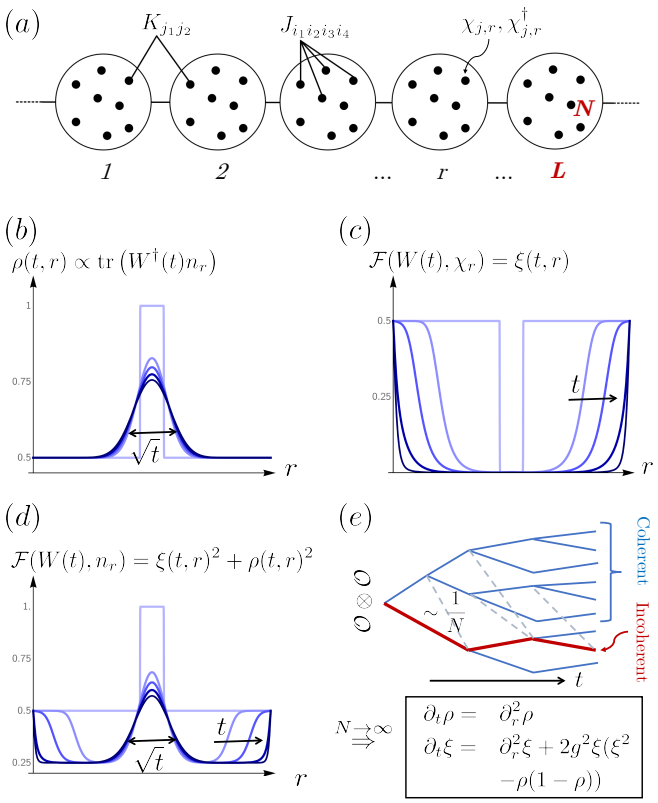

Figure 4.1: (a) The Brownian SYK model with L clusters of N complex fermions, with on-site interaction J and nearest neighbor hopping K. The total fermion number operator $\sum n_{r,i}$ is the conserved operator, leading to a $U(1)$ symmetric circuit. (b-d) The time evolution of charge ρ (b),the OTOC $\mathcal{F}(W(t),\chi_r)$ (c), and OTOC $\mathcal{F}(W(t),n_r)$ (d), when the initial operator W has an initial charge distribution as shown in (b). In each of the graphs the darkness of the plots increases with increasing times. The charge (b) and conserved part of the operator (d) have diffusive behavior, while the OTOC $\mathcal{F}(W(t),\chi_r)$ (c) and the uncharged part of OTOC $\mathcal{F}(W(t),n_r)$ propagates ballistically. (e) Schematic of the time evolution of two copies of the operator, which is involved in the OTOC computation. Due to the $U(1)$ symmetry, the super-operator develops coherence, which makes the hydrodynamic description hard. In this work, we argue that for certain probing operators, the correction from this induced coherence is $1/N$ suppressed. In the $N \to \infty$ limit, we directly obtain the hydrodynamical equations 4.17, which lead to the dynamical evolution in (b-d).

$W(t=0)$ in Eq. (2.1). Hence the operator W carries information about two separate modes, the charge, and the 'complexity' of the operator within the charge subspace. Following this, the operator is evolved using Eq. (4.17), where it is observed that the mode ξ spreads ballistically while ρ is governed by diffusion.

- The evolved operator is then measured via the use of a probing operator V. The choice of whether V is chosen to be a conserved (has overlap with charge) or non-conserved operator determines which modes the OTOC detects:

$$\begin{aligned} \mathcal{F}(t)|_{V=\chi_{r_0}} &= \xi(r_0,t) \\ \mathcal{F}(t)|_{V=n_{r_0}} &= \xi^2(r_0,t) + \rho^2(r_0,t) \end{aligned} \tag{4.18}$$

The operator χ_{r_0} refers to the local creation operator on site r_0 of the chain, while n_{r_0} is the local number operator, which has overlap with the charge. This formalism distinguishes the time-ordered Green's function from the OTOC, as the former can only detect the charged mode and not the fixed-charge operator transitions (Fig. 4.1). It is important to mention that W is a non-local operator as it fixes the initial charge profile (Sec. 4.3.2). This is necessary if one wishes to obtain a precise description of how information dynamics are related to charge dynamics, as local operators do not have a well-defined charge. This is perhaps also related to other works which have observed that locality has non-trivial implications in the presence of symmetries [106]. The equations in Eq. (4.17) correctly reproduce all known features of charged chaotic models, such as the charge-dependent Lyapunov exponent/butterfly velocity [82, 80], and the late-time diffusive tail of the OTOC [77, 78, 75]. Moreover, since they are valid for arbitrary initial charge/operator profile, we simulate the coupled equations in inhomogeneous backgrounds to obtain new phenomena.

The formalism developed in this work encodes the microscopic operator dynamics in terms of transitions between states in a particular irrep of the SU(4) algebra. Since the OTOC is computed on four time-contours, this allows us to track the dynamics of the four

corresponding conserved charges in terms of the weights of the SU(4) algebra, and explains the emergence of the coupled equations describing the OTOC in terms of a single charged mode (ρ) and a non-conserved ballistic mode (ξ). This derivation reveals new features of operator dynamics in the presence of conservation laws. Namely, in contrast with models that do not have continuous symmetries, the operator dynamics in the model with a U(1) symmetry allow for transitions that introduce quantum coherence at the operator level. Therefore, while usual noisy/random models are well described by a classical stochastic process, for U(1) symmetric models the time-evolution of the operator can only be modeled by a probability in a fixed subspace, and in the infinite-N limit, this gives rise to a Fokker-Planck equation which only describes a conserved quantity in the 'incoherent' sector of the operator-states.

4.3.2 Charged operator basis

In this work we will be concerned with computing the OTOC, which can be viewed through the lens of operator spreading. Due to the charge conservation, we work with a specific choice of operator basis. We assume the degrees of freedom are represented by complex fermions, which satisfy the anti-commutation relations:

$$\{\chi_i^\dagger, \chi_j\} = \delta_{ij} \; ; \; \{\chi_i, \chi_j\} = 0$$

The relevant operators we consider are left and right eigen-operators with respect to the U(1) symmetry:

$$\Big(\sum_i n_i\Big) O = q_a O; \quad O\Big(\sum_i n_i\Big) = q_b O \tag{4.19}$$

where ($n = \chi^\dagger \chi$) is the number operator. It can be easily checked that for a model with U(1) conservation, the charges (q_a, q_b) are a constant of motion during the dynamics of the operator string. For a single fermionic operator, we choose the relevant four dimensional

eigen-operator basis and the charges take the following respective values:

$$\chi^\dagger : (1,0) \quad \chi : (0,1) \quad n : (1,1) \quad \bar{n} : (0,0) \tag{4.20}$$

where $\bar{n} = I - n$. Following this insight, we will work with operator strings $\mathcal{S}$ when the system contains N fermions, where each element of the string is picked from the U(1) operator basis defined above:

$$\mathcal{S} = 2^{N/2} s_1 s_2 \cdots s_N, \quad s_i \in \{\chi_i^\dagger, \chi_i, n_i, \bar{n}_i\}. \tag{4.21}$$

This ensures that the entire operator string is also an eigen-operator of the global U(1) symmetry. The factor of $2^{N/2}$ in the string is picked to ensure the following orthogonal and completeness relations

$$\frac{1}{\mathrm{Tr}I}\mathrm{Tr}(\mathcal{S}^\dagger \mathcal{S}') = \delta(\mathcal{S}', \mathcal{S}), \quad \frac{1}{\mathrm{Tr}I}\sum_{\mathcal{S}} \mathcal{S}^\dagger_{mn}\mathcal{S}_{pq} = \delta_{mq}\delta_{np}. \tag{4.22}$$

The procedure to compute the OTOC, on the other hand, begins by rearranging the correlator to write it in the operator state language:

$$\begin{aligned} \mathcal{F}(W(t), V) &= \frac{1}{\mathrm{Tr}I}\mathrm{Tr}(W^\dagger(t)V^\dagger W(t)V) = \mathrm{Tr}I \,\langle \mathrm{out}|\, \mathbb{U} \,|\mathrm{in}\rangle \\ |\mathrm{in}\rangle &= \frac{1}{\mathrm{Tr}I}\sum W^\dagger_{mn} W_{pq} \,|m \otimes n \otimes p \otimes q\rangle \\ |\mathrm{out}\rangle &= \frac{1}{\mathrm{Tr}I}\sum V^\dagger_{mq} V_{pn} \,|m \otimes n \otimes p \otimes q\rangle \\ \mathbb{U} &= U \otimes U^* \otimes U \otimes U^* \end{aligned} \tag{4.23}$$

Hence the computation of the OTOC involves four copies of the Unitary and in a charge-conserving model, four corresponding conserved charges as well. These conserved charges, which we label as (q_a, q_b, q_c, q_d), are the left and right charges of the double-copy of the operator-state involved in the OTOC. Therefore, an exact dynamical description of the OTOC would depend on the evolution of these four independent charges as well.

To complete the formalism and ensure a proper overlap between the input and output

state, we insert the resolution of identity in the output state (Fig. 2.1(a))

$$\begin{aligned} |\text{out}\rangle &= \frac{1}{\text{tr}^2\, I} \sum V^\dagger_{mm'} \mathcal{S}^\dagger_{m'n'} V_{n'n} \mathcal{S}_{pq} |m \otimes n \otimes p \otimes q\rangle \\ &= \frac{1}{\text{tr}^2\, I} \sum_{\mathcal{S}} \left| V^\dagger \mathcal{S}^\dagger V \otimes \mathcal{S} \right\rangle \end{aligned} \tag{4.24}$$

4.3.3 General procedure and emergent SU(4) algebra

The model we work with is the complex Brownian SYK chain, defined through the all-to-all quartic on-site and quadratic two-site interaction Hamiltonians

$$\begin{aligned} H_{\text{intra}} &= g \sum_{i_1,i_2,i_3,i_4,r} J^r_{i_1,i_2,i_3,i_4}(t) \chi^\dagger_{i_1,r} \chi^\dagger_{i_2,r} \chi_{i_3,r} \chi_{i_4,r} + \text{h.c.} \\ H_{\text{inter}} &= \sum_{j_1,j_2,r} K^r_{j_1,j_2}(t) \chi^\dagger_{j_1,r} \chi_{j_2,r+1} + \text{h.c.} \end{aligned} \tag{4.25}$$

where i, j, k, l are indices labelling fermions on each site and r is the site/cluster index. Each cluster contains N fermions and the number of clusters can be chosen to be L. Although we consider the one-dimensional model, the formalism is easily generalized to higher dimensions. The couplings in the Brownian model break the time-translation symmetry and satisfy the constraints

$$\begin{aligned} \overline{J^r_{i_1,i_2,i_3,i_4}(t) J^{r'*}_{j_1,j_2,j_3,j_4}(t')} &= \frac{1}{N^3} \delta_{i_1,j_1} ... \delta_{i_4,j_4} \delta_{r,r'} \delta(t-t') \\ \overline{K^r_{i_1,i_2}(t) K^{r'*}_{j_1,j_2}(t')} &= \frac{1}{N} \delta_{i_1,j_1} \delta_{i_2,j_2} \delta_{r,r'} \delta(t-t') \end{aligned} \tag{4.26}$$

Hence the couplings are uncorrelated at different times, and this property makes the Brownian model more analytically and numerically tractable. The on-site Hamiltonian discussed above conserves charge on each site, whereas the inter-site term facilitates the flow of charge between clusters but preserves the global charge. The inter-site model is also chosen to be non-interacting, in contrast to its intra-site counterpart which scrambles quantum information within each cluster. In this work we will precisely explore this interplay between transport and scrambling.

After disorder averaging, the composite unitary $\mathbb{U}$ in Eq. (4.23) for the Brownian model is mapped to an emergent Hamiltonian $\mathbb{H}$ which evolves in imaginary time

$$\overline{\mathbb{U}} = \overline{U^a U^{b*} U^c U^{d*}} = e^{\mathbb{H}t}. \tag{4.27}$$

Here we have labelled individual time-contours by the labels a, b, c, d. For complex fermionic models, after the disorder average, each copy is occupied by anti-commuting fermions after a Jordan-Wigner like transformation

$$\{\psi^{\dagger\alpha}_{i,r}, \psi^{\beta}_{j,r'}\} = \delta_{i,j}\delta_{\alpha,\beta}\delta_{r,r'}; \quad \alpha, \beta = a, b, c, d \tag{4.28}$$

The details of this transformation are present in the appendix. An important point to note is that we have performed a particle-hole transformation on replicas b and d, for future mathematical convenience. While for general fermionic models this procedure does not make computations simpler, one can show that for the Brownian SYK models considered in this work, the emergent Hamiltonian can be written purely in terms of permutation symmetric inter and intra replica number operators which are the generators of the SU(4)$\otimes$U(1) algebra:

$$\begin{aligned} &\mathbb{H} = \mathbb{H}(S^{\alpha\beta}_r); \quad S^{\alpha\beta}_r = \sum_i \psi^{\dagger\alpha}_{i,r}\psi^{\beta}_{i,r}, \quad \alpha, \beta = a, b, c, d \\ &[S^{\alpha\beta}_r, S^{\gamma\sigma}_r] = \delta^{\beta\gamma} S^{\alpha\sigma}_r - \delta^{\alpha\sigma} S^{\beta\gamma}_r. \end{aligned} \tag{4.29}$$

The 16 generators $S^{\alpha\beta}_r$ can be split into the 15 generators of SU(4) plus one given by $\sum_\alpha S^{\alpha\alpha}_r = Q_r$ which forms the U(1) part of the algebra and commutes with the SU(4) generators. Hence we have exactly mapped the dynamics of a Brownian all-to-all interacting model to the dynamics of an SU(4) spin chain that evolves in imaginary time. As an example, for the free-model, i.e. H_{inter} term in Eq. (4.25), the emergent Hamiltonian takes

the form of the SU(4) Heisenberg model:

$$\mathbb{H}_{\text{inter}} = \frac{1}{N}\Big(\sum_{\alpha,\beta,r} S_r^{\alpha\beta} S_{r+1}^{\beta\alpha} - N\sum_r Q_r\Big) \tag{4.30}$$

This has an appealing format, as it makes the global SU(4) invariance of the emergent model manifest. Models that have interactions, on the other hand, will lack this exact symmetry. However, if the model has global charge conservation, it will be reflected in terms of global weight conservation in the emergent SU(4) spin model. In other words, while the emergent Hamiltonian corresponding to the free model commutes with all global SU(4) operators and is therefore SU(4) symmetric, more general models, which conserve charge but have interactions, will only commute with the Cartan-subalgebra and conserve weights.

Physically, the structure of charges in terms of weights can be understood as follows: Each replica has its own copy of the globally conserved charge labelled by $\sum_r (S_r^{aa}, N - S_r^{bb}, S_r^{cc}, N - S_r^{dd}) = \sum_r (q_{a,r}, q_{b,r}, q_{c,r}, q_{d,r})$ respectively, where the $S_r^{\alpha\alpha}$ operators are defined in Eq. (4.29). The physical charge is counted differently on replicas b, d due to the particle-hole transformation (App. B.1). On the right hand side of the equation, q_r's are essentially the left and right charges of the two copies of the operator on each site, as defined in Eq. (4.19). However, not all four of them are independent as the Brownian nature of the model fixes the sum $\sum_\alpha S_r^{\alpha\alpha} = Q_r$, which forms the U(1) part of the algebra. For example, for the irrep $(0, N, 0)$, we have a fixed $Q = 2N$ as it commutes with all generators of the SU(4) algebra. The remaining three charges can be mapped to the three weights of the SU(4) algebra, which will be made more precise in the next section.

4.3.4 Map from operator strings to SU(4) basis

For a single complex fermion, the four copies a, b, c, d together span a 16 dimensional Hilbert space, which can be thought of as the double-copy of four-dimensional operator basis. For the Brownian model, as discussed in the previous section, the emergent Hamiltonian is composed of SU(4) operators, which suggests that the corresponding states should be viewed

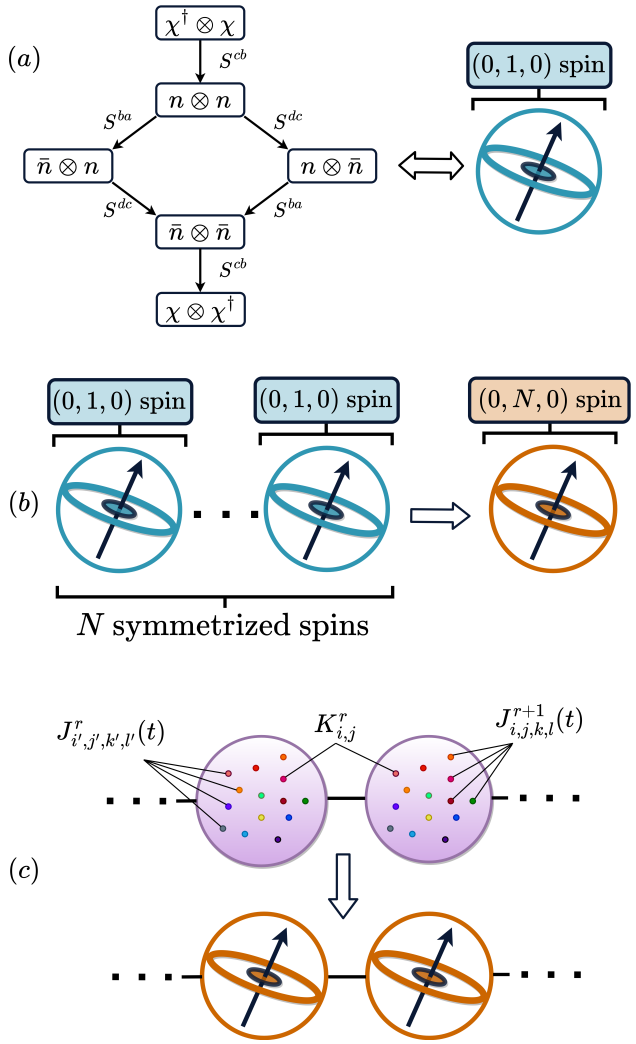

Figure 4.2: (a) The SU(4) representation $(0, 1, 0)$ for the relevant operator-states corresponding to a single fermion, along with the rules that govern transitions between the operator-states. Here $\bar{n} = I - n$ is the operator orthogonal to the number operator n. (b) The emergence of the SU(4) spin $(0, N, 0)$ as the permutation-symmetric combination of N fermions within each cluster in the Brownian SYK chain. (c) After disorder average, each cluster in the chain maps to a $(0, N, 0)$ spin, and in this work we consider the limit of infinite-N.

in terms of the representations of the algebra. The 16 states split into irreps as:

$$\mathbf{16} = \mathbf{1} \oplus \mathbf{4} \oplus \mathbf{6} \oplus \bar{\mathbf{4}} \oplus \mathbf{1}. \tag{4.31}$$

In this work, we will be concerned with the **6** or in fundamental weight notation, the $(0, 1, 0)$ irrep, as it contains the operators of interest. The states in this irrep are listed in Fig. 4.2(a), along with how the SU(4) operators act on them. This six-dimensional operator space is similar to the one presented in [78].

Now we will move on to the discussion of representations which involve multiple fermions. As is well known, for SU(n) with $n > 2$, there are $n-1$ weights and multiple states with the same weights in an irrep, hence states cannot be uniquely labeled by just using the Casimir and the weights. To study the large-N dynamics, we will therefore begin by discussing the basis labeling the states on each site in the SU(4) spin chain. The scheme to label the states relies on Gelfand-Tsetlin patterns, where 10 numbers are used to label each state within each SU(4) irrep [99]:

$$\begin{pmatrix} m_{1,4} & & m_{2,4} & & m_{3,4} & & m_{4,4} \\ & m_{1,3} & & m_{2,3} & & m_{3,3} & \\ & & m_{1,2} & & m_{2,2} & & \\ & & & m_{1,1} & & & \end{pmatrix}$$

The numbers have to satisfy the constraint:

$$m_{k,l} \geq m_{k,l-1} \geq m_{k+1,l}$$

in order to represent a valid GT-pattern. In this work, we will fix the irrep on each cluster to be $(0, N, 0)$, which is the unique permutation symmetric tensor composition of N $(0, 1, 0)$

irreps (Fig. 4.2(b)).

$$\underbrace{(0,1,0)\otimes ...\otimes (0,1,0)}_{N \text{ times}} = (0,N,0)\oplus \underbrace{(1,N-2,1)}_{N-1 \text{ copies}}\oplus ..., \tag{4.32}$$

Physically, this corresponds to restricting the operator-strings of N fermions on each cluster to be permutation symmetric among the indices which label the fermions. This is justifiable for two reasons, firstly, it is expected that in the case of scrambling dynamics, the non-symmetric operator-strings will decay exponentially fast, leaving behind only the symmetric strings after a short time. Secondly, it has also been shown that features such as Lyapunov growth and the scrambled steady-state are entirely contained within this symmetric irrep, making it the only relevant sector to study the chaotic behavior of the model [28]. For the Brownian model, starting from a symmetric operator-string completely restricts the dynamics to the symmetric sector, which can be seen from the emergent algebra structure.

Fixing the irrep also completely fixes the first row of the GT-pattern to

$$(m_{1,4}, m_{2,4}, m_{3,4}, m_{4,4}) = (N, N, 0, 0) \tag{4.33}$$

Along with this, the entries $m_{1,3} = N, m_{3,3} = 0$ are also fixed due to the constraints of the GT-pattern. This leaves us with four variables on each site r, which can be understood in terms of the SU(4) algebra as the three independent weights $w_{1,r}, w_{2,r}, w_{3,r}$ plus an index n_r which labels the state within each fixed-weight subspace.

$$\begin{pmatrix} N & & N & & 0 & & 0 \\ & N & & w_{1,r} & & 0 & \\ & & w_{2,r}-n_r & & n_r & & \\ & & & w_{3,r} & & & \end{pmatrix} \equiv |w_{1,r}, w_{2,r}, w_{3,r}, n_r\rangle \tag{4.34}$$

As has been discussed in the previous section, the four emergent charges on the four time-contours $(q_{a,r}, q_{b,r}, q_{c,r}, q_{d,r})$ map to the three weights of the SU(4) algebra plus one overall

total charge, which is not dynamical once the irrep is fixed. The variables $w_{1,r}, w_{2,r}, w_{3,r}$ encode the three remaining dynamical charges, and the variable n_r controls the fluctuations within each fixed-weight sector, i.e. it represents the dynamics of the operator within a fixed charge subspace. The weights are related to the physical charges on the four contours in the following way:

$$\begin{aligned} q_{a,r} &= w_{3,r}\,;\; q_{b,r} = N - w_{2,r} + w_{3,r} \\ q_{c,r} &= N - w_{2,r} + w_{1,r}\,;\; q_{d,r} = w_{1,r} \end{aligned} \tag{4.35}$$

4.3.5 Quantum operator coherence due to U(1) symmetry

This section will be devoted to the comparison of operator dynamics in Brownian models with and without charge conservation. An example of a model without charge conservation is the Brownian SYK model built with Majorana fermions. The operator transitions in such a model strictly follow the general rule:

$$|O_1^\dagger \otimes O_1\rangle \to |O_2^\dagger \otimes O_2\rangle \tag{4.36}$$

Such transitions can be seen as 'incoherent' when translating from the operator state to super-operator language:

$$|O_1 \otimes O_2^\dagger\rangle \to |O_1\rangle \langle O_2| \tag{4.37}$$

which means that diagonal elements in the super-operator can only transition to other diagonal elements. This general rule is also compatible with the parity symmetry in the Majorana model, which restricts all operators of the form $|O^\dagger \otimes O\rangle$ to one symmetry sector since all such operators have even parity [28].

On the other hand, in the complex model, only a part of the symmetry-resolved emergent Hilbert space consists of incoherent operator-states (Fig. 4.2). Specifically, the operator-states $|\bar{n} \otimes n\rangle$ and $|n \otimes \bar{n}\rangle$ break the incoherence. Requiring this incoherence in the operator-state forces the charges to obey the necessary constraints $q_{a,r} = q_{d,r}, q_{b,r} = q_{c,r} \implies w_{1,r} =$

$w_{3,r}$, which in general is not true for a random state in the Hilbert space. One can use the information in Fig. 4.2 to reproduce the following transition generated by a global-charge conserving operator $S_1^{ca}S_2^{ac}$ on an operator string over 2 fermions:

$$S_1^{ca}S_2^{ac}\,|\chi_1^\dagger\chi_2 \otimes \chi_1\chi_2^\dagger\rangle \to |\bar{n}_1 n_2 \otimes n_1\bar{n}_2\rangle\,. \tag{4.38}$$

This can be viewed as a toy model with two sites and one fermion per site. The operator $S_1^{ca}S_2^{ac}$ is one of the terms in the emergent Hamiltonian corresponding to the hopping term in Eq. (4.25), which conserves charge over the two fermions. Even though the transition conserves the four global charges $(q_a, q_b, q_c, q_d) = (1, 1, 1, 1)$ of the entire operator-string, it introduces operator coherence on each fermion, which means the operators on the right hand side cannot be written in the form $|O^\dagger \otimes O\rangle$ and the corresponding super-operator develops off-diagonal entries. This insight distinguishes the cases with and without charge conservation, and also explicitly affects the large-N hydrodynamics of the operators. In this work, we will utilize permutation symmetric operator-states on each site, which are chosen from the irrep $(0, N, 0)$, and labelling the states as incoherent is equivalent to the condition $w_{1,r} = w_{3,r}$.

4.3.6 The large-N formalism and the 'restricted' Fokker-Planck equation

The strategy to obtain the large-N hydrodynamical equations of motion relies on a similarity transformation that turns the effective Hamiltonian $\mathbb{H}$ into a (partially) stochastic matrix. As can be seen from Fig. 2.1, the operator-state $\sum_{\mathcal{S}} |\mathcal{S}^\dagger \otimes \mathcal{S}\rangle$ is an exact eigenstate of $\mathbb{H}$ due to the unitary nature of the underlying dynamics:

$$\mathbb{H}\sum_{\mathcal{S}} |\mathcal{S}^\dagger \otimes \mathcal{S}\rangle = 0. \tag{4.39}$$

This steady-state represents the late-time distribution of an initially simple operator under scrambling dynamics. For non-conserved local operators which have overlap with this state,

all other states which are orthogonal to the steady-state decay to zero at late time, due to the chaotic nature of the Brownian model. The steady-state can be resolved into different charge sectors, where each component acts as a scrambled steady-state for the specific charge sector (App. B.2). Thus, when starting from a specific charge sector, the operator evolves into the charge-resolved steady-state at late times, which also signals the decay of the OTOC. The full steady state on the chain can be written as a product state of the steady state on every site r:

$$\sum_{\mathcal{S}} |\mathcal{S}^\dagger \otimes \mathcal{S}\rangle = \bigotimes \sum_{\mathcal{S}_r} |\mathcal{S}_r^\dagger \otimes \mathcal{S}_r\rangle \tag{4.40}$$

In the GT-pattern basis, this steady-state on each site is written as:

$$\begin{aligned} \sum_{\mathcal{S}_r} |\mathcal{S}_r^\dagger \otimes \mathcal{S}_r\rangle &= \sum_{w_{1r},w_{2r},n_r} c_{w_{2r},n_r} \, |w_{1r}, w_{2r}, w_{3r} = w_{1r}, n_r\rangle \\ c_{w_{2r},n_r} &= \sqrt{\frac{(w_{2r}+1-2n_r)}{N+1}\binom{N+1}{N-(w_{2r}-n_r)}\binom{N+1}{n_r}} \end{aligned} \tag{4.41}$$

One can understand the restriction $w_{1r} = w_{3r}$ here from the perspective that the steady state $\sum_{\mathcal{S}_r} |\mathcal{S}_r^\dagger \otimes \mathcal{S}_r\rangle$ is strictly within the incoherent subspace of the larger Hilbert space. However, fixing $w_{1r} = w_{3r}$ is merely the necessary condition to obtain the state, whereas the sufficient condition involves also specifying the correct coffecients c_{w_{2r},n_r}. Following this, we define a diagonal matrix $\mathbb{S}_r$ with the entries:

$$\langle w_{1r}, w_{2r}, w_{3r}, n_r| \, \mathbb{S}_r \, |w_{1r}, w_{2r}, w_{3r}, n_r\rangle = c_{w_{2r},n_r} \tag{4.42}$$

We use the matrix $\mathbb{S}_r$ to perform a similarity transformation in Eq. (4.23)

$$\begin{aligned} \langle \text{out}| \, e^{\mathbb{H}t} \, |\text{in}\rangle &= \langle \tilde{\text{out}}| \, e^{\tilde{\mathbb{H}}t} \, |\tilde{\text{in}}\rangle \\ \tilde{\mathbb{H}} = \mathbb{S}\mathbb{H}\mathbb{S}^{-1} \, ; \, |\tilde{\text{in}}\rangle = \mathbb{S} \, |\text{in}\rangle \; ; \; |\tilde{\text{out}}\rangle &= \mathbb{S}^{-1} \, |\text{out}\rangle \end{aligned} \tag{4.43}$$

The global transformation $\mathbb{S}$ is the tensor product of local transformations $\mathbb{S}_r$. This procedure has a two-fold advantage. Firstly, it removes the non-uniform N-dependence usually contained in the output state. As an example, if the probing operator V in the OTOC is chosen to be the identity, the output state is the resolution of identity, meaning the steady state in Eq. (4.41). Hence the output state will contain combinatorial factors, which are not compatible with a continuum analysis. The Similarity transformation strips away these factors and makes the output state amenable to a large-N expansion. Secondly, due of the choice of the Similarity matrix $\mathbb{S}$, the coefficients of the steady state corresponding to the resolution of identity (from the left) all become 1, and hence the transformed Hamiltonian obeys the equation

$$\sum_{\vec{w}_1,\vec{w}_2,\vec{n}} \tilde{\mathbb{H}}_{(\vec{w}_1,\vec{w}_2,\vec{w}_3=\vec{w}_1,\vec{n}),(\vec{w}'_1,\vec{w}'_2,\vec{w}'_3=\vec{w}'_1,\vec{n}')} = 0 \tag{4.44}$$

due to having a uniform left eigenvector. Here the vectors $\vec{w}_i, \vec{n}$ have components $(w_{i,r}, n_r)$ over the space of all sites r. Therefore the matrix $\tilde{\mathbb{H}}$ has become stochastic, but only in the sector $\vec{w}_1 = \vec{w}_3$ that contains the full steady state. This can be contrasted with the Majorana and spin version of the model, where the steady state occupies the entire Hilbert space and therefore the entire emergent Hamiltonian can be made stochastic [31, 107, 33, 28]. The stark difference between these two scenarios is precisely a consequence of the U(1) symmetry in the complex model. We write the inner product which governs the OTOC in the wavefunction notation:

$$\langle \tilde{\text{out}}| \, e^{\tilde{\mathbb{H}}t} \, |\tilde{\text{in}}\rangle = \sum_{\vec{w}_1,\vec{w}_2,\vec{w}_3,\vec{n}} \psi_{\text{out}}(\vec{w}_1,\vec{w}_2,\vec{w}_3,\vec{n})\psi_{\text{in}}(\vec{w}_1,\vec{w}_2,\vec{w}_3,\vec{n},t) \tag{4.45}$$

where the input state is evolved using the emergent Hamiltonian

$$\partial_t \psi_{\text{in}}(\vec{w}_1,\vec{w}_2,\vec{w}_3,\vec{n},t) = \sum_{\vec{w}'_1,\vec{w}'_2,\vec{w}'_3,\vec{n}'} \tilde{\mathbb{H}}_{(\vec{w}_1,\vec{w}_2,\vec{w}_3,\vec{n}),(\vec{w}'_1,\vec{w}'_2,\vec{w}'_3,\vec{n}')} \psi_{\text{in}}(\vec{w}'_1,\vec{w}'_2,\vec{w}'_3,\vec{n}',t) \tag{4.46}$$

Due to the (partially) stochastic nature of $\tilde{\mathbb{H}}$, $\psi_{\rm in}$ behaves as a probability distribution, but only in the incoherent sector, and therefore

$$\partial_t\big(\sum_{\vec{w}_1,\vec{w}_2,\vec{n}} \psi_{\rm in}(\vec{w}_1,\vec{w}_2,\vec{w}_3=\vec{w}_1,\vec{n},t)\big)=0 \tag{4.47}$$

This will be explicitly reflected in the large-N equation we obtain. We now follow the standard operating procedure and expand the SU(4) operators in $\mathbb{H}$, in the large-N limit. The explicit matrix elements of simple raising/lowering operators in SU(n) are known in the GT-pattern basis [99]. For the purpose of expanding the operators, we use the variables

$$\begin{aligned} w_{1r}-w_{3r}&\to 2Nv_r, \quad w_{2r}\to Ny_r,\\ w_{1r}+w_{3r}&\to 2N\rho_r, \quad n_r\to Nu_r. \end{aligned} \tag{4.48}$$

The resulting equation, which is the continuum version of Eq. (4.46), can be written in the form of a 'restricted' Fokker-Planck as follows:

$$\partial_t\psi_{\rm in}=\sum_r \beta_r\psi_{\rm in}+\alpha_{v_r}\partial_{v_r}\psi_{\rm in}+\partial_{u_r}(\alpha_{u_r}\psi_{\rm in})+\partial_{\rho_r}(\alpha_{\rho_r}\psi_{\rm in})+\partial_{y_r}(\alpha_{y_r}\psi_{\rm in}) \tag{4.49}$$

The explicit expressions for the functions α,β depend on the underlying model, but the 'restricted' nature of the equation is always valid. As one can immediately check, $\int\psi_{\rm in}$ is not conserved due to the β_r and α_{v_r} terms as they are not total derivative terms [2]. However, they satisfy the important property:

$$\beta_r|_{\vec{v}=0}=0, \quad \alpha_{v_r}|_{\vec{v}=0}=0 \tag{4.50}$$

for all r. Therefore, $\int\delta(\vec{v})\psi_{\rm in}$ is conserved, which is expected from Eq. (4.47) because $\vec{v}=0$ restricts to the incoherent sector. In what follows, we can restrict our analysis to this sector by

[2]For models that conserve charge on each site, there is no α_{v_r} term due to the corresponding weight conservation.

choosing an output state strictly contained in it, since the overlap (and therefore the OTOC) will be blind to growth of the input state outside the sector. For example, choosing $V = {\chi_{r_0}}^3$ will satisfy this criterion, since $v_{r_0} = 1/N$ for the resulting output state and therefore it is in the sector to leading order in the infinite-N limit. Hence we impose the condition $\vec{v}_r = 0$ on the 'restricted' Fokker-Planck by starting with an input state sufficiently well localized around $\vec{v} = 0$ and obtain Langevin equations for the variables y_r, ρ_r, u_r (Appendix B.3). Since the input state is chosen to be localized functions which evolve according to these Langevin equations, the OTOC will be given by:

$$\mathcal{F}(t) = \psi_{\text{out}}(y_r(t), \rho_r(t), u_r(t)) \tag{4.51}$$

4.3.7 The OTOC at large N

This section will be devoted to the study of the OTOC in the large-N limit. We will probe various cases of the OTOC, such as when the dynamics are driven by interacting vs non-interacting Hamiltonians. We will also study how the behavior of the OTOC changes with the choice of operators involved. Before we discuss specific models, it is beneficial to recast the variables y_r, ρ_r in terms of the more 'physical' left and right charges ρ_a and ρ_b defined in Sec. 4.3.2:

$$\rho_{a,r} = \rho_r \; ; \; \rho_{b,r} = 1 - y_r + \rho_r \tag{4.52}$$

This relation is true in the incoherent sector ($w_{1,r} = w_{3,r}$) as can be seen from the equations Eq. (4.35) and Eq. (4.48). Choosing the probing operator as $V = \chi_{r_0}$ means that the output state after the similarity transformation and in the continuum limit becomes:

$$\sqrt{(1 - \rho_{b,r} - u_r)(\rho_{a,r} - u_r)} = \xi_r \; ; \; \psi_{\text{out}} = \xi_{r_0} \tag{4.53}$$

[3]We suppress the fermionic index and only display the cluster/site index since it is assumed that this operator will be restricted to the symmetric irrep, and therefore will be symmetrized between all the fermions in the cluster.

where we transform to the variable $u_r \to \xi_r$ at every site, in which case the OTOC is captured by the variable $\mathcal{F}(t) = \xi_{r_0}(t)$. The input operator W on the other hand, is determined by fixing the initial value of $\xi_r, \rho_{a,r}$ and $\rho_{b,r}$ on every site.

4.3.7.1 Free-fermionic chain

In this section we will discuss the large-N analysis for the free-fermion complex brownian SYK chain, namely the H_{inter} term in Eq. (4.25). For this strictly non-interacting case, the emergent Hamiltonian is simply the SU(4) Heisenberg model:

$$\mathbb{H}_{\text{inter}} = \frac{1}{N}\Big(\sum_{\alpha,\beta,r} S_r^{\alpha\beta} S_{r+1}^{\beta\alpha} - N \sum_r Q_r \Big) \tag{4.54}$$

and is therefore SU(4) invariant. This property can be used to exactly solve the OTOC even at finite N (Appendix B.4.2). In the new co-ordinates ξ, ρ_a, ρ_b, we write down the restricted Fokker-Planck for the model and the corresponding equations of motion (Langevin equation) are:

$$\partial_t \rho_a = \partial_r^2 \rho_a; \quad \partial_t \rho_b = \partial_r^2 \rho_b; \quad \partial_t \xi = \partial_r^2 \xi \tag{4.55}$$

As a reminder, the charges ρ_a and ρ_b are the left and right continuum charge densities of the charges q_a and q_b in Eq. (4.19) and ξ measures the OTOC. Here we have treated r as a continuous variable. Notice that since we have restricted to the incoherent sector, the four emergent charges on the time-contours of the OTOC are not all independent and have collapsed into just two separate charges. We see some important features of the free fermionic chain from these equations of motion. The first observation is that the charges ρ_a, ρ_b completely decouple from the OTOC ξ. Secondly, all three quantities show diffusive behavior, which is expected for the two charges from the global charge conservation, and for the OTOC due to the non-interacting nature of the underlying model.

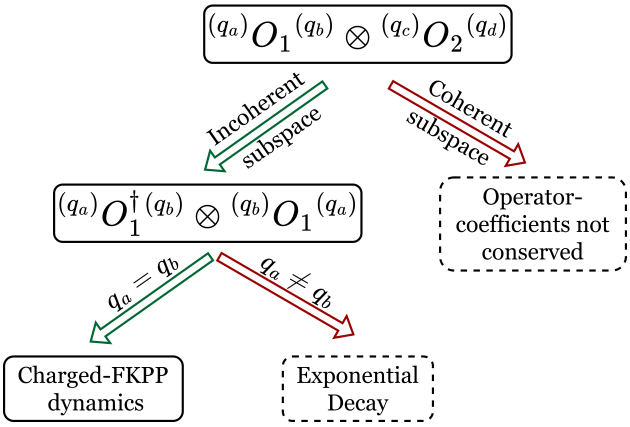

Figure 4.3: Figure depicts the reduction of four charges involved in the computation of the OTOC, to a single charged mode. An operator-state of the form $O_1 \otimes O_2$, where each operator has two associated charges, has to be restricted to the incoherent subspace ($q_c = q_b$; $q_d = q_a$) in order for its coefficients to represent a conserved probability distribution. This reduces the four charges to two. Following this, the sector $q_a \neq q_b$ represents dynamics with pure exponential decay (as seen from Eq. (4.56)). Restricting to the single charge ($q_a = q_b$) sector enables the operator to show interesting dynamics such as Lyapunov growth and butterfly velocity.

4.3.7.2 Charge-dependent FKPP equation

Adding interactions to the model, i.e. $H = H_{\text{inter}} + H_{\text{intra}}$, does not change the nature of the charge transport, as the added on-site interaction conserves charge on each site. However, this does change the behavior of the OTOC as the interaction term scrambles quantum information within each cluster. We write the equation obtained for ξ in terms of the left(ρ_a) and right(ρ_b) charge densities as follows:

$$\begin{aligned} \partial_t \xi &= g^2 \xi(2\xi^2 - \rho_a(1-\rho_a) - \rho_b(1-\rho_b)) + \partial_r^2 \xi \\ \partial_t \rho_{a/b} &= \partial_r^2 \rho_{a/b} \end{aligned} \tag{4.56}$$

In general, the term proportional to g^2 hosts two roots, $\xi = 0$ which is a stable solution and $\xi = \sqrt{(\rho_a(1-\rho_a) + \rho_b(1-\rho_b))/2}$ which is an unstable zero. However, one can obtain the physical range of ξ by in turn determining the range of $n \to Nu$ through the constraints on the GT-pattern (Eq. (4.34)) and also remembering the coordinate transformation in

Eq. (4.53):

$$0 \leq \xi \leq \min(\sqrt{\rho_a(1-\rho_b)}, \sqrt{(1-\rho_a)\rho_b})$$

Thus, when $\rho_a \neq \rho_b$, the physically maximal allowed value of ξ is smaller than the unstable solution of the non-linear term in Eq. (4.56). Therefore in this case, regardless of the initial profile of ξ, the non-linear term will be negative and the solution on every site will exponentially decay till it reaches the stable solution $\xi = 0$. Physically, the stable root corresponds to the charge-resolved fully scrambled state $\sum_{\mathcal{S}} |\mathcal{S}^\dagger \otimes \mathcal{S}\rangle$. The unstable root on the other hand is not a physical solution in general because it would physically correspond to the vanishing of the identity operator under the emergent Hamiltonian (Fig. 2.1). For $\rho_a \neq \rho_b$, however, the charge sector does not host a component of the Identity (App. B.2). Therefore, the maximal allowed value of ξ is not a solution and only the stable solution is physical. Hence no butterfly velocity or Lyapunov growth is observed when $\rho_a \neq \rho_b$. In terms of operators, the maximal value of ξ in such a sector corresponds to a string with a large number of χ or $\chi^\dagger$, which means the strings are 'far away' from any component of the identity and therefore have very high energy (in terms of magnitude) with respect to the emergent Hamiltonian.

Now we will analyze the situation when $\rho_a = \rho_b$. Due to their equations of motion being structurally identical, $\partial_t(\rho_a - \rho_b) = 0$ and we can conclude that starting with this condition will fix it for all time. For the charge sector where $\rho_a = \rho_b = \rho$, the coupled equations become:

$$\partial_t \rho = \partial_r^2 \rho \ ; \ \partial_t \xi = 2g^2 \xi(\xi^2 - \rho(1-\rho)) + \partial_r^2 \xi. \tag{4.57}$$

This charge-dependent FKPP equation is one of the primary results of our work, which summarizes the effect of charge conservation on the OTOC. To briefly recap, we originally started with four variables, namely, three weights which represent charges on the OTOC-contour and one variable describing operator fluctuations within fixed-charge subspaces. One charge was fixed by requiring incoherence of the operators. Finally, we set the left and right

charges to be equal to obtain the above equation describing the charge-dependent OTOC in terms of a single charged mode. This reduction in charges is depicted in Fig. 4.3. For the rest of this work, we will assume the use of the condition $\rho_a = \rho_b$.

4.3.7.3 Constant charge density

When ρ is constant, the physically maximal allowed of ξ, $\sqrt{\rho(1-\rho)}$, corresponds to the unstable solution of the FKPP-equation. The equation therefore supports travelling wave solutions $\xi(r,t) = f(r - v_B t)$ with minimal velocity v_B when one starts with a source which is sufficiently well localized. Along with this, there is exponential growth of the field with Lyapunov exponent λ_L ahead of the wave-front. The butterfly velocity and Lyapunov exponent can be computed as

$$\begin{aligned} \lambda_L &= 8g^2\rho(1-\rho) \\ v_B &= 4g\sqrt{\rho(1-\rho)} \end{aligned} \tag{4.58}$$

in terms of the charge density. Let's analyze these results in terms of operator-strings. The sector $\rho_a = \rho_b$ hosts null-eigenstates corresponding to the charge resolution of the identity $I_{q,N}$ (App. B.2), and starting from a state 'near' $\xi = \sqrt{\rho(1-\rho)}$ corresponds to these operator-strings, which contain mostly n and $\bar{n}$ and very few $\chi^\dagger$ and χ. These strings constitute the ground states of the emergent Hamiltonian, and perturbations to this ground state grow exponentially fast at early times and allow the solution to move with a well-defined velocity across the chain. The number of n's in the said string determines the value ρ, and therefore also the speed of the butterfly velocity and the rate of exponential growth. On the other hand, the stable solution $\xi = 0$ represents the charge-resolved, fully scrambled steady-state, i.e. $\sum_{\mathcal{S}} |\mathcal{S}^\dagger \otimes \mathcal{S}\rangle$ restricted to the region $\rho_a = \rho_b = \rho$.

4.3.7.4 Charge-transport and late-time behavior

So far we have considered the operator χ_{r_0}, which means that the OTOC is given by the variable $\mathcal{F} = \xi_{r_0}(t)$. This ensures that the OTOC decays to 0, which is related to the fact that the operator χ_{r_0} has zero overlap with the charge. In this case, the late-time behavior

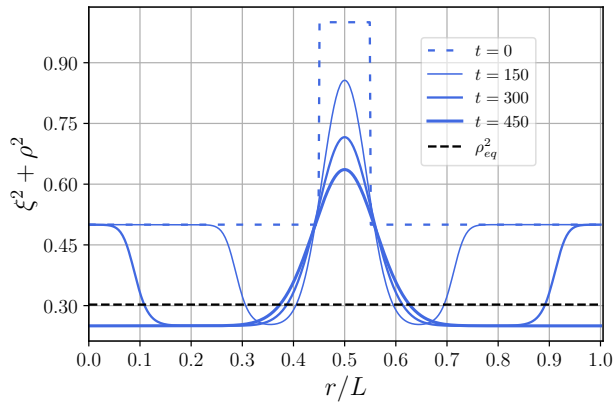

Figure 4.4: The function $\xi^2+\rho^2$, which corresponds to the OTOC when the probing operator is $V = n_{r_0}$, is plotted at equal time-intervals. In this scenario, we start with $\rho = 1/2$ at every site except near the center where we place $\rho = 1$ for sites $0.45 \leq r/L \leq 0.55$. The variable ξ starts with its maximal value given by $\xi(t = 0) = \sqrt{\rho(1-\rho)}$ on every site. We also impose open boundary conditions and set $2g^2 = 0.1$. The two equations in Eq. (4.57) are then simulated and we observe that while a part of the function corresponding to the non-conserved ξ expands ballistically, the conserved part ρ spreads out diffusively near the center. This slower mode controls the late-time behavior after the ballistic part has travelled across the chain, as can be seen from the $t = 450$ time-step. The OTOC relaxes diffusively to the equilibrium value given by $\rho^2_{eq} \sim 0.3$ (the dashed black line) at very late times.

of the OTOC is always determined by the non-linear term in the FKPP equation, which is represented by an exponential decay.

In contrast, fixing the probe operator in the OTOC to be $V = n_{r_0}$ modifies the output state and makes it so that the OTOC is given by $\mathcal{F} = \xi^2_{r_0}(t)+\rho^2_{r_0}(t)$. This function is plotted in Fig. 4.4, where we start with an initial charge-profile which is non-uniform. We observe that there is a mode, which does not have overlap with the charge, that travels ballistically as well a charged mode which is 'left-behind' near the center [77, 78]. Since the equations of motion (Eq. (4.57)) remain unchanged, the OTOC does not decay to 0, but instead at late-times is determined by the equilibrium value of the charge-distribution. In such a scenario, the late-time behavior of the OTOC is controlled by the nature of the charge-transport, since ρ decays slower than ξ and is therefore the dominant mode at late times. As an example, generalizing the model in this work to d spatial dimensions will cause the charge to decay

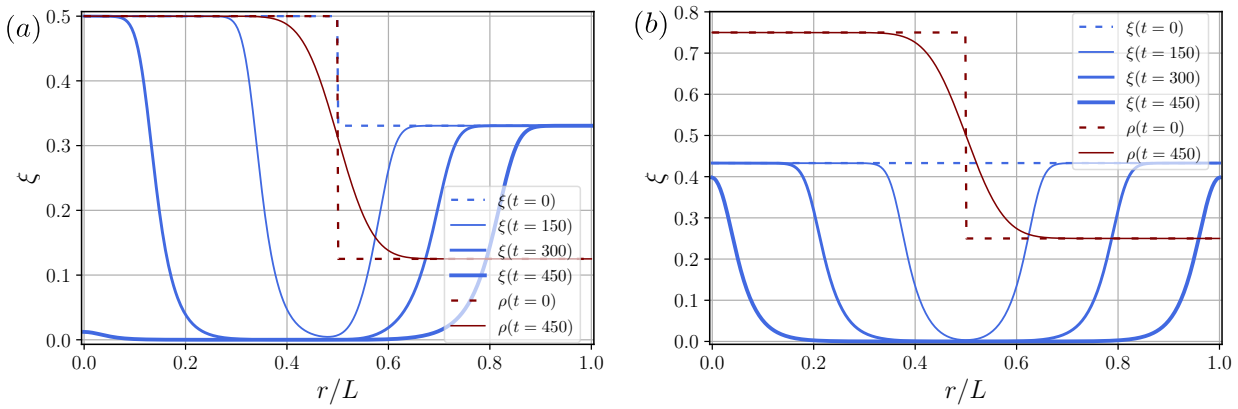

Figure 4.5: The solutions of Eq. (4.57) are plotted for two different charge profiles. We start with the maximally allowed value of $\xi(t=0) = \sqrt{\rho(1-\rho)}$ and impose open boundary conditions in both cases, along with the condition $2g^2 = 0.1$. In (a), a charge domain wall is used with density $1/2$ on the left and $1/8$ on the right. This causes the operator to acquire an asymmetric velocity which is evident when observing the wavefront at equal time-intervals. In (b), the left and right charge densities are $3/4$ and $1/4$ respectively, causing the operator to have a flat profile which is static by itself. However, the melting of the domain-wall at early times forces the operator to have dynamics, even though it has zero overlap with the charge.

diffusively with the power-law $\sim t^{-d/2}$, which will therefore be the late-time behavior of the OTOC as well. This explains the observed behavior of the OTOC studied in similar models with U(1) conservation [75, 77, 78].

4.3.8 A case study: operator dynamics in a domain wall density background

In this section we will discuss operator dynamics in the case where the charge-background starts in a domain-wall configuration. Depending on the initial left and right density, i.e. ρ_L and ρ_R, we gain different insights into how the charge dynamics can affect operator growth. We will assume that ξ always starts with its maximal initial value $\sqrt{\rho(1-\rho)}$.

4.3.8.1 Asymmetric butterfly velocity

The first case we consider involves the left-half of the chain initialized in density-profile $\rho_L = 1/2$ and the right-half being in $\rho_R = 1/8$. The operator starts with its maximal value $\sqrt{\rho(1-\rho)}$ on every site. In this scenario, both the varying ρ and ξ are perturbed by the

diffusion term at $t = 0$, and the non-linear term for ξ then carries the perturbation along the chain with a butterfly velocity. Due to the nature of the domain wall, the left and right halves of the operator can travel with different speeds. This phenomenon is depicted in Fig. 4.5(a), where the wavefront plotted at equal time intervals clearly demonstrates that the operator moves faster through the left half of the chain, as expected from Eq. (4.58). It is also clear that the domain wall melts at a rate much slower than the evolution of the operator, which makes the dynamics of the charge largely inconsequential to the dynamics of the operator χ, in this scenario.

4.3.8.2 Conserved vs. non-conserved operator

If one starts with a completely filled density on one half ($\rho_L = 1$) while the other remains completely unoccupied ($\rho_R = 0$), the variable ξ can only take one value, i.e. 0, at every site. Since this is a stable solution of the FKPP-equation, the OTOC involving the operator χ remains completely static, even though the charge and therefore the on-site scrambled-state changes with time. However, if one uses a conserved operator, such as n, the OTOC is captured by the variable $\xi^2 + \rho^2$. Since the charge moves diffusively as the domain wall melts, it causes the OTOC to have diffusive behavior at all times. Hence, in this situation, the OTOC involving an operator such as χ remains perfectly static, whereas the OTOC for a conserved operator such as n shows diffusive behavior.

4.3.8.3 Charge dynamics influences the dynamics of non-conserved operators

Let's consider a scenario where the left and right densities are chosen to be $\rho_L = 3/4$ and $\rho_R = 1/4$ respectively (Fig. 4.5(b)). This makes it so that the value of $\rho(1-\rho)$ is equal on both sides of the chain, even though the density has different values. Thus, at $t = 0$, the operator-profile which starts at its maximal value, is flat and static, although the charge is not. This case is different from the previous one because the operator dynamics are kick-started purely due to the charge dynamics, where at early times the diffusion for the charge causes the domain wall to melt and therefore forces the operator to start moving as well.

In fact, this can be generalized further. When starting with some specific operator-profile $\xi(r, t = 0) = f(r)$, there are two available solutions for the corresponding charge density since $\xi = \sqrt{\rho(1-\rho)}$. Each solution for ρ individually gives the same behavior for ξ, however starting from different solutions on the left and right half of the chain creates a perturbation in the center as the charge moves to bridge the gap between the two solutions. This is especially interesting because usually one expects the transport to only be relevant when conserved operators such as n are involved, which have overlap with the charge. However, even though the operator χ does not have overlap with the charge, the charge dynamics in the background forces the Hilbert-space dimension and therefore the maximum allowed value of ξ to change in the middle of the chain. This causes a local perturbation that then travels ballistically across the chain.

4.4 Conclusion and Discussions

In this chapter we utilized the symmetry structures present in Brownian SYK models, which emerge after the disorder averaging procedure, to study the relation between charge-transport and operator growth. We measured operator growth and scrambling by computing the OTOC in the complex Brownian SYK chain with U(1) symmetry. For this calculation, the model maps to an SU(4) spin chain which evolves in imaginary time and conserves weights. The computation of the OTOC involves four time-contours, and therefore four conserved charges as well. In our formalism, we show that the dynamics of these charges can be encoded in terms of the evolution of the conserved weights. Moreover, the evolution of operator-states is represented by transitions between states in the SU(4) algebra.

Tracking these transitions reveals distinct features of operator dynamics in many-body models with symmetries. While usual Brownian/random models can be modeled by a classical stochastic process, we show that the U(1) symmetry introduces quantum-coherence at the operator level, which only allows for a classical description in a subspace of the operator-space. In the infinite-N limit, the model therefore is described by a 'restricted' Fokker-Planck equation, which represents a probability distribution only in the sector where

the operator-states have no coherence.

We utilized the mapping to solve the OTOC and charge-transport exactly at finite-N, for the non-interacting model. For the model with both transport and scrambling, we computed the OTOC involving simple operators, which can be shown to lie in the incoherent subspace, in the large-N limit. This enables us to derive an FKPP-equation governing the evolution of the operator coupled to the charge which is valid for all charge-density profiles and at all time-scales. For constant charge-density background, the coupled FKPP equation provides us with the Lyapunov exponent and the butterfly velocity as a function of the charge density. Using these equations we also explain known results for charged-operator dynamics, such as the diffusive late-time behavior, and explore new regimes of varying charge-density backgrounds. When starting with different domain-wall solutions, we obtain novel solutions for operator dynamics, including one where the dynamics even for a non-conserved operator such as χ are kick-started purely due to the charge dynamics. Next, we share some additional insights involving operator growth in the presence of symmetries.

In this work, we have considered a model which moves the charge and scrambles quantum information simultaneously. However, it is possible to decouple the movement of the charge from the spatial movement of the operator, by considering a Brownian Hamiltonian like:

$$H = \sum_{i,j,k,l,r} J_{i,j,k,l,r}(t)\chi^{\dagger}_{i,r}\chi_{j,r}\chi^{\dagger}_{k,r+1}\chi_{l,r+1} + \text{h.c.} \tag{4.59}$$

This model is interacting, yet does not allow the transfer of charge as it conserves charge on each site r. It can be solved in the large-N limit as well, where the equation for ξ (the OTOC) has a stable zero at $\xi = 0$ and a transport term for ξ, but not the charge. This can be contrasted with the case in Sec. 4.3.8.2, in which case the charge transport was required to kickstart the operator dynamics. Thus, if one were to consider the model in Eq. (4.59) instead, the OTOC in that scenario would remain completely static.

In contrast with this, if one considers a model which conserves energy, it does not seem

possible to construct scenarios which scramble information yet do not simultaneously transport energy. This marks a stark difference between a gauge symmetry, such as charge conservation, and energy conservation.

REFERENCES

[1] M. Srednicki, "Chaos and quantum thermalization," *Phys. Rev. E*, vol. 50, pp. 888–901, aug 1994.

[2] J. M. Deutsch, "Quantum statistical mechanics in a closed system," *Phys. Rev. A*, vol. 43, pp. 2046–2049, feb 1991.

[3] A. M. Kaufman, M. E. Tai, A. Lukin, M. Rispoli, R. Schittko, P. M. Preiss, and M. Greiner, "Quantum thermalization through entanglement in an isolated many-body system," *Science*, vol. 353, no. 6301, pp. 794–800, 2016.

[4] L. Amico, R. Fazio, A. Osterloh, and V. Vedral, "Entanglement in many-body systems," *Rev. Mod. Phys.*, vol. 80, pp. 517–576, May 2008.

[5] P. Calabrese, J. Cardy, and B. Doyon, "Entanglement entropy in extended quantum systems," *J. Phys. A*, vol. 42, no. 50, p. 500301, 2009.

[6] J. Eisert, M. Cramer, and M. B. Plenio, "Colloquium: Area laws for the entanglement entropy," *Rev. Mod. Phys.*, vol. 82, pp. 277–306, Feb 2010.

[7] M. Headrick, "Lectures on entanglement entropy in field theory and holography," *arXiv:1907.08126*, 2019.

[8] A. Polkovnikov, K. Sengupta, A. Silva, and M. Vengalattore, "Colloquium: Nonequilibrium dynamics of closed interacting quantum systems," *Rev. Mod. Phys.*, vol. 83, pp. 863–883, Aug 2011.

[9] M. Rigol, V. Dunjko, and M. Olshanii, "Thermalization and its mechanism for generic isolated quantum systems," *Nature*, vol. 452, no. 7189, pp. 854–858, 2008.

[10] D. A. Roberts, D. Stanford, and A. Streicher, "Operator growth in the syk model," *J. High Energy Phys.*, vol. 2018, no. 6, pp. 1–20, 2018.

[11] A. Nahum, S. Vijay, and J. Haah, "Operator spreading in random unitary circuits," *Phys. Rev. X*, vol. 8, p. 021014, Apr 2018.

[12] S. Xu and B. Swingle, "Scrambling dynamics and out-of-time ordered correlators in quantum many-body systems: a tutorial," *arXiv:2202.07060*, 2022.

[13] B. Swingle, "Unscrambling the physics of out-of-time-order correlators," *Nat. Phys.*, vol. 14, no. 10, pp. 988–990, 2018.

[14] P. Hosur, X.-L. Qi, D. A. Roberts, and B. Yoshida, "Chaos in quantum channels," *J. High Energy Phys.*, vol. 2016, p. 004, Feb 2016.

[15] J. Li, R. Fan, H. Wang, B. Ye, B. Zeng, H. Zhai, X. Peng, and J. Du, "Measuring out-of-time-order correlators on a nuclear magnetic resonance quantum simulator," *Phys. Rev. X*, vol. 7, p. 031011, Jul 2017.

[16] K. X. Wei, C. Ramanathan, and P. Cappellaro, "Exploring localization in nuclear spin chains," *Phys. Rev. Lett.*, vol. 120, no. 7, p. 070501, 2018.

[17] X. Nie, Z. Zhang, X. Zhao, T. Xin, D. Lu, and J. Li, "Detecting scrambling via statistical correlations between randomized measurements on an NMR quantum simulator," *arXiv:1903.12237*, 2019.

[18] C. Sánchez, A. Chattah, K. Wei, L. Buljubasich, P. Cappellaro, and H. Pastawski, "Perturbation independent decay of the loschmidt echo in a many-body system," *Phys. Rev. Lett.*, vol. 124, no. 3, p. 030601, 2020.

[19] M. Gärttner, J. G. Bohnet, A. Safavi-Naini, M. L. Wall, J. J. Bollinger, and A. M. Rey, "Measuring out-of-time-order correlations and multiple quantum spectra in a trapped-ion quantum magnet," *Nat. Phys.*, vol. 13, p. 781, May 2017.

[20] K. A. Landsman, C. Figgatt, T. Schuster, N. M. Linke, B. Yoshida, N. Y. Yao, and C. Monroe, "Verified quantum information scrambling," *Nature*, vol. 567, p. 61, Mar 2019.

[21] M. K. Joshi, A. Elben, B. Vermersch, T. Brydges, C. Maier, P. Zoller, R. Blatt, and C. F. Roos, "Quantum information scrambling in a trapped-ion quantum simulator with tunable range interactions," *Phys. Rev. Lett.*, vol. 124, no. 24, p. 240505, 2020.

[22] M. R. Geller, "Sampling and scrambling on a chain of superconducting qubits," *Phys. Rev. Applied*, vol. 10, p. 024052, Aug 2018.

[23] J. Braumüller, A. H. Karamlou, Y. Yanay, B. Kannan, D. Kim, M. Kjaergaard, A. Melville, B. M. Niedzielski, Y. Sung, A. Vepsäläinen, R. Winik, J. L. Yoder, T. P. Orlando, S. Gustavsson, C. Tahan, and W. D. Oliver, "Probing quantum information propagation with out-of-time-ordered correlators," *arXiv:2102.11751*, 2021.

[24] X. Mi, P. Roushan, C. Quintana, S. Mandra, J. Marshall, C. Neill, F. Arute, K. Arya, J. Atalaya, R. Babbush, *et al.*, "Information scrambling in computationally complex quantum circuits," *arXiv:2101.08870*, 2021.

[25] M. Blok, V. Ramasesh, T. Schuster, K. O'Brien, J. Kreikebaum, D. Dahlen, A. Morvan, B. Yoshida, N. Yao, and I. Siddiqi, "Quantum information scrambling on a superconducting qutrit processor," *Phys. Rev. X*, vol. 11, no. 2, p. 021010, 2021.

[26] T. Schuster, B. Kobrin, P. Gao, I. Cong, E. T. Khabiboulline, N. M. Linke, M. D. Lukin, C. Monroe, B. Yoshida, and N. Y. Yao, "Many-body quantum teleportation via operator spreading in the traversable wormhole protocol," *Phys. Rev. X*, vol. 12, p. 031013, Jul 2022.

[27] A. R. Brown, H. Gharibyan, S. Leichenauer, H. W. Lin, S. Nezami, G. Salton, L. Susskind, B. Swingle, and M. Walter, "Quantum gravity in the lab: teleportation by size and traversable wormholes," *arXiv:1911.06314*, 2019.

[28] L. Agarwal and S. Xu, "Emergent symmetry in brownian syk models and charge dependent scrambling," *J. High Energy Phys.*, vol. 2022, no. 2, pp. 1–57, 2022.

[29] Y. Bao, S. Choi, and E. Altman, "Symmetry enriched phases of quantum circuits," *Annals of Physics*, vol. 435, p. 168618, 2021.

[30] C. Sünderhauf, L. Piroli, X.-L. Qi, N. Schuch, and J. I. Cirac, "Quantum chaos in the Brownian SYK model with large finite N: OTOCs and tripartite information," *J. High Energy Phys.*, vol. 2019, p. 038, Nov 2019.

[31] S. Xu and B. Swingle, "Locality, quantum fluctuations, and scrambling," *Phys. Rev. X*, vol. 9, p. 031048, Sep 2019.

[32] S.-K. Jian and B. Swingle, "Note on entropy dynamics in the brownian SYK model," *J. High Energy Phys.*, vol. 2021, p. 042, Mar 2021.

[33] T. Zhou and X. Chen, "Operator dynamics in a brownian quantum circuit," *Phys. Rev. E*, vol. 99, p. 052212, May 2019.

[34] S. Sachdev and J. Ye, "Gapless spin-fluid ground state in a random quantum Heisenberg magnet," *Phys. Rev. Lett.*, vol. 70, no. 21, pp. 3339–3342, 1993.

[35] A. Kitaev, "A simple model of quantum holography," in *KITP Program: Entanglement in Strongly-Correlated Quantum Matter*, 2015.

[36] S. Sachdev, "Bekenstein-hawking entropy and strange metals," *Phys. Rev. X*, vol. 5, no. 4, p. 041025, 2015.

[37] J. Polchinski and V. Rosenhaus, "The spectrum in the Sachdev-Ye-Kitaev model," *J. High Energy Phys.*, vol. 2016, no. 04, p. 001, 2016.

[38] J. Maldacena and D. Stanford, "Remarks on the Sachdev-Ye-Kitaev model," *Phys. Rev. D*, vol. 94, p. 106002, Nov 2016.

[39] Y. Sekino and L. Susskind, "Fast scramblers," *J. High Energy Phys.*, vol. 2008, p. 065, Oct 2018.

[40] N. Lashkari, D. Stanford, M. Hastings, T. Osborne, and P. Hayden, "Towards the fast scrambling conjecture," *J. High Energy Phys.*, vol. 2013, p. 022, Apr 2013.

[41] J. Maldacena, S. H. Shenker, and D. Stanford, "A bound on chaos," *J. High Energy Phys.*, vol. 2016, no. 08, p. 106, 2016.

[42] D. E. Parker, X. Cao, A. Avdoshkin, T. Scaffidi, and E. Altman, "A universal operator growth hypothesis," *Phys. Rev. X*, vol. 9, no. 4, p. 041017, 2019.

[43] S. H. Shenker and D. Stanford, "Black holes and the butterfly effect," *J. High Energy Phys.*, vol. 2014, p. 067, Mar 2014.

[44] I. L. Aleiner, L. Faoro, and L. B. Ioffe, "Microscopic model of quantum butterfly effect: out-of-time-order correlators and traveling combustion waves," *Annals of Physics*, vol. 375, pp. 378–406, 2016.

[45] D. A. Roberts and B. Swingle, "Lieb-robinson bound and the butterfly effect in quantum field theories," *Phys. Rev. Lett.*, vol. 117, no. 9, p. 091602, 2016.

[46] M. Blake, "Universal charge diffusion and the butterfly effect in holographic theories," *Phys. Rev. Lett.*, vol. 117, no. 9, p. 091601, 2016.

[47] Y. Gu, X.-L. Qi, and D. Stanford, "Local criticality, diffusion and chaos in generalized Sachdev-Ye-Kitaev models," *J. High Energy Phys.*, vol. 2017, no. 05, p. 125, 2017.

[48] D. J. Luitz and Y. B. Lev, "Information propagation in isolated quantum systems," *Phys. Rev. B*, vol. 96, no. 2, p. 020406, 2017.

[49] A. Bohrdt, C. B. Mendl, M. Endres, and M. Knap, "Scrambling and thermalization in a diffusive quantum many-body system," *New J. Phys.*, vol. 19, no. 6, p. 063001, 2017.

[50] A. Nahum, S. Vijay, and J. Haah, "Operator spreading in random unitary circuits," *Phys. Rev. X*, vol. 8, p. 021014, Apr 2018.

[51] C. von Keyserlingk, T. Rakovszky, F. Pollmann, and S. Sondhi, "Operator hydrodynamics, OTOCs, and entanglement growth in systems without conservation laws," *Phys. Rev. X*, vol. 8, p. 021013, Apr 2018.

[52] C.-J. Lin and O. I. Motrunich, "Out-of-time-ordered correlators in a quantum ising chain," *Phys. Rev. B*, vol. 97, no. 14, p. 144304, 2018.

[53] S. Xu and B. Swingle, "Accessing scrambling using matrix product operators," *Nat. Phys.*, vol. 16, pp. 199–204, Nov 2019.

[54] V. Khemani, D. A. Huse, and A. Nahum, "Velocity-dependent lyapunov exponents in many-body quantum, semiclassical, and classical chaos," *Phys. Rev. B*, vol. 98, no. 14, p. 144304, 2018.

[55] S. Gopalakrishnan, D. A. Huse, V. Khemani, and R. Vasseur, "Hydrodynamics of operator spreading and quasiparticle diffusion in interacting integrable systems," *Phys. Rev. B*, vol. 98, p. 220303, Dec 2018.

[56] G. Bentsen, T. Hashizume, A. S. Buyskikh, E. J. Davis, A. J. Daley, S. S. Gubser, and M. Schleier-Smith, "Treelike interactions and fast scrambling with cold atoms," *Phys. Rev. Lett.*, vol. 123, no. 13, p. 130601, 2019.

[57] G. Bentsen, Y. Gu, and A. Lucas, "Fast scrambling on sparse graphs," *Proc. Natl. Acad. Sci.*, vol. 116, no. 14, pp. 6689–6694, 2019.

[58] S. K. Zhao, Z.-Y. Ge, Z. Xiang, G. M. Xue, H. S. Yan, Z. T. Wang, Z. Wang, H. K. Xu, F. F. Su, Z. H. Yang, H. Zhang, Y.-R. Zhang, X.-Y. Guo, K. Xu, Y. Tian, H. F. Yu, D. N. Zheng, H. Fan, and S. P. Zhao, "Probing operator spreading via floquet engineering in a superconducting circuit," *Phys. Rev. Lett.*, vol. 129, p. 160602, Oct 2022.

[59] S. H. Shenker and D. Stanford, "Stringy effects in scrambling," *J. High Energy Phys.*, vol. 2015, no. 05, p. 132, 2015.

[60] P. Saad, S. H. Shenker, and D. Stanford, "A semiclassical ramp in SYK and in gravity," *arXiv:1806.06840*, 2018.

[61] W.-T. Kuo, A. Akhtar, D. P. Arovas, and Y.-Z. You, "Markovian entanglement dynamics under locally scrambled quantum evolution," *Phys. Rev. B*, vol. 101, no. 22, p. 224202, 2020.

[62] Y.-Z. You and Y. Gu, "Entanglement features of random hamiltonian dynamics," *Phys. Rev. B*, vol. 98, no. 1, p. 014309, 2018.

[63] M. Knap, "Entanglement production and information scrambling in a noisy spin system," *Phys. Rev. B*, vol. 98, no. 18, p. 184416, 2018.

[64] D. A. Rowlands and A. Lamacraft, "Noisy coupled qubits: Operator spreading and the fredrickson-andersen model," *Phys. Rev. B*, vol. 98, no. 19, p. 195125, 2018.

[65] D. A. Roberts and B. Yoshida, "Chaos and complexity by design," *J. High Energy Phys.*, vol. 2017, no. 04, p. 121, 2017.

[66] D. Stanford, Z. Yang, and S. Yao, "Subleading weingartens," *J. High Energy Phys.*, vol. 2022, no. 2, pp. 1–50, 2022.

[67] S. Grozdanov, K. Schalm, and V. Scopelliti, "Black hole scrambling from hydrodynamics," *Phys. Rev. Lett.*, vol. 120, no. 23, p. 231601, 2018.

[68] M. Blake, R. A. Davison, S. Grozdanov, and H. Liu, "Many-body chaos and energy dynamics in holography," *J. High Energy Phys.*, vol. 2018, no. 10, p. 035, 2018.

[69] C. Choi, M. Mezei, and G. Sárosi, "Pole skipping away from maximal chaos," *J. High Energy Phys.*, vol. 2021, no. 2, pp. 1–38, 2021.

[70] A. Lucas, "Operator size at finite temperature and planckian bounds on quantum dynamics," *Phys. Rev. Lett.*, vol. 122, no. 21, p. 216601, 2019.

[71] X.-L. Qi and A. Streicher, "Quantum epidemiology: operator growth, thermal effects, and SYK," *J. High Energy Phys.*, vol. 2019, p. 012, Aug 2019.

[72] X. Han and S. A. Hartnoll, "Quantum scrambling and state dependence of the butterfly velocity," *SciPost Phys.*, vol. 7, p. 045, 2019.

[73] Y. Huang, F. G. Brandao, Y.-L. Zhang, *et al.*, "Finite-size scaling of out-of-time-ordered correlators at late times," *Phys. Rev. Lett.*, vol. 123, no. 1, p. 010601, 2019.

[74] S. Sahu and B. Swingle, "Information scrambling at finite temperature in local quantum systems," *Phys. Rev. B*, vol. 102, no. 18, p. 184303, 2020.

[75] G. Cheng and B. Swingle, "Scrambling with conservation laws," *J. High Energy Phys.*, vol. 2021, no. 11, pp. 1–30, 2021.

[76] A. A. Patel, D. Chowdhury, S. Sachdev, and B. Swingle, "Quantum butterfly effect in weakly interacting diffusive metals," *Phys. Rev. X*, vol. 7, p. 031047, Sep 2017.

[77] V. Khemani, A. Vishwanath, and D. A. Huse, "Operator spreading and the emergence of dissipative hydrodynamics under unitary evolution with conservation laws," *Phys. Rev. X*, vol. 8, p. 031057, Sep 2018.

[78] T. Rakovszky, F. Pollmann, and C. von Keyserlingk, "Diffusive hydrodynamics of out-of-time-ordered correlators with charge conservation," *Phys. Rev. X*, vol. 8, p. 031058, Sep 2018.

[79] A. J. Friedman, A. Chan, A. De Luca, and J. Chalker, "Spectral statistics and many-body quantum chaos with conserved charge," *Phys. Rev. Lett.*, vol. 123, p. 210603, Nov 2019.

[80] X. Chen, R. M. Nandkishore, and A. Lucas, "Quantum butterfly effect in polarized floquet systems," *Phys. Rev. B*, vol. 101, no. 6, p. 064307, 2020.

[81] L. Piroli, C. Sünderhauf, and X.-L. Qi, "A random unitary circuit model for black hole evaporation," *J. High Energy Phys.*, vol. 2020, p. 063, Apr 2020.

[82] X. Chen, Y. Gu, and A. Lucas, "Many-body quantum dynamics slows down at low density," *SciPost Phys.*, vol. 9, p. 71, Nov 2020.

[83] P. Kos, B. Bertini, and T. Prosen, "Chaos and ergodicity in extended quantum systems with noisy driving," *Phys. Rev. Lett.*, vol. 126, p. 190601, May 2021.

[84] S. Pai, M. Pretko, and R. M. Nandkishore, "Localization in fractonic random circuits," *Phys. Rev. X*, vol. 9, no. 2, p. 021003, 2019.

[85] S. Moudgalya, A. Prem, D. A. Huse, and A. Chan, "Spectral statistics in constrained many-body quantum chaotic systems," *Phys. Rev. Research*, vol. 03, p. 023176, Jun 2021.

[86] J. Feldmeier and M. Knap, "Critically slow operator dynamics in constrained many-body systems," *Phys. Rev. Lett.*, vol. 127, p. 235301, Dec 2021.

[87] J. Kudler-Flam, R. Sohal, and L. Nie, "Information scrambling with conservation laws," *SciPost Phys.*, vol. 12, p. 117, 2022.

[88] S. A. Hartnoll, "Theory of universal incoherent metallic transport," *Nat. Phys.*, vol. 11, no. 1, p. 54, 2015.

[89] B. Kobrin, Z. Yang, G. D. Kahanamoku-Meyer, C. T. Olund, J. E. Moore, D. Stanford, and N. Y. Yao, "Many-body chaos in the Sachdev-Ye-Kitaev model," *Phys. Rev. Lett.*, vol. 126, no. 3, p. 030602, 2021.

[90] R. Vasseur, A. C. Potter, Y.-Z. You, and A. W. Ludwig, "Entanglement transitions from holographic random tensor networks," *Phys. Rev. B*, vol. 100, no. 13, p. 134203, 2019.

[91] T. Zhou and A. Nahum, "Entanglement membrane in chaotic many-body systems," *Phys. Rev. X*, vol. 10, no. 3, p. 031066, 2020.

[92] C.-M. Jian, Y.-Z. You, R. Vasseur, and A. W. Ludwig, "Measurement-induced criticality in random quantum circuits," *Phys. Rev. B*, vol. 101, no. 10, p. 104302, 2020.

[93] A. Nahum, S. Roy, B. Skinner, and J. Ruhman, "Measurement and entanglement phase transitions in all-to-all quantum circuits, on quantum trees, and in landau-ginsburg theory," *PRX Quantum*, vol. 2, no. 1, p. 010352, 2021.

[94] Y. Bao, S. Choi, and E. Altman, "Theory of the phase transition in random unitary circuits with measurements," *Phys. Rev. B*, vol. 101, no. 10, p. 104301, 2020.

[95] S.-K. Jian, C. Liu, X. Chen, B. Swingle, and P. Zhang, "Measurement-induced phase transition in the monitored sachdev-ye-kitaev model," *Phys. Rev. Lett.*, vol. 127, no. 14, p. 140601, 2021.

[96] S.-K. Jian, C. Liu, X. Chen, B. Swingle, and P. Zhang, "Quantum error as an emergent magnetic field," *arXiv:2106.09635*, 2021.

[97] M. Winer, S.-K. Jian, and B. Swingle, "Exponential ramp in the quadratic sachdev-ye-kitaev model," *Phys. Rev. Lett.*, vol. 125, no. 25, p. 250602, 2020.

[98] P. Zhang, S.-K. Jian, C. Liu, and X. Chen, "Emergent Replica Conformal Symmetry in Non-Hermitian SYK_2 Chains," *Quantum*, vol. 5, p. 579, Nov. 2021.

[99] A. Alex, M. Kalus, A. Huckleberry, and J. von Delft, "A numerical algorithm for the explicit calculation of su(n) and sl(n,c) clebsch–gordan coefficients," *Journal of Mathematical Physics*, vol. 52, p. 023507, Feb 2011.

[100] A. Keselman, L. Nie, and E. Berg, "Scrambling and lyapunov exponent in spatially extended systems," *Phys. Rev. B*, vol. 103, no. 12, p. L121111, 2021.

[101] L. Agarwal, S. Sahu, and S. Xu, "Charge transport, information scrambling and quantum operator-coherence in a many-body system with u(1) symmetry," *arXiv:2210.14828*, 2022.

[102] X.-L. Qi and A. Streicher, "Quantum epidemiology: operator growth, thermal effects, and syk," *J. High Energy Phys.*, vol. 2019, no. 8, pp. 1–28, 2019.

[103] T. Zhou and B. Swingle, "Operator growth from global out-of-time-order correlators," *arXiv:2112.01562*, 2021.

[104] Z.-Y. Zhou, G.-X. Su, J. C. Halimeh, R. Ott, H. Sun, P. Hauke, B. Yang, Z.-S. Yuan, J. Berges, and J.-W. Pan, "Thermalization dynamics of a gauge theory on a quantum simulator," *Science*, vol. 377, no. 6603, pp. 311–314, 2022.

[105] I. Golding, Y. Kozlovsky, I. Cohen, and E. Ben-Jacob, "Studies of bacterial branching growth using reaction–diffusion models for colonial development," *Physica A: Statistical Mechanics and its Applications*, vol. 260, no. 3-4, pp. 510–554, 1998.

[106] I. Marvian, "Restrictions on realizable unitary operations imposed by symmetry and locality," *Nat. Phys.*, vol. 18, no. 3, pp. 283–289, 2022.

[107] X. Chen and T. Zhou, "Quantum chaos dynamics in long-range power law interaction systems," *Phys. Rev. B*, vol. 100, no. 6, p. 064305, 2019.

APPENDIX A

APPENDIX FOR NON-EQUILIBRIUM DYNAMICS IN 0+1 DIMENSIONS

A.1 The emergent Hamiltonian

A.1.1 The Majorana model

The Emergent Hamiltonian for the Majorana case, for $q_{\text{syk}} = 2$ and $q_{\text{syk}} = 4$ body couplings in the original Hamiltonian, is given by:

$$\begin{aligned}\mathbb{H}_{q_{\text{syk}}=2} &= \frac{1}{2N}\left(-2\binom{N}{2} - 3N - \frac{1}{2}\sum_{(\alpha\neq\beta)} (S^{\alpha\beta})^2 \right) \\ \mathbb{H}_{q_{\text{syk}}=4} &= \frac{3}{N^3}\left(-2\binom{N}{4} + \frac{1}{4!}\sum_{(\alpha\neq\beta)} (-1)^{\gamma_{\alpha,\beta}} \left[(S^{\alpha\beta})^4 - (S^{\alpha\beta})^2(-6N+8) + 3N(N-2)\right] \right)\end{aligned} \tag{A.1}$$

Where

$$S^{\alpha\beta} = \sum_{i=1}^{N} \psi_i^\alpha \psi_i^\beta; \quad (-1)^{\gamma_{\alpha,\beta}} = \begin{cases} 1 & (\alpha,\beta) = (a,b),(a,d),(b,c),(c,d) \\ -1 & (\alpha,\beta) = (a,c),(b,d) \end{cases} \tag{A.2}$$

The emergent Hamiltonians for larger q_{syk} can be obtained iteratively, and are always functions of the 6 operators $S^{\alpha\beta}$.

We will devote the rest of the Majorana section to the discussion of the qualitative behavior of the OTOC for larger q_{syk} in the Brownian SYK model. We will use $q_{\text{syk}} = 8$ as an example to build intuition about the behavior for general q_{syk}. The emergent Hamiltonian for $q_{\text{syk}} = 8$ in terms of the SU(2) algebra takes the manifestly square symmetric form:

$$\mathbb{H}_{q_{\text{syk}}=8} = \frac{7!}{2N^7}\left(-2\begin{pmatrix} N \\ 8 \end{pmatrix} + \frac{1}{8!}\left((H_x)_{q_{\text{syk}}=8} + (H_z)_{q_{\text{syk}}=8} - (H_y)_{q_{\text{syk}}=8} \right) \right) \tag{A.3}$$

Where

$$(H_\alpha)_{q_{\rm syk}=8} = 512L_\alpha^8 - 3584(-4+N)L_\alpha^6 + 448(176+5N(-22+3N))L_\alpha^4 \\ +32(2112-7N(424+15(-10+N)N))L_\alpha^2 \\ +210(-6+N)(-4+N)(-2+N)N; \quad \alpha = x,y,z \tag{A.4}$$

Now we expand the Hamiltonian obtained within the $L = N/2$ irrep, in the infinite-N limit, keeping the input and output states the same as in Sec. 3.2.6. The Logistic equation in this case is given by:

$$\xi'(t) = 2\xi(\xi^6 - 1)\ ;\ \xi(0) = 1 - 2\delta\ ,\ \delta \ll 1 \tag{A.5}$$

with the solution:

$$(\mathcal{F}_{N/2}(t))_{q_{\rm syk}=8} = -\frac{1}{\sqrt[6]{1+12e^{12t}\delta}}. \tag{A.6}$$

This solution has the following early and late-time behavior:

$$(\mathcal{F}_{N/2}(t))_{q_{\rm syk}=8} \sim \begin{cases} -1+2e^{12t}\delta & t \ll -\frac{1}{12}\ln\delta \\ e^{-2t} & t \gg -\frac{1}{12}\ln\delta \end{cases} \tag{A.7}$$

The Hamiltonian for larger $q_{\rm syk}$ can be derived iteratively through the equation:

$$(H_\alpha)_{q_{\rm syk}+1} = 2iL_\alpha(H_\alpha)_{q_{\rm syk}} + q_{\rm syk}(N+1-q_{\rm syk})(H_\alpha)_{q_{\rm syk}-1}\ ; \\ (H_\alpha)_{q_{\rm syk}=0} = 2\ ;\ (H_\alpha)_{q_{\rm syk}=1} = 2iL_\alpha \tag{A.8}$$

The emergent Hamiltonian for general $q_{\rm syk}$ can then be written as the square or cubic symmetric function of $(H_\alpha)_{q_{\rm syk}}$, depending on whether $q_{\rm syk}/2$ is even or odd. Based on the results obtained so far, we can conjecture that the logistic equation and OTOC for general $q_{\rm syk}$ will take the form:

$$\xi'(t) = 2\xi(\xi^{(q_{\rm syk}-2)} - 1) \implies (\mathcal{F}_{N/2}(t))_{q_{\rm syk}} = -\frac{1}{\sqrt[(q_{\rm syk}-2)]{1+2(q_{\rm syk}-2)e^{2(q_{\rm syk}-2)t}\delta}}. \tag{A.9}$$

which implies that the ratio of the early to late exponent is $(\lambda_L/\lambda_{late})_{q_{\rm syk}} = (q_{\rm syk}-2)$, for $q_{\rm syk} > 2$. Therefore changing the $q_{\rm syk}$ leads to a larger Lyapunov exponent but leaves the late-time exponent unchanged ($\lambda_{late} = 2$).

A.1.2 The complex model

To derive the emergent Hamiltonian, one has to account for the fact that the Hamiltonian on the replicas a, c looks slightly different from the one on the replicas b, d due to the particle-hole transformation.

$$\begin{aligned} H^{\alpha} &= \sum_{i,j,k,l} J_{i,j,k,l}\, \psi_i^{\alpha\dagger}\, \psi_j^{\alpha\dagger}\, \psi_k^{\alpha}\, \psi_l^{\alpha} \quad ;\alpha = a, c \\ H^{\alpha *} &= \sum_{i,j,k,l} J^*_{i,j,k,l}\, \psi_i^{\alpha}\, \psi_j^{\alpha}\, \psi_k^{\alpha\dagger}\, \psi_l^{\alpha\dagger} \quad ;\alpha = b, d. \end{aligned} \tag{A.10}$$

Since the couplings are complex, J only couples to J^*, and when the disorder average is computed, the resultant operator depends on which sites are paired together. As an example, for $q_{\rm syk} = 4$:

$$\overline{H^a H^a} \propto \sum_{i,j,k,l} \psi_i^{a\dagger}\psi_j^{a\dagger}\psi_k^{a}\psi_l^{a}\psi_l^{a\dagger}\psi_k^{a\dagger}\psi_j^{a}\psi_i^{a} \;;\; \overline{H^a H^{b*}} \propto \sum_{i,j,k,l} \psi_i^{a\dagger}\psi_j^{a\dagger}\psi_k^{a}\psi_l^{a}\psi_i^{b}\psi_j^{b}\psi_k^{b\dagger}\psi_l^{b\dagger}. \tag{A.11}$$

The emergent Hamiltonian after disorder average reads

$$\begin{aligned} \mathbb{H} = -\frac{1}{2}\left(\overline{H^a H^a} + \overline{H^{b*} H^{b*}} + \overline{H^c H^c} + \overline{H^{d*} H^{d*}}\right) + \left(\overline{H^a H^{b,*}} + \overline{H^{b,*} H^c} + \overline{H^c H^{d,*}} + \overline{H^{d,*} H^a}\right) \\ - \left(\overline{H^a H^c} + \overline{H^{b,*} H^{d,*}}\right). \end{aligned} \tag{A.12}$$

To simplify the notation for $q_{\rm syk} = 4$, we define the operators $\mathcal{P}_{\alpha\beta}$ which sends the index $\alpha \to \beta$ and the conjugation operator $\mathcal{C}$ which sends $\psi^{a,c} \to (\psi^{b,d})^\dagger$ and therefore $\mathcal{C}S^{aa} \to N - S^{bb}$ and $\mathcal{C}S^{ac} \to -S^{db}$. One can then write :

$$\mathbb{H}_{q_{\rm syk}=4} = -\frac{1}{2}(1+\mathcal{C})(1+\mathcal{P}_{ac})\overline{H^a H^a} + (1+\mathcal{P}_{bd})(1+\mathcal{P}_{ac})\overline{H^a H^{b,*}} - (1+\mathcal{C})\overline{H^a H^c} \tag{A.13}$$

Where

$$\begin{aligned}
\overline{H^a H^a} &= S^{aa}(S^{aa}-1)(N-S^{aa}+2)(N-S^{aa}+1) \\
\overline{H^a H^{b,*}} &= [(S^{ab}S^{ba})^2 + (S^{aa}-S^{bb}-2)S^{ab}S^{ba}] \\
\overline{H^a H^c} &= [2(S^{aa}-1)(S^{aa}) - (3S^{aa}+S^{cc}-2)S^{ac}S^{ca} + (S^{ac}S^{ca})^2]
\end{aligned} \tag{A.14}$$

and $S^{\alpha\beta} = \sum_i \psi_i^{\alpha\dagger}\psi_i^{\beta}$. It is evident that this Hamiltonian, although more complicated than the $q_{\text{syk}} = 2$ case, also preserves the charge profile $(S^{aa}, N-S^{bb}, S^{cc}, N-S^{dd})$ since it commutes with $S^{\alpha\alpha}$, $\alpha = \{a,b,c,d\}$.

A.2 Consistency checks

We will dedicate this section to independent consistency checks to make sure our results are accurate.

A.2.1 Invariance of the identity operator

First we will note that within our formalism, we expect operator-states which correspond to symmetries of the Hamiltonian to vanish under the emergent Hamiltonian. One such operator that vanishes identically without depending on the details of the theory, is the identity operator $|I\rangle$. A generalised version of this statement for an operator O can be written as

$$\big[H,O\big] = 0 \implies UOU^\dagger = O \implies \big(U\otimes U^*\big)\,|O\rangle = |O\rangle \tag{A.15}$$

What is theory dependent however, are the details of how the identity state splits into the representations of the algebra respected by the Hamiltonian. For the complex Brownian SYK model, the identity state splits into different states within the $(0,N,0)$ irrep as

$$\begin{aligned}
|I\otimes I\rangle &= \sum_{l,m=0}^{N} \left| \sum_{\alpha_1<\ldots<\alpha_l} \bar{n}_{\alpha_1}\ldots\bar{n}_{\alpha_l} n_{i_1}\ldots n_{i_{N-l}} \otimes \sum_{\beta_1<\ldots<\beta_m} \bar{n}_{\beta_1}\ldots\bar{n}_{\beta_m} n_{j_1}\ldots n_{j_{N-m}} \right\rangle \\
&= \sum_{l,m=0}^{N} (-1)^{N/2} \frac{(S^{dc})^m (S^{ba})^l (S^{cb})^N}{(N-1)!\,l!\,m!}\,|W_{(0,N,0)}\rangle
\end{aligned} \tag{A.16}$$

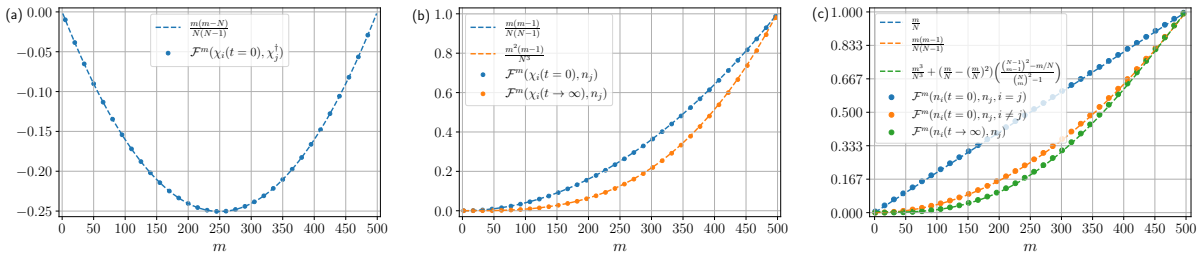

Figure A.1: (a) Benchmarking of the initial values of the OTOC $\mathcal{F}^m(\chi_i(t), \chi_j^\dagger)$, for $N = 500$ and different m. (b) Benchmarking of the initial and final values of the OTOCs $\mathcal{F}^m(\chi_i(t), n_j)$, for $N = 500$ and different m. (c) Benchmarking of the initial and final values of the OTOCs $\mathcal{F}^m(n_i(t), n_j)$, for $N = 500$ and different m. All of the benchmarking has been performed using the numerical values obtained using the Lie Algebra method and the values obtained analytically listed in Table. 3.1.

This shows that the identity splits into $(N+1)^2$ different states with different weights. Since the identity cannot have dynamics, it must vanish under the action of the emergent Hamiltonian, i.e. $\mathbb{H}\,|I \otimes I\rangle = 0$. Because the emergent Hamiltonian conserves weights, it implies that each state in the decomposition of the identity with a unique weight must vanish independently as well. We have already seen that this happens for the free case, i.e. $\mathbb{H}^{(0,N,0)}_{q_{\text{syk}}=2}\,|I \otimes I\rangle = 0$, in the section 3.3.5.1, because the operator vanishes for the entire irrep $(0, N, 0)$. One can check that the identity indeed does vanish even under the action of the emergent Hamiltonian for $q_{\text{syk}} = 4$, which completes our first consistency check.

A.2.2 Comparison of initial and final values obtained numerically vs analytically

The second consistency check comes from comparing the theoretical and numerical values of the initial and final values of the OTOCs. We plot this check in Fig. A.1. The numerical values are obtained using the Lie Algebra method and the theoretical values are listed in Table. 3.1

A.2.3 Benchmarking with small systems using explicit random averaging

Another consistency check comes from comparing the prediction of the OTOC obtained using the emergent Lie Algebra in Eq. (3.26), with the numerical results obtained from

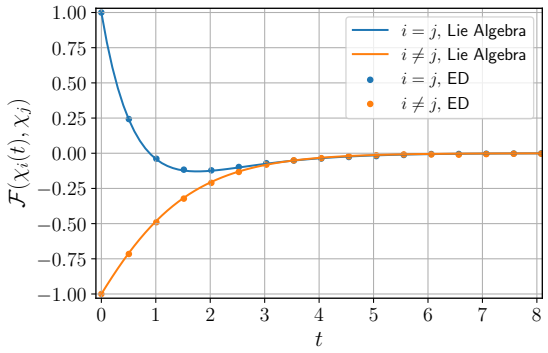

Figure A.2: A plot of the OTOC $\mathcal{F}(\chi_i(t), \chi_j)$ in the Majorana model vs time, from both the ED of the original model in Eq. (3.5) with explicit disorder average, and Lie Algebra (SU(2)) methods. Here $N = 12$, $q_{\text{syk}} = 4$ and the numerical ED results are computed using 200 disorder averages.

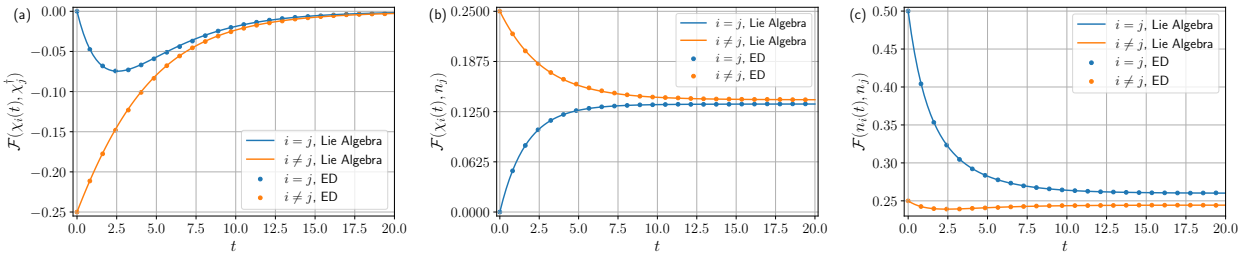

Figure A.3: A plot of the OTOCs $\mathcal{F}(\chi_i(t), \chi_j^\dagger)$ in (a), $\mathcal{F}(\chi_i(t), n_j)$ in (b) and $\mathcal{F}(n_i(t), n_j)$ in (c) vs time, from both the ED of the original model in Eq. (3.53) and Lie Algebra (SU(4)) methods. Here $N = 6$, $q_{\text{syk}} = 4$ and the numerical ED results are computed using 500 disorder averages.

directly computing the OTOC via ED. We display the plot in Fig. A.2 for $N = 12$ particles in the Majorana model using 200 disorder averages.

We also make the same comparison for the complex model in Fig. A.3, for OTOCs involving different local operators. The Lie Algebra method corresponds to computing the OTOC using the contribution from each irrep after evolving the input state and taking the overlap with the output state. As an example, Eq. (3.77) shows how to do this for the OTOC $\mathcal{F}(\chi_i(t), \chi_j^\dagger)$, and the ED is computed for $N = 6$ particles over 500 disorder averages for all the OTOCs considered.

A.3 Gelfand-Tsetlin pattern calculus

To label states in the SU(4) irreps and explicitly build the matrices in the group for numerical purposes, we will make use of Gelfand-Tsetlin patterns. In this section we will provide a brief introduction to GT-patterns (a more detailed review can be found in [99]) and demonstrate their utility for the purpose of solving problems that involve SU(n) algebras. For SU(4), GT-patterns are labelled by 10 non-negative integers arranged in the triangular pattern depicted below:

$$\begin{pmatrix} m_{1,4} & & m_{2,4} & & m_{3,4} & & m_{4,4} \\ & m_{1,3} & & m_{2,3} & & m_{3,3} & \\ & & m_{1,2} & & m_{2,2} & & \\ & & & m_{1,1} & & & \end{pmatrix}$$

Each entry in the pattern is uniquely labelled by the 2 integers k, l such that the entry $m_{k,l}$ lies along the k^{th} diagonal and in the l^{th} row. A valid GT-pattern has entries that satisfy the constraint $m_{k,l} \geq m_{k,l-1} \geq m_{k+1,l}$. The top-most row of the pattern is determined by the irrep and stays fixed for all states within the irrep. To label the highest-weight state of an irrep, one needs to compute the values of $(S^{aa}, S^{bb}, S^{cc}, S^{dd})$ corresponding to the state, and the values in the highest row of the corresponding pattern $(m_{1,4}, m_{2,4}, m_{3,4}, m_{4,4})$ take these values respectively. The values in the lower rows are given by the maximum values that are allowed in a valid GT-pattern. A subtle point here is that the charge sensitivity of the Hamiltonian that emerges after disorder-averaging makes it important to label the patterns differently for irreps with the same young diagrams but different charges. For example, the states $|{\chi_1}^\dagger ... {\chi_N}^\dagger \otimes {\chi_1}^\dagger ... {\chi_N}^\dagger\rangle$ and $|\chi_1 ... \chi_N \otimes \chi_1 ... \chi_N\rangle$ are both singlets but have charge profiles (N, N, N, N) and $(0, 0, 0, 0)$ respectively and therefore have different eigenvalues with respect to the emergent Hamiltonian. Often this charge is 'gauged' away by requiring that the element $m_{N,N}$ be set to zero, however it is unwise to do so for this problem. The Young-diagrams for the irreps can be read off using the rule that $m_{k,4}$ labels the number of boxes

in the k^{th} row of the diagram. For the highest-weight states in Eq. (3.70) (with the correct normalizations) :

$$N\,|W_{(0,N,0)}\rangle = \begin{pmatrix} N & & N & & 0 & & 0 \\ & N & & N & & 0 & \\ & & N & & N & & \\ & & & N & & & \end{pmatrix} \in$$

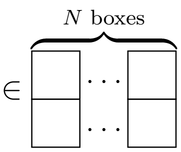

$$\frac{\sqrt{N}\,|W_{(1,N-2,1)}\rangle}{\sqrt{(N-1)}} = \begin{pmatrix} N & & N-1 & & 1 & & 0 \\ & N & & N-1 & & 1 & \\ & & N & & N-1 & & \\ & & & N & & & \end{pmatrix} \in \qquad \text{(A.17)}$$

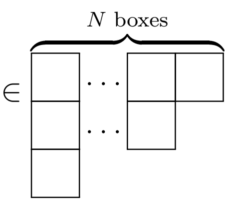

To construct states lower in these irreps, the rule states that the action of the operators $E_{\pm\alpha_l}$ results in adding(subtracting) $M^{k,l}$, the pattern with all entries 0 except for the position k, l which has value 1 ($M^{k,l}$ is not a valid GT-pattern by itself). If $|M\rangle$ represents a GT-pattern then the raising(lowering) action is given by:

$$E_{\pm\alpha_l}|M\rangle = \sum_k c_k^{\pm}|M \pm M^{k,l}\rangle. \qquad \text{(A.18)}$$

Thus it is possible to act on a single pattern and generate multiple ones, all corresponding to states with the same weight. The coefficients $c_k^{\pm}$ have been determined as:

$$\begin{aligned} c_k^{-} &= \left\langle M - M^{k,l}\,|E_{-\alpha_l}|\,M\right\rangle = \left(\frac{\prod_{k'=1}^{l+1}\left(m_{k',l+1}-m_{k,l}+k-k'+1\right)\prod_{k'=1}^{l-1}\left(m_{k',l-1}-m_{k,l}+k-k'\right)}{\prod_{\substack{k'=1\\k'\neq k}}^{l}\left(m_{k',l}-m_{k,l}+k-k'+1\right)\left(m_{k',l}-m_{k,l}+k-k'\right)} \right)^{\frac{1}{2}} \\ c_k^{+} &= \left\langle M + M^{k,l}\,|E_{+\alpha_l}|\,M\right\rangle = \left(\frac{\prod_{k'=1}^{l+1}\left(m_{k',l+1}-m_{k,l}+k-k'\right)\prod_{k'=1}^{l-1}\left(m_{k',l-1}-m_{k,l}+k-k'-1\right)}{\prod_{\substack{k'=1\\k'\neq k}}^{l}\left(m_{k',l}-m_{k,l}+k-k'\right)\left(m_{k',l}-m_{k,l}+k-k'-1\right)} \right)^{\frac{1}{2}}. \end{aligned} \qquad \text{(A.19)}$$

If $|M \pm M^{k,l}\rangle$ is not a valid pattern, $c_k^{\pm}$ will be 0. These equations can be used to build the matrix elements of raising/lowering operators in any SU(n) algebra. The 'traditional'

weight of a state, which is composed of the eigenvalues of the Cartan subalgebra, is given by 'z-weights' which are

$$\lambda_l^M = \sigma_l^M - \frac{1}{2}\left(\sigma_{l+1}^M + \sigma_{l-1}^M\right); \quad \left(\sigma_l^M = \sum_{k=1}^{l} m_{k,l}, \quad \sigma_0^M = 0\right) \tag{A.20}$$

However one can also use an equivalent formalism called 'p-weights' ($w_l^M = \sigma_l^M - \sigma_{l-1}^M$) which can be mapped to the z-weights. Patterns with the same sum of individual rows have the same p-weights and therefore the same z-weights and form the subspaces in the irrep with the same weight. For the irrep $(0, N, 0)$, one can write down the states appearing in the decomposition of the input state as individual GT-patterns, owing to the symmetrisation of indices in the irrep. The states that occur within the sum in Eq. (3.71) when restricted to the $(0, N, 0)$ irrep can be represented as:

$$\frac{(S^{dc})^m (S^{ba})^l}{l!m!} \left|\chi_1^\dagger n \otimes \chi_1 n\right\rangle_{(0,N,0)} \propto \begin{pmatrix} N & & N & & 0 & & 0 \\ & N & & N-m & & 0 & \\ & & N & & 1 & & \\ & & & N-l & & & \end{pmatrix} \tag{A.21}$$

One can take advantage of this feature to gain analytical leverage. Since the Hamiltonian conserves weights, it is important to know the multiplicity of the weights that reside in the input states within each irrep. For the $(0, N, 0)$ irrep, this can be calculated by realising that the patterns with the same weight(p-weight) are the ones that differ along the second row but give the same sum. This is because they are the only valid GT-patterns that have the

same row sums as Eq. (A.21). These patterns look like

$$\begin{pmatrix} N & & N & & 0 & & 0 \\ & N & & N-m & & 0 & \\ & & x & & y & & \\ & & & N-l & & & \end{pmatrix} \qquad \begin{aligned} &x+y=N+1; \qquad N \geq x \geq N-m; \\ &N-m \geq y \geq 0; \qquad x \geq N-l \geq y \end{aligned} \tag{A.22}$$

The number of different non-negative x, y that satisfy these constraints determine the weight multiplicity I, and can be computed for both the irreps that contribute to the OTOC

$$\begin{aligned} &I\big((S^{dc})^m (S^{ba})^l \, |\chi_1^\dagger n \otimes \chi_1 n\rangle_{(0,N,0)}\big) = \min(l+1, m+1, N-l, N-m) \\ &I\big((S^{dc})^m (S^{ba})^l \, |\chi_1^\dagger n \otimes \chi_1 n\rangle_{(1,N-2,1)}\big) = 2\min(l+1, m+1, N-l, N-m) \\ &+ min(l+1, m+2, N-l, N-m-1) + \min(l+1, m, N-l, N-m+1) - 2. \end{aligned} \tag{A.23}$$

This means the subspaces that the Hamiltonian can have dynamics within are at most of size $\mathcal{O}(N)$.

A.4 Decomposition of operator states to SU(4) irreps

In this section, we present more details on how to organize the input and output operator states into irreps of SU(4) algebra. We consider the initial operators that take the form $|O_1 I \otimes O_1^\dagger I\rangle$, where O_1 acts on the first fermion. The operator states on the first fermion belongs to the six dimensional $(0,1,0)$ irrep of SU(4). The operator state acting on the remaining fermions is $I \otimes I$ belongs to $(0, N-1, 0)$. As a result, the total states can be decomposed into three irreps,

$$(0,1,0) \otimes (0,N-1,0) = (0,N,0) \oplus (1,N-2,1) \oplus (0,N-2,0). \tag{A.24}$$

The operator states corresponding to the highest weight states in $(0, N, 0)$ and $(1, N-1, 1)$ are

$$|W_{(0,N,0)}\rangle = \frac{1}{N}|\chi^\dagger \otimes \chi\rangle\,, \quad |W_{(1,N-1,1)}\rangle = -|n_1\chi^\dagger \otimes n_1\chi\rangle + \frac{1}{N}\sum_i |n_i\chi^\dagger \otimes n_i\chi\rangle \tag{A.25}$$

A.4.1 $W = n_1$ as the input state

Now we consider the decomposition of $|n_1 I \otimes n_1 I\rangle$ in the interest of computing correlators involving this state. We first perform the double rotation in the SU(2)⊗SU(2) subgroup of SU(4) to rotate the state to $|(n_1 - \bar{n}_1)n \otimes (n_1 - \bar{n}_1)n\rangle$. We study the states in the expansion, which have fixed weights, term by term. The most involved term is $|\bar{n}_1 n \otimes \bar{n}_1 n\rangle$. Based on the weight counting, in the basis of GT patterns, there are two states in $(0, N, 0)$, 4 states in $(1, N-1, 1)$ and 1 state in $(0, N-2, 0)$ contributing to the decomposition. The state $|g\rangle$ in the irrep $(0, N-2, 0)$ is

$$\begin{aligned}|g\rangle = &\sum_{i\neq 1}\Big(|(\bar{n}_1 n_i - n_1\bar{n}_i)\otimes(\bar{n}_1 n_i - n_1\bar{n}_i)\rangle + |\chi_1^\dagger\chi_i n \otimes \chi_1\chi_i^\dagger n\rangle + |\chi_1\chi_i^\dagger n \otimes \chi_1^\dagger\chi_i n\rangle\Big)\\ &- \frac{1}{2N}\left(\sum_{i,j\neq 1}|(\bar{n}_i n_j - n_i\bar{n}_j)\otimes(\bar{n}_i n_j - n_i\bar{n}_j)\rangle + |\chi_i^\dagger\chi_j n \otimes \chi_i\chi_j^\dagger n\rangle + |\chi_i\chi_j^\dagger n \otimes \chi_i^\dagger\chi_j n\rangle\right).\end{aligned} \tag{A.26}$$

The two independent states in the irrep $(0, N, 0)$ that are required for the construction are:

$$|a\rangle = \frac{1}{N!}S^{dc}S^{ba}(S^{cb})^N|\chi^\dagger \otimes \chi\rangle\ ;\ |b\rangle = S^{bc}S^{cb}|a\rangle\,. \tag{A.27}$$

For the contribution from the $(1, N-2, 1)$ irrep, we will begin by defining the state $|X\rangle$

$$(-1)^{N/2+1}\frac{(S^{cb})^{N-2}}{(N-2)!}|W\rangle_{1,N-2,1} = |\chi_1^\dagger n \otimes \chi_1 n\rangle - \frac{1}{N}\sum_j |\chi_j^\dagger n \otimes \chi_j n\rangle = |X\rangle\,. \tag{A.28}$$

Using this state, one can construct the 4 independent states in $(1, N-2, 1)$ irrep required:

$$|k\rangle = S^{cb}S^{dc}S^{ba}\,|X\rangle \;;\; |l\rangle = S^{dc}S^{cb}S^{ba}\,|X\rangle \;;\; |m\rangle = S^{ba}S^{cb}S^{dc}\,|X\rangle \;;\; |j\rangle = S^{bc}S^{cb}\,|m\rangle \tag{A.29}$$

and we use a linear combination of the 4 states above to build the required state:

$$\begin{aligned}\implies |g\rangle + \frac{N+2}{N^2}(|b\rangle + |a\rangle) + (1+1/N)(|j\rangle - |k\rangle + 2(|l\rangle + |m\rangle)) \\ = (N+3+2/N)|\bar{n}_1 n \otimes \bar{n}_1 n\rangle.\end{aligned} \tag{A.30}$$

Hence we have built the desired operator-state using states from all three contributing irreps. The other parts of the state $|(n_1-\bar{n}_1)n \otimes (n_1-\bar{n}_1)n\rangle$ can be built using just two of the three irreps in the young decomposition:

$$\begin{aligned}|\bar{n}_1 n \otimes n\rangle &= (-1)^{\frac{N}{2}+1}\frac{(S^{cb})^{N-1}S^{ba}}{(N-1)!}(S^{cb}\,|W_{(0,N,0)}\rangle - |W_{(1,N-2,1)}\rangle) \\ |n \otimes \bar{n}_1 n\rangle &= (-1)^{\frac{N}{2}+1}\frac{(S^{cb})^{N-1}S^{dc}}{(N-1)!}(S^{cb}\,|W_{(0,N,0)}\rangle - |W_{(1,N-2,1)}\rangle) \\ |n \otimes n\rangle &= (-1)^{N/2}\frac{(S^{cb})^{N}}{(N-1)!}\,|W_{(0,N,0)}\rangle\end{aligned} \tag{A.31}$$

Now the overall state can be rotated back into the desired z-basis by applying the following rotation operator:

$$\sum_{l,m=0}^{N}\frac{(S^{ba})^l(S^{dc})^m}{l!m!}\,|(n_1-\bar{n}_1)n \otimes (n_1-\bar{n}_1)n\rangle = |n_1 I \otimes n_1 I\rangle\,. \tag{A.32}$$

The OTOC $\mathcal{F}(n_1(t), \chi_j^\dagger)$ in each charge sector, labelled by the charge m, has the charge-profile $(m, m, m+1, m+1)$ on the four replicas. This state can therefore be split into different charge-profiles that contribute to the OTOC by applying the appropriate part of the rotation operator. The full output state $\sum_{\mathcal{S}}|\chi_j \mathcal{S}\chi_j^\dagger \otimes \mathcal{S}^\dagger\rangle$ has been built in the main text, which can also be rotated into the relevant charge profiles to find the output state restricted to each charge sector. Hence the equation above builds the charge resolved input

and output states required to compute the OTOC $\mathcal{F}^m(n_1(t), \chi_j^\dagger)$. This OTOC can also be used to compute the charge resolved OTOC $\mathcal{F}^m(\chi_i(-t), n_1)$ in the following way:

$$\mathrm{Tr}(P_m\, n_1(t)\, \chi_j\, n_1(t)\, \chi_j^\dagger) = \mathrm{Tr}(P_{m+1}\, \chi_j^\dagger(-t)\, n_1\, \chi_j(-t)\, n_1) \tag{A.33}$$

Hence the OTOCs can be equated once the charge-sector is shifted by 1.

A.4.2 $V = n_1$ as the output state

Next, we task ourselves with computing $|n_1 I \otimes n_1 I\rangle$ as the output state in the interest of computing the correlator $\mathcal{F}(n_i(t), n_1)$. Since we know how to build the input state $|n_i I \otimes n_i I\rangle$, we will build the output state using the SU(2) $\otimes$ SU(2) subalgebra formed by the operators S^{da} and S^{cb}. Inserting the resolution of the identity into the output state, we get

$$|\mathrm{out}\rangle = \frac{1}{4^N}\sum_S |n_1 \mathcal{S}^\dagger n_1 \otimes \mathcal{S}\rangle = \frac{1}{2^{2N-1}}\sum_{\mathcal{S}^c} |n_1 \mathcal{S}^{c\dagger} \otimes n_1 \mathcal{S}^c\rangle\,, \tag{A.34}$$

where the sum S^c is over operator-strings on all sites except 1. This state can be rotated into just four states and then rotated back in the following way:

$$\begin{aligned}\sum_{\mathcal{S}^c} |n_1 \mathcal{S}^{c\dagger} \otimes n_1 \mathcal{S}^c\rangle = (-1)^{N/2}\sum_{k=0}^{N}\sum_{l=0}^{N-1}(-1)^l \frac{(S^{da})^k}{k!}\frac{(S^{cb})^l}{l!}(1+S^{bc}) \\ \Big(\, |\chi^\dagger \otimes \chi\rangle - |\chi_1 \chi^\dagger \otimes \chi_1^\dagger \chi\rangle + |\bar{n}_1 \chi^\dagger \otimes \bar{n}_1 \chi\rangle - |n_1 \chi^\dagger \otimes n_1 \chi\rangle \,\Big)\end{aligned} \tag{A.35}$$

The state $|\chi^\dagger \otimes \chi\rangle$ is proportional to the highest weight state $|W_{(0,N,0)}\rangle$. Two of the other states are simple to build using

$$|n_1 \chi^\dagger \otimes n_1 \chi\rangle = S^{cb}\,|W_{(0,N,0)}\rangle - |W_{(1,N-2,1)}\rangle \;\;;\;\; |\bar{n}_1 \chi^\dagger \otimes \bar{n}_1 \chi\rangle = S^{ba} S^{dc}\,|n_1 \chi^\dagger \otimes n_1 \chi\rangle \tag{A.36}$$

Now we move onto building the fourth state and to build this, we first construct the highest weight state in $(0, N-2, 0)$:

$$\begin{aligned}|W_{(0,N-2,0)}\rangle = (N-1)\,|\chi_1\chi^\dagger \otimes \chi_1^\dagger\chi\rangle + \sum_{i\neq 1}(|\bar{n}_1 n_i\chi^\dagger \otimes \bar{n}_1 n_i\chi\rangle - |n_1\bar{n}_i\chi^\dagger \otimes \bar{n}_1 n_i\chi\rangle \\ - |\bar{n}_1 n_i\chi^\dagger \otimes n_1\bar{n}_i\chi\rangle + |n_1\bar{n}_i\chi^\dagger \otimes n_1\bar{n}_i\chi\rangle) + \frac{2}{N}\sum_{i\neq 1}|\chi_i\chi^\dagger \otimes \chi_i^\dagger\chi\rangle \\ -\frac{1}{N}\sum_{i,j\neq 1}(|\bar{n}_i n_j\chi^\dagger \otimes \bar{n}_i n_j\chi\rangle - |\bar{n}_i n_j\chi^\dagger \otimes n_i\bar{n}_j\chi\rangle)\end{aligned} \tag{A.37}$$

The state in the $(0, N, 0)$ irrep relevant to the construction is:

$$\begin{aligned}|c\rangle = (S^{cb}S^{ba}S^{dc}S^{cb} - \frac{1}{4}S^{ba}S^{dc}(S^{cb})^2)\,|W_{(0,N,0)}\rangle \\ = \sum_i |\chi_i\chi^\dagger \otimes \chi_i^\dagger\chi\rangle - \frac{1}{2}\sum_{i,j}(|\bar{n}_i n_j\chi^\dagger \otimes \bar{n}_i n_j\chi\rangle - |\bar{n}_i n_j\chi^\dagger \otimes n_i\bar{n}_j\chi\rangle)\end{aligned} \tag{A.38}$$

Hence

$$\begin{aligned}|W\rangle_{(0,N-2,0)} - \frac{2}{N}|c\rangle = (N-1-2/N)\,|\chi_1\chi^\dagger \otimes \chi_1^\dagger\chi\rangle \\ + (1+1/N)\sum_{i\neq 1}(|\bar{n}_1 n_i\chi^\dagger \otimes \bar{n}_1 n_i\chi\rangle - |n_1\bar{n}_i\chi^\dagger \otimes \bar{n}_1 n_i\chi\rangle \\ - |\bar{n}_1 n_i\chi^\dagger \otimes n_1\bar{n}_i\chi\rangle + |n_1\bar{n}_i\chi^\dagger \otimes n_1\bar{n}_i\chi\rangle)\end{aligned} \tag{A.39}$$

Now in the irrep $(1, N-2, 1)$, we build the 4 states:

$$\begin{aligned}|x\rangle = S^{dc}S^{cb}S^{ba}\,|W_{(1,N-2,1)}\rangle \;;\; |y\rangle = S^{ba}S^{cb}S^{dc}\,|W_{(1,N-2,1)}\rangle \;; \\ |z\rangle = S^{cb}S^{ba}S^{dc}\,|W_{(1,N-2,1)}\rangle \;;\; |w\rangle = S^{ba}S^{dc}S^{cb}\,|W_{(1,N-2,1)}\rangle\end{aligned} \tag{A.40}$$

And using these, we can build the fourth state required to rotate into the overall state $\sum_{S^c} |n_1 S^{c\dagger} \otimes n_1 S^c\rangle$

$$\begin{aligned} |W\rangle_{(0,N-2,0)} + \left(\frac{2N+4}{N^2}\right)|c\rangle + \left(1+\frac{1}{N}\right)(2(|x\rangle + |y\rangle) - |w\rangle - 4\,|z\rangle) \\ = (N+3+2/N)\,|\chi_1\chi^\dagger \otimes \chi_1^\dagger \chi\rangle \end{aligned} \tag{A.41}$$

For the correlator $\mathcal{F}^m(n_i(t), n_1)$, the values of $S^{\alpha\alpha}$ on each replica corresponding to the overall charge $m(\in [1, N])$ are $(m, N-m, m, N-m)$. Therefore, the input and output state built can be rotated appropriately into these charge sectors to compute the OTOC.

A.5 Additional irreps

The OTOC $\mathcal{F}^m(\chi_i(t), \chi_j^\dagger)$ contains contributions from two irreps. The early and late time behavior of sectors in the $(1, N-2, 1)$ irrep displays an exponential decay (for large enough N) governed by eigenvalues similar to λ^ρ_{late}, shown in Fig. 3.7(a), for large N

$$\mathcal{F}^m_{(1,N-2,1)}(\chi(t), \chi^\dagger) \simeq \rho(1-\rho)e^{-\lambda^\rho_{late} t} \tag{A.42}$$

where smaller sectors have larger eigenvalues and therefore decay slower. This behavior has been plotted in Fig. A.4(a) and is similar to the behavior of the irrep $L = N/2 - 1$ in the Majorana case. It should be noted that this irrep shows similar behavior for other OTOCs. The OTOC $\mathcal{F}(n_i(t), n_j)$ is unique amongst the ones discussed in this work because it contains the contribution from the third irrep $(0, N-2, 0)$. This irrep also shows an exponential decay as well, with eigenvalues picked from the λ^ρ_L distribution

$$\mathcal{F}^m_{(0,N-2,0)}(n(t), n) \simeq \rho(1-\rho)e^{-\lambda^\rho_L t} \tag{A.43}$$

We plot this behavior in Fig. A.4(b).

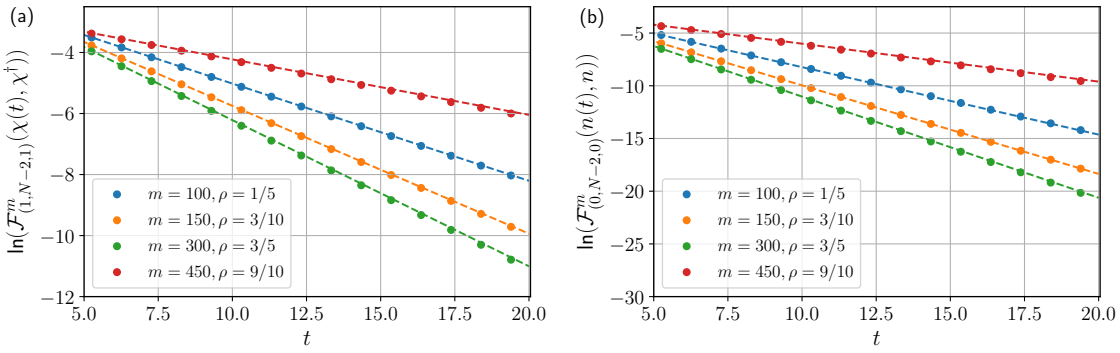

Figure A.4: (a) The log-behavior of different sectors within the $(1, N-2, 1)$ contribution to the $\mathcal{F}^m(\chi_i(t), \chi_j^\dagger)$ OTOC for $N = 500$, compared with straight line fits with slope $-\lambda^\rho_{late}$ and intercept $\ln(\rho(1-\rho))$ for the corresponding ρ. (b) The log-behavior of different sectors within the $(0, N-2, 0)$ contribution to the $\mathcal{F}^m(n_i(t), n_j)$ OTOC for $N = 500$, compared with straight line fits with slope $-\lambda^\rho_L$ and intercept $\ln(\rho(1-\rho))$ for the corresponding ρ. The irreps in both (a) and (b) exponentially decay in each charge sector and therefore do not contribute to the scrambling dynamics.

APPENDIX B

APPENDIX FOR NON-EQUILIBRIUM DYNAMICS IN 1+1 DIMENSIONS

B.1 Anti-commuting fermions on multiple time-contours

This short section will elucidate the procedure to arrive at anti-commuting fermions on four time contours. In the original model, we begin with a Brownian model built with fermions $\chi_{i,r}$ where i is the fermion index and r is the site/cluster index. These satisfy the anti-commutation relation $\{\chi^\dagger_{i,r}, \chi_{j,r'}\} = \delta_{i,j}\delta_{r,r'}$. When generalizing to four time contours, we use the 'replica fermions' on replicas a, b, c, d:

$$\begin{aligned} \chi^a_{i,r} &:= \chi_{i,r} \otimes I \otimes I \otimes I \qquad & \chi^b_{i,r} &:= I \otimes \chi^\top_{i,r} \otimes I \otimes I \\ \chi^c_{i,r} &:= I \otimes I \otimes \chi_{i,r} \otimes I \qquad & \chi^d_{i,r} &:= I \otimes I \otimes I \otimes \chi^\top_{i,r} \end{aligned} \tag{B.1}$$

where $\chi^\top$ refers to the transpose, and we have performed a particle-hole transformation on replicas b, d for future mathematical convenience. It's clear that the fermions on different replicas commute with each other due to the tensor-product structure. To make them anti-commute, we use the global parity operator $\mathcal{Q}$

$$\mathcal{Q}^\alpha = \prod_{j,r} \exp(i\pi n^\alpha_{j,r}), \quad \alpha = a, b, c, d \tag{B.2}$$

Following this, we define the fermions $\psi^\alpha_{i,r}$ using the parity operator:

$$\begin{aligned} \psi^a_j &= \mathcal{Q}^a \chi^a_j, \qquad & \psi^b_j &= \mathcal{Q}^a \chi^b_j, \\ \psi^c_j &= \mathcal{Q}^a \mathcal{Q}^b \mathcal{Q}^c \chi^c_j, \qquad & \psi^d_j &= \mathcal{Q}^a \mathcal{Q}^b \mathcal{Q}^c \chi^d_j. \end{aligned} \tag{B.3}$$

These new fermions now anti-commute even on separate replicas, $\{\psi^{\dagger\alpha}_{i,r}, \psi^\beta_{j,r'}\} = \delta_{i,j}\delta_{\alpha,\beta}\delta_{r,r'}$, and can be used to define the SU(4) algebra as highlighted in the main text.

B.2 Charge-resolution of null-eigenstates

In this section of the appendix, we will discuss the properties of the Identity operator state and other null-eigenstates in a model with charge conservation. As was noted in Sec. 4.3.2, we work with an operator basis with a well defined left and right charge, which are both constants of motion. Since the identity is invariant due to the unitary dynamics (Fig. 2.1), the corresponding operator state vanishes under the action of the emergent Hamiltonian:

$$UIU^\dagger = I \implies \overline{U \otimes U^*}\,|I\rangle = |I\rangle \implies \mathbb{H}\,|I\rangle = 0\,;\; |I\rangle \;= \sum_{i,j} \delta_{ij}\,|i \otimes j\rangle \tag{B.4}$$

While the above statement is true for any unitary Brownian model, in a charge-conserving model this identity splits into multiple charge sectors. For a complex fermionic model with N fermions:

$$I = \prod_{i=1}^{N}(n_i + \bar{n}_i) = \sum_{q=0}^{N} I_{q,N}\;;\; I_{q,N} = \sum_{i_1<\ldots<i_q} n_{i_1}\ldots n_{i_q}\bar{n}_{i_{q+1}}\ldots\bar{n}_{i_{N-q}} \tag{B.5}$$

where we have split the identity into strings $I_{q,N}$, each with charge profile (q, q). Since both the identity and the charge profiles are conserved, each string $I_{q,N}$ is also a constant of motion $\mathbb{H}\,|I_{q,N}\rangle = 0$. This means that due to charge conservation, we have multiple constants of motion from the invariance of the identity, instead of just one. There exists one in each sector with profile (q, q), hence $q_a = q_b$ is a necessary condition to restrict to a sector with a component of the identity. Apart from the identity, any other operator which represents a symmetry will also have corresponding charge-resolved null eigenstates. On the four-contour level, there emerges another null-eigenstate of the emergent Hamiltonian which is due to the unitary nature of the dynamics as well. This is the complete set of states $\sum_{\mathcal{S}} |\mathcal{S}^\dagger \otimes \mathcal{S}\rangle$ (Fig. 2.1), and this as well will split into different charge sectors, each with profile of the form (q_1, q_2, q_2, q_1). This is because the charge profiles of an operator and its complex conjugate

are related in the following way:

$$(\sum_i n_i)O = q_a O \implies O^\dagger(\sum_i n_i) = q_a O^\dagger \tag{B.6}$$

B.3 Solving the restricted Fokker-Planck equation

In this section, we will study simple toy versions of the 'restricted' differential equations we obtain in the main section. The goal is to show that once we restrict to the sector which describes a stochastic process, the usual process of obtaining a Langevin equation still remain valid.

Let's consider a function $P(x, y, t)$ which satisfies the following differential equation:

$$\partial_t P = \partial_x((xy + x)P) + \partial_y(yP) \tag{B.7}$$

Hence P describes a probability distribution since $\int P dxdy$ is a constant. It is well known that the equations of motion for x, y can be described by the followin Langevin equations:

$$x'(t) = -(xy + x); \quad y'(t) = -y \tag{B.8}$$

Now we modify the equation such that it only describes a probability distribution in the sector $y = 0$, which means it is the incoherent sector:

$$\partial_t P = \partial_x((xy + x)P) + y\partial_y P \implies \partial_t \int \delta(y) P dxdy = 0 \tag{B.9}$$

We begin with an input state which is well localized around the fixed probability sector $P(x, y, t = 0) \propto e^{-y^2}\delta(x - \epsilon)$, and we are interested in computing the quantity $\mathcal{F}$ is given by $\mathcal{F}(t) = \int \delta(y) x P(x, y, t) dxdy$. This model is a simplified version of the situation in the main text, with $y = 0$ representing the 'incoherent' sector. The restricted differential equation

above supports solutions of the form:

$$P(x,y,t) = \frac{1}{x} f\left(y - \ln\left(\frac{x}{y}\right),\, \ln y + t\right) = \frac{1}{x}\delta\left(\ln x + y(e^t - 1) + t - \ln\epsilon\right) e^{-y^2 e^{2t}} \tag{B.10}$$

where we have reshaped $P(x, y, t = 0)$ to be of the from f, time-evolved it, and then simplified it to be the expression on the right. Hence $\mathcal{F}$ is given by:

$$\mathcal{F}(t) = \int x\delta(y) P(x,y,t) dx dy = \int x\, \delta(x - e^{-t} - \epsilon) dx \tag{B.11}$$

which implies that x satisfies the equation of motion $x'(t) = -x$ which is precisely what one gets upon setting $y = 0$ in Eq. (B.8). The overall equations of motion have changed, but in the fixed probability sector, variables follow Langevin equations as expected, and there is no 'feedback' effect from the non-conserved sector.

B.4 Analytic solution of the free-fermionic chain

In this section we analytically solve the transport properties and OTOC in the free fermionic chain which is represented by the Hamiltonian:

$$H_{\text{inter}} = \sum_{j_1, j_2, r} K^r_{j_1, j_2}(t) \chi^\dagger_{j_1, r} \chi_{j_2, r+1} + h.c. \tag{B.12}$$

This represents a fermionic model with N fermions on each cluster, while driven hopping is allowed between L such clusters.

B.4.1 Charge transport at finite-N

The transport occurs on two-time contours, as it can be diagnosed by analyzing the two-point function of the charge density:

$$\langle \rho(r_1, t) \rho(r_2, 0) \rangle = \frac{\text{Tr}(\rho(r_1, t)\rho(r_2, 0))}{\text{Tr}(I)}; \quad \rho = \sum_{i=1}^{N} \frac{n_i}{N} \tag{B.13}$$

For operator dynamics in the Brownian model, we consider the two-replica level emergent Hamiltonian, which will show an emergent SU(2) $\otimes$ U(1) symmetry. Defining the operator $S^{\alpha\beta} = \sum_i \chi_i^{\dagger\alpha}\chi_i^{\beta}$, we can show that it can be used to define the algebra as follows:

$$L^+ = S^{ab}; \quad L^- = S^{ba}; \quad [L^+, L^-] = 2L_z = S^{ab} - S^{ba}; \quad Q = S^{ab} + S^{ba} \tag{B.14}$$

where Q is the U(1) part of the algebra. In the SU(2) algebra on each site, the input state $|\rho\rangle$ can be decomposed as:

$$\begin{aligned}
&|n_1\rangle = |n_1(n_2 + \bar{n}_2)...(n_N + \bar{n}_N)\rangle = \frac{1}{\sqrt{2}}|\uparrow \rightarrow ... \rightarrow\rangle \\
&= \frac{1}{2}|(\rightarrow + \leftarrow) \rightarrow ... \rightarrow\rangle = \frac{1}{2}|\rightarrow\rightarrow ... \rightarrow\rangle + \frac{1}{2}|\leftarrow\rightarrow ... \rightarrow\rangle \\
&|\leftarrow\rightarrow ... \rightarrow\rangle = \frac{1}{N}\sum_i |\rightarrow ... \leftarrow_i ... \rightarrow\rangle + \left(|\leftarrow\rightarrow ... \rightarrow\rangle - \frac{1}{N}|\rightarrow ... \leftarrow_i ... \rightarrow\rangle\right) \\
&\implies |\rho\rangle = \frac{1}{2}|N/2, N/2\rangle_x + \frac{1}{2\sqrt{N}}|N/2, N/2-1\rangle_x \\
&\implies |\rho(r_1)\rangle = |I\rangle_1 \otimes |I\rangle_2 \otimes ... |\rho\rangle_{r_1} ... \otimes |I\rangle_L
\end{aligned} \tag{B.15}$$

The identity is the fully polarized state along the x-direction on every site, and is a constant of motion for the unitary dynamics (Appendix B.2). The trace is given by:

$$\frac{\mathrm{Tr}(\rho(r_1, t)\rho(r_2, 0))}{\mathrm{Tr}(I)} = \langle\rho(r_2)|U \otimes U^*|\rho(r_1)\rangle \tag{B.16}$$

One can verify that these give the correct values at $t = 0$ according to the spin decomposition, i.e. 1/4 for $r_1 \neq r_2$ and 1/4(1+1/N) for $r_1 = r_2$. Now that we have the state-decomposition, we can analyze the emergent Hamiltonian, which for the free fermionic chain is:

$$\mathbb{H} = \frac{1}{N}\left(\sum_{r=1}^{L} 2L_r^z L_{r+1}^z + L_r^+ L_{r+1}^- + L_r^- L_{r+1}^+ - \frac{N^2 L}{2}\right) \tag{B.17}$$

This is simply the SU(2) Heisenberg model, and we can exploit the SU(2) invariance to

solve the two-point function exactly. The 'physical' charge conservation manifests itself as conservation of global weights $\sum_r L_r^i = \text{const}$, $i = x, y, z$. This should be contrasted with the mathematical charge conservation (Q) within each irrep. Since the input state of interest splits into two states, one of which is static under the emergent Hamiltonian, we only need to focus on the lower weight state. We define a basis:

$$|\psi_r\rangle = |N/2\rangle_{x,1} \otimes ... \, |N/2-1\rangle_{x,r} \otimes ... \, |N/2\rangle_{x,L} \tag{B.18}$$

such that a general state may be written as:

$$|\psi(t)\rangle = \sum_r q_r(t) \, |\psi_r\rangle \implies \sum_r q_r(t) = const, \tag{B.19}$$

hence $q_r(t)$ can be viewed as the charge distribution. The equation of motion for the state is:

$$\begin{aligned} &\partial_t \, |\psi(t)\rangle = \mathbb{H} \, |\psi(t)\rangle \implies \sum_r \partial_t q_r(t) \, |\psi_r\rangle = \sum_i q_r(t)(|\psi_{r+1}\rangle + |\psi_{r-1}\rangle - 2 \, |\psi_r\rangle) \\ &\implies \partial_t q_r(t) = (q_{r+1}(t) + q_{r-1}(t) - 2q_r(t)) \longrightarrow \partial_t \rho(r,t) = \partial_r^2 \rho(r,t) \end{aligned} \tag{B.20}$$

where the last equation involves taking the continuum limit of the spatial direction r. Starting with a delta function localized at $r = r_1$, we get the solution:

$$\rho(r,t) = \frac{1}{\sqrt{8\pi N t}} \exp\bigg(- \frac{(r-r_1)^2}{4t} \bigg) \tag{B.21}$$

which means the expression for the 2-pt func. is:

$$\langle \rho(r_1,t)\rho(r_2,0)\rangle = \frac{1}{4} + \frac{1}{4N\sqrt{4\pi t}} \exp\bigg(- \frac{(r_2-r_1)^2}{4t} \bigg) \tag{B.22}$$

B.4.2 OTOC at finite-N

In this section we will exactly solve the OTOC for the free fermion at finite N, for a chain with L clusters. We will choose both the input operator and output operator, W and V, to be χ but on clusters r and r', because it makes the computations simpler. The Emergent Hamiltonian for the free-fermion case, assuming periodic boundary conditions, is given by:

$$\mathbb{H}_{\text{inter}} = \frac{1}{N}\Big(\sum_{\alpha,\beta,r} S_r^{\alpha\beta} S_{r+1}^{\beta\alpha} - N\sum_r Q_r\Big) \tag{B.23}$$

This has been written explicitly in terms of the Casimir of SU(4) to make the SU(4) invariance manifest. The OTOC we will study will be of the form $\sum_{i,j}\mathcal{F}(\chi_{i,r},\chi_{j,r'})$. The input state is the operator-state $|\chi^\dagger\otimes\chi\rangle$ on site r and the identity $|I\otimes I\rangle$ on all the other sites.

$$\begin{aligned} |\text{in}_r\rangle &= \frac{1}{2^{NL}}\,|I\otimes I\rangle_1\otimes\ldots|\chi^\dagger\otimes\chi\rangle_r\otimes\ldots|I\otimes I\rangle_L\,; \\ |\chi^\dagger\otimes\chi\rangle_r &= \frac{1}{N}\sum_{i=1}^{N}|\chi_i^\dagger\otimes\chi_i\rangle_r\,. \end{aligned} \tag{B.24}$$

The second line is due to the restriction of the operator to the symmetric irrep $(0,N,0)$. Note that since the identity-state is automatically contained within this irrep, we have fixed the irrep to be the same on every site. This overall state is complicated in terms of its decomposition into different charge sectors which have independent dynamics. Now we utilize the SU(4) invariance of the Emergent Hamiltonian and specifically the SU(2) $\otimes$ SU(2) sub-algebra formed by the operators S^{ba} and S^{dc} (Fig. 4.2) to rotate the input state into one strict charge-sector:

$$|\widetilde{\text{in}}_r\rangle = \frac{1}{2^{NL}}\,|\Pi n\otimes\Pi n\rangle_1\otimes\ldots|\chi^\dagger\Pi n\otimes\chi\Pi n\rangle_r\otimes\ldots|\Pi n\otimes\Pi n\rangle_L \tag{B.25}$$

where $|\widetilde{\text{in}}\rangle_r$ is the rotated input state. We have simply rotated the identity $I = n+\bar{n}$ into n on both the left and right halves of the string via the SU(2) $\otimes$ SU(2) rotation. This leaves

the emergent Hamiltonian unchanged due to the SU(4) invariance. We will now demonstrate that this state performs a random walk under the dynamics. Let there be a general state given by:

$$\begin{aligned} |\widetilde{\psi}(t)\rangle &= \sum_r c_r(t)\,|\widetilde{\text{in}}\rangle_r \\ \partial_t\,|\widetilde{\psi}(t)\rangle &= \mathbb{H}\,|\widetilde{\psi}(t)\rangle \end{aligned} \tag{B.26}$$

where on the second line we have demonstrated the rule which governs the dynamics of the said state. Since the input-state now has fixed values of $\sum_r S_r^{\alpha\alpha} S_{r+1}^{\alpha\alpha}$ after the rotation, it is simple to check that it satisfies:

$$\begin{aligned} &\mathbb{H}(\sum_r c_r(t)\,|\widetilde{\text{in}}_r\rangle) = \sum_r c_r(t)(|\widetilde{\text{in}}_{r+1}\rangle + |\widetilde{\text{in}}_{r-1}\rangle - 2\,|\widetilde{\text{in}}_r\rangle) \\ &\implies \partial_t c_r(t) = (c_{r+1} + c_{r-1} - 2c_r) \to \partial_t c(r,t) = \partial_r^2 c(r,t) \end{aligned} \tag{B.27}$$

In the second line we have used the continuum limit along the spatial dimension r. This result is exact for all N and L. One can now rotate the states back into the form $|\text{in}\rangle_r$ and show that it performs a random walk under the time evolution. Since the output operator is also chosen to be χ, it is simple to verify that it satisfies the following overlap condition:

$$2^{NL}\,\langle \text{out}_{r'}|\text{in}_r\rangle = \begin{cases} \frac{1}{4N} - \frac{1}{4}, & \text{if } r = r' \\ -\frac{1}{4}, & \text{otherwise} \end{cases} \tag{B.28}$$

Hence the overall overlap with the state ψ, which is the state $\widetilde{\psi}$ rotated back, takes the form:

$$\mathcal{F}(W(t), V) = 2^{NL}\,\langle \text{out}_{r'}|\psi(t)\rangle = -\frac{1}{4}\sum_r c_r(t) + \frac{1}{4N} c_{r'}(t) \tag{B.29}$$

The sum of the coefficients c_r is conserved due to the random-walk nature of the dynamics and the initial state can be chosen to guarantee that it is fixed at 1. Hence the OTOC in the continuum limit is determined by the value of $c(r', t)$ which shows diffusive growth/decay (Eq. (B.27)). The exact OTOC at finite N therefore matches the OTOC in the infinite N

limit.